SOLUTION COMBUSTION SYNTHESIS OF CERIUM-, IRON-, AND TUNGSTEN-PROMOTED ALUMINA FOR CONVERSION OF SUGARCANE LEAVES TO FURFURAL

By
MR. Navee AMPOLSING

A Thesis Submitted in Partial Fulfillment of the Requirements
for Master of Engineering (CHEMICAL ENGINEERING)
Department of CHEMICAL ENGINEERING
Graduate School, Silpakorn University
Academic Year 2021

การสังเคราะห์แบบเผาไหม้สารละลายของอะลูมินาส่งเสริมด้วยซีเรียม เหล็ก และทังสเตน สำหรับการเปลี่ยนใบอ้อยเป็นเฟอร์ฟูรัล

โดย
นายนาวี อำพลสิงห์

วิทยานิพนธ์นี้เป็นส่วนหนึ่งของการศึกษาตามหลักสูตรวิศวกรรมศาสตรมหาบัณฑิต
สาขาวิชาวิศวกรรมเคมี แผน ก แบบ ก 2 ระดับปริญญามหาบัณฑิต
ภาควิชาวิศวกรรมเคมี
บัณฑิตวิทยาลัย มหาวิทยาลัยศิลปากร
ปีการศึกษา 2564

SOLUTION COMBUSTION SYNTHESIS OF CERIUM-, IRON-, AND TUNGSTEN-PROMOTED ALUMINA FOR CONVERSION OF SUGARCANE LEAVES TO FURFURAL

By

MR. Navee AMPOLSING

A Thesis Submitted in Partial Fulfillment of the Requirements
for Master of Engineering (CHEMICAL ENGINEERING)
Department of CHEMICAL ENGINEERING
Graduate School, Silpakorn University
Academic Year 2021

Title	Solution combustion synthesis of cerium-, iron-, and tungsten-promoted alumina for conversion of sugarcane leaves to furfural
By	MR. Navee AMPOLSING
Field of Study	(CHEMICAL ENGINEERING)
Advisor	Nutchapon Chotigkrai, D.Eng.

Graduate School Silpakorn University in Partial Fulfillment of the Requirements for the Master of Engineering

.....Dean of graduate school
(Associate Professor Jurairat Nunthanid, Ph.D.)

Approved by

.....Chair person
(Assistant Professor Tarawipa Puangpetch, Ph.D.)

.....Advisor
(Nutchapon Chotigkrai, D.Eng.)

.....Committee
(Assistant Professor Choowong Chaisuk, D.Eng.)

.....External Examiner
(Assistant Professor Patcharaporn Weerachawanasak, Ph.D.)

620920032 : Major (CHEMICAL ENGINEERING)
Keyword : Solution combustion synthesis, cerium, iron, tungsten, alumina, sulfated metals catalyst, furfural, sugarcane leaves

MR. NAVEE AMPOLSING : SOLUTION COMBUSTION SYNTHESIS OF CERIUM-, IRON-, AND TUNGSTEN-PROMOTED ALUMINA FOR CONVERSION OF SUGARCANE LEAVES TO FURFURAL THESIS ADVISOR : NUTCHAPON CHOTIGKRAI, D.Eng.

The valorization of abundant agricultural wastes such as sugarcane leaves into furfural is significant and challenging. The solution combustion method (SC) was used to synthesize cerium-, iron-, and tungsten-promoted alumina and the effect of metal loadings (1, 5, 10, and 20 wt.%) on the one-pot conversion of sugarcane leaves to furfural was investigated. The prepared catalysts were characterized by X-ray diffraction (XRD), N_2-physisorption, scanning electron microscopy (SEM), and ammonia temperature-programmed desorption (NH_3-TPD). The XRD results showed that SC-derived catalysts were gamma-phase alumina and suggested the highly dispersed of metals on the alumina surface. The specific surface area and pore volume of unpromoted alumina were 189 m^2/g and 0.24 cm^3/g, respectively. These monotonically increased to 272 m^2/g and 0.31 cm^3/g with increasing tungsten loading. In contrast for cerium and iron, the specific surface of cerium increased to 212 and 245 and then decreased to 169 and 214 m^2/g, with increasing cerium and iron loading, respectively. Moreover, the pore size distribution was narrow with the average pore diameter around 4-5 nm for all series. The SEM images indicated the aggregation of uniform small particles and EDS analysis of tungsten-promoted alumina indicated a high dispersion of tungsten on alumina. The NH_3-TPD results showed that the acidity of tungsten-promoted alumina catalysts was increased with increasing tungsten loading but decreased for cerium-, and iron-promoted alumina catalysts. The highest furfural yield (29.3 mg per 1 g of sugarcane leaves) was achieved at 170°C, 10 bars of N_2, and 5 h using 5Ce-Al. Furthermore, the effect of reaction times was investigated for tungsten-promoted aluminas and the amount of sulfate impregnation on 10W-Al was also investigated. This work suggested that metal-oxide catalysts play an important role in reducing reaction time, and this work illustrated the advantage of solution combustion for synthesizing solid acid catalysts which can be used in the valorization of biomass.

ACKNOWLEDGEMENTS

First, I would like to express my gratitude to my advisor, Dr. Nutchapon Chotigkrai, for the chance of working and learning under his guidance at the Department of Chemical Engineering, Silpakorn University. In addition to his kind encouragement and support, I have learned and improved my perspective on science and life.

Additionally, I would like to thank Dr. Nardrapee Karuna Sanchez for her support of experiments and discussion of High-performance liquid chromatography (HPLC) results.

I would like to further thank Assistant Professor Dr. Tarawipa Puangpetch, Assistant Professor Dr. Choowong Chaisuk, and Assistant Professor Dr. Patcharaporn Weerachawanasak, who has been the members of my thesis committee. I have gained valuable suggestions and enhancements for the thesis and also for myself.

I would like to thank all members of the Chemical Engineering Lab at Silpakorn University that I have benefited from the academic and social interactions we have had over the years.

Most importantly, I would like to thank my family, for all of their invaluable support and love.

Finally, this work was supported by the Research Team Promotion grant (Professor Dr. Joongjai Panpranot) from the National Research Council of Thailand (NRCT). The authors also would like to thank the Center of Excellence on Catalysis and Catalytic Reaction Engineering (CECC), Chulalongkorn University for providing NH3-TPD results.

MR. Navee AMPOLSING

TABLE OF CONTENTS

Page

LIST OF TABLES

Page

LIST OF FIGURES

Page

Chapter I
Introduction

1.1 Motivation

Nowadays, the world has to face a problem shortage of energy, especially energy from fossil fuels such as crude oil, natural gas, and coal. Energy shortages are a result of the rapid growth of various industrial sectors. Resulting in the use of large amounts of fossil energy. Especially Thailand, which does not have sufficient fossil energy sources, needs to import fossil fuels from foreign countries. Therefore, we need to find alternative energy to replace the fossil energy. In which biomass is one of the alternative energies obtained from agricultural waste. That can be used to produce energy, fuel, and chemicals. Thailand is an agricultural country with forests, crops, and many livestock, which were one of the countries with the top export of agricultural products in the world. Thailand is a country that is mainly engaged in the agricultural industry country. Agricultural residues have been leftovered. In addition to being used for further benefits in livestock farming. However, there is still a lot of it until burning in the end. This is useless and also causes air pollution. Therefore, promoting the use of energy from biomass is one of ways that can benefit the nation. There are many types of biomass utilized for energy such as rice straw, corncobs, sugarcane, and palm bunches, etc. Currently, lignocellulosic biomass has been interested to be used in the production of biomass energy, the conversion to fuels and various chemicals. In this research, sugarcane leaves (SCL) was used as a raw material because a large amount of the leaves was leftovered from the agriculture industry. Mostly, it will be burned by farmers after being harvested. From the database of biomass potential in Thailand, crop year 2013, found that sugarcane leaves are utilized only about 1.8 million tons out of about 17 million tons produced. There are still unused sugarcane leaves and discarded about 15.2 million tons [1]. Sugarcane leaves contain three main components cellulose, hemicellulose, and lignin. Which can be converted into other forms of chemical platforms such as furfural and 5-HMF. Therefore, the sugarcane leaves have higher value.

There are many ways to convert biomass to furfural such as using a solvent, catalyst, or both. Brønsted acidic ionic liquids (BAILs), such as using 1-methyl-3(3-sulfopropyl)-imidazolium hydrogen sulfate ($[C_3SO_3HMIM][HSO_4]$) was applied and showed very high yield (73%)

of furfural [2]. Using the deep eutectic solvents (DESs) without additional catalyst can produce a high furfural yield [3, 4]. P. Zhou and Z. Zhang review the transformation of biomass into value-added chemicals and biofuels. Furfural and HMF can be easily produced from the dehydration of xylose and fructose over acid catalysts [5]. The solid-acid catalyst ZSM-5 was used for the furfural production from corn cobs. The results showed that the highest furfural yield of 78.5% was obtained from catalyzation corn cob by ZSM-5 [6]. The addition of a heterogeneous acid catalyst (solid acid catalyst) in the conversion of biomass has been interested for this research. The addition of solid acid catalyst to the reaction was able to prove the use of sugarcane leaves as a raw material to get high yield furfural and other related products in a one-pot process. Both processes were needed help getting the desired product Lewis' acidity and Brønsted. [7], [8], [9]. The other research report showed the yield of furfural 56% by using a solid catalyst (HUSY) from crop waste in the biphasic system (water+p-xylene) [10]. M. N. Catrinck, et al. [11], study the production of furfural from sugarcane bagasse by using niobic acid (NbO) and niobium phosphate (NbP) in water, they achieve the yield of furfural 52.1 g/kg for NbO and 59.3 g/kg for NbP. This work is interested in using the solid acid heterogeneous catalyst such as WO_3, CeO_2, and Fe_2O_3 on Al_2O_3 support to improve the yield of furfural. Al_2O_3 has many properties. For example, having high surface area [12, 13], that helps the Fe_2O_3 was added to dispersed well [14], Al_2O_3 is inert ceramic support, produce highly dispersed metal nanoparticles [15], and Al_2O_3 is the strong Lewis acid site [16, 17], etc. For WO_3/Al_2O_3, in the research of A. E. Kerenkan et al., various WO_3/Al_2O_3 ratios 1/10, 5/10, and 10/10 when increasing WO_3 the specific surface area and pore volume were decreased but the yield of products was increased [13]. Cerium was good dispersion over the surface of the Al_2O_3 support [18], which might predict the increase of yield of products and Ce could improve the ability of the catalyst to hydrothermal aging and against the water [19-21]. The study of Fe_2O_3 supported Al_2O_3 showed Fe_2O_3 was well dispersed on Al_2O_3 [14]. Which the same as the cerium case. This might predict the increase yield of product. M.Mu et al., [22] reported, the conversion of benzoyl chloride increased rapidly when the Fe_2O_3 loading increased was obtained. When the Fe_2O_3 loading increased, Lewis acidic sites increase, which enhance the activity of the catalyst.

The catalyst preparation is important for catalyst properties. The most of research using synthesis methods based on precipitation, thermal decomposition, and sol-gel which give a high surface area and oxygen vacancies. However, these methods require long time, large amount of solvent, and many steps for synthesis. Solution combustion synthesis (SCS) is a catalyst preparation using metal oxidizer and fuel in an aqueous solution, the mixture is combusted to get the catalyst nanoparticles size and high surface area. And SCS is a facile one-pot method to prepare material and relatively new compared to other methods [23]. Solid catalyst products can be formed easily and fast because the combustion reaction is completed in a short time and at a high temperature. The mixture of metal precursors, fuels in an aqueous solution and gaseous byproducts was generated during the combustion reaction, provides the formation of homogeneous composition solids with highly porous characteristics. Furthermore, the properties of solid catalysts can be changed by adjusting the parameters in the synthesis such as metal precursor, fuel type, fuel-to-oxidizer ratio, and gas generating agent.

1.2 Objective of research

To develop cerium-, iron-, and tungsten-promoted alumina using solution combustion method for one-pot conversion of sugarcane leaves for furfural production.

1.3 Scopes of research

1.3.1 Effect of metals (Ce, Fe, and W) of metal-promoted alumina on catalytic properties.

1.3.2 Effect of metals loadings of metal-promoted alumina on catalytic properties.

1.3.3 The effect of sulfate concentrations of sulfated metal-promoted alumina on catalytic properties.

Table 1 All samples of catalyst.

Part 1			**Part 2**
WO_3-Al_2O_3	CeO_2-Al_2O_3	Fe_2O_3-Al_2O_3	SO_4^{2-}/MOx[a]-Al_2O_3
Unpromoted Al_2O_3			
1 wt.% WO_3	1 wt.% CeO_2	1 wt.% Fe_2O_3	5 wt.% SO_4^{2-}
5 wt.% WO_3	5 wt.% CeO_2	5 wt.% Fe_2O_3	10 wt.% SO_4^{2-}
10 wt.% WO_3	10 wt.% CeO_2	10 wt.% Fe_2O_3	15 wt.% SO_4^{2-}
20 wt.% WO_3	20 wt.% CeO_2	20 wt.% Fe_2O_3	

[a] The best catalyst selected from part 1.

Chapter II
Theory and Literature review

This chapter discusses the theory and the research related to the thesis. Which has been studied, researched, summarized, and collected to guide the operation of the thesis.

2.1 Lignocellulosic biomass

Thailand is an agricultural country with many types of crops such as rice, sugarcane, corn, palm oil, and cassava. These economic crops contain residue that cannot be used. Only some of these wastes have been utilized, for heat and electricity generation. However, there are still have large amounts of residues that cannot be utilized. For example, rice straw, leaves, and sugarcane shoots, and palm leaves (**Table 2**).

Table 2 Results of the evaluation of biomass potential in Thailand.

Biomass	**Born (Million tons)**	**Utilized (Million tons)**	**Remain (Million tons)**
Rice straw	19	8.1	10.9
Sugarcane leaves	17	1.8	15.2
Shoots, leaves, and corn stalks	9.3	0.5	8.8
Cassava rhizome	6	0.2	5.8

Reference: Database of biomass potential in Thailand, crop year 2 0 1 3 , Department of Alternative Energy Development and Efficiency, Ministry of energy. [1]

The wastes from these economic crops are lignocellulosic biomass with three major components: cellulose, hemicellulose, and lignin. The amount of the three components depends on the type of biomass, cultivated place, and different species of those crops.

All of the components of this lignocellulosic biomass have many potential applications in the biofuel and biochemical industries, which are new and potential for Thailand. It is also in demand in the world market as well. Especially in European countries with clear renewable energy targets and seriously pushing to use products from biomass.

2.1.1 Components of lignocellulosic biomass [24]

- Lignin

Lignin is an aromatic component, which is found in the cell wall. Lignin has to protect cellulose decompose from the enzyme. Lignin is a heteropolymer, has form in 3 dimensions consist with tran-p-coumaryl alcohol, trans-coniferyl alcohol, and trans-p-sinapyl alcohol.

- Cellulose

Cellulose is the largest quantity component in lignocellulose which is found in the cell wall. The quantity of cellulose depends on the type of plant. Cellulose is a homopolymer-like chain, consist of beta-D-Glucopyranose connect by beta bond, 1 , 4 -glycosidic then forms to polymer glucan anchor with a hydrogen bond. The form of cellulose can find in crystalline cellulose and amorphous cellulose.

- Hemicellulose

Hemicellulose is the component in lignocellulose. Hemicellulose is a heteropolymer, consists of many types of sugar such as glucose, mannose, xylose, and arabinose. The length of hemicellulose is estimated at around 2 0 0 units. In the wilan polymer, the quantity of D-xylose is largest, around 85-93%.

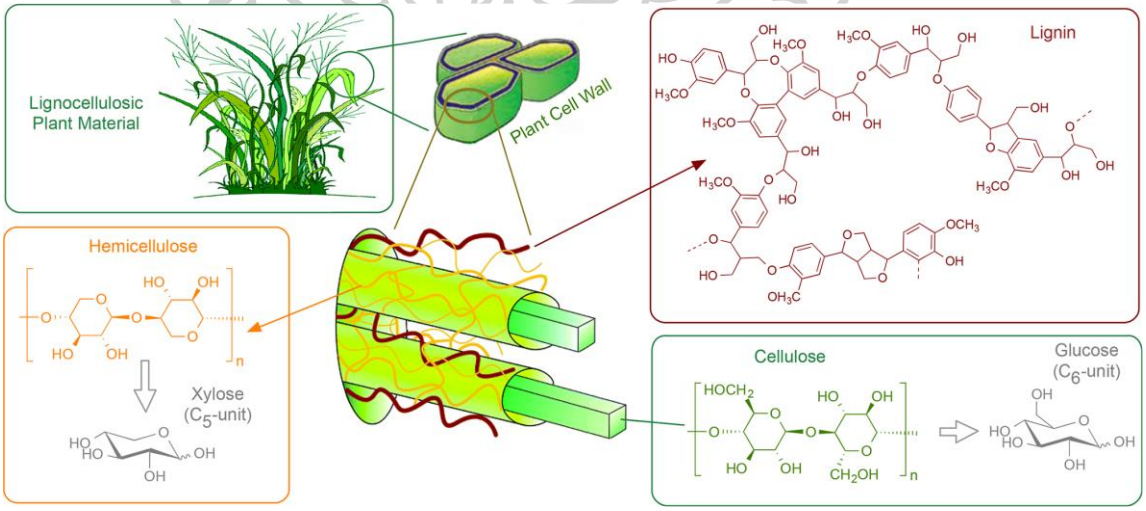

Figure 1 : Schematic illustration of lignocellulose., Chem. Rev., 2018, 118, 505−613. [25]

2.1.2 Potential of each component in lignocellulosic biomass

Direct utilization and changing to biological chemistry.

- Hemicellulose is a precursor of important products such as furfural and furfuryl alcohol. This research focuses on furfural products, a high-value substance that can be utilized in many industries.

- Cellulose is a precursor of important products, glucose, ethanol, 5-HMF, levulinic acid. And it can be converted to fuels and valuable platform chemicals using catalytic reactions [26].

- Lignin is an important substrate for the production of other substances in many industries such as adhesives, waterproofing, coatings in the paper industry, drilling fluids in the oil drilling industry, used as an additive in the rubber industry, or as an ingredient in the cement production industry for strength, etc. [27]

As above, the potential to utilize the three important components are many options. But the important step in making use of all three components is to separate each component from lignocellulosic biomass. The separation process must be effective for medium-sized factories as it avoids the limitations of transporting biomass from various sources to a large factory center.

2.2 Furfural [28]

Furfural ($C_5H_4O_2$) is a chemical platform aldehyde, colorless liquid with a characteristic “almond-benzaldehyde” odor. It’s one of the top valuable chemicals, expensive if it separated to high purity. And furfural can be converted to many products, which is a product that has been used in many industries. Furfural was first isolated in 1 8 2 1 by a German scientist, Dobereiner. Nowadays, furfural is one of the top valuable chemicals with a huge potential to be produced from the lignocellulosic biomass, can be produced from the agricultural industrial residues, it was converted from hemicellulose from the previous topic. Simultaneously, furfural can be produced from fossil-based raw materials, but it’s not economical as compared to the lignocellulosic biomass-based sources. And furfural used for many precursor chemicals, such as furfurylamine, furoic acid, furan, furfuryl alcohol, etc.

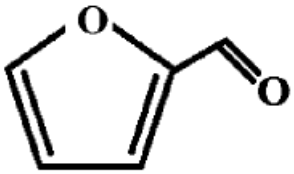

Figure 2 : Chemical structure of furfural., Waste and Biomass Valorization, 2021, 12, 531–552, [28].

Applications of furfural such as used as a nematocide, fungicide, and preservative. Used as an extractant for aromatics from lubricating oils, Purification solvent for hydrocarbons, reactive solvent, and wetting agent. And used Platform chemicals such as furfurylamine, furoic acid, furan, α-(methyl)-furfuryl alcohol, furfuryl alcohol, 2-methylfuran, furoic esters, levulinic acid, 2-methyl-tetra-hydrofuran, tetra-hydrofurfurylamine, tetra-hydrofuroic acid, tetra-hydro-furfuryl alcohol, α-Acetyl-furan, and piperidine. Some products from furfural, showing in **Figure 3**.

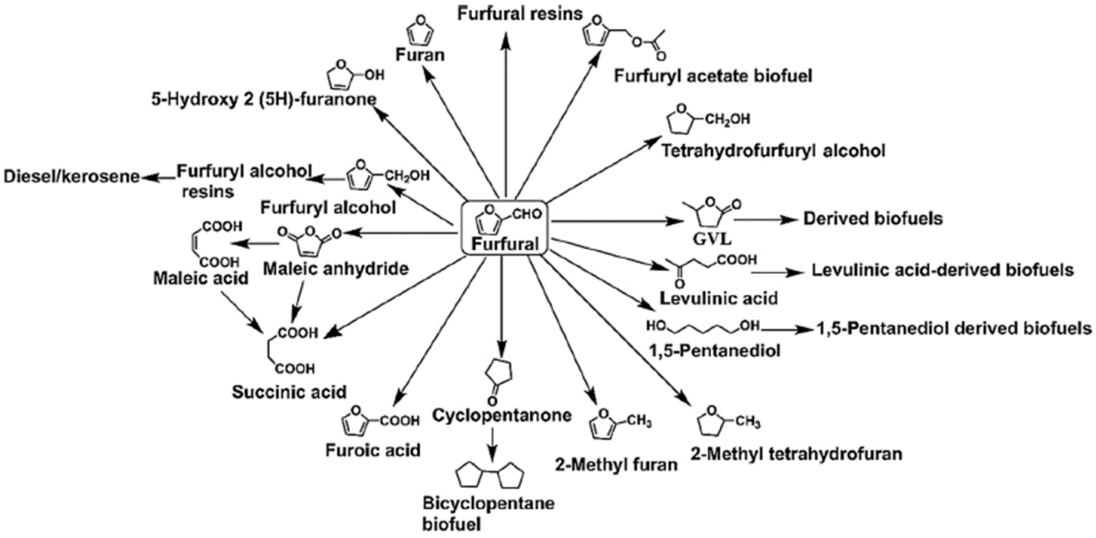

Figure 3 : The pathways for the conversion of furfural as platform molecule into chemicals and fuels., Catalysis Today, 2019, 319, 14–24. [29]

2.3 Sugarcane leaves (SCL) [30]

Sugarcane is a plant in the grass family, and originating on the island of New Guinea in the Pacific Ocean. The external characteristics consist of stems with clear joints, have switching leaves, the leaf sheath covering the trunk in which the leaf is also hairy. The root of the sugar cane is a fibrous root system but strong, able to penetrate deep into the soil. The stems of sugarcane can sprout from the buds of various joints that are close to the soil.

Sugarcane is a plant that grows well in the tropics and subtropical areas. Need an area with heavy rainfall and sunlight. Grows well at temperatures above 20 degrees Celsius with uniform distribution of rain. Must have 1,500 millimeters of rainfall per year. Sugarcane grew slowly in the first months. Older sugarcane will have a long growing period and provide high yields. In many countries that grow sugarcane, sugarcane is harvested at the age of 11-16 months.

Sugarcane grows well in almost all soil types with air and water transferable. Because sugarcane while still young is not able to withstand flooding conditions. The soil for planting must not be too acid or base, and complete with nutrients. The area should look like a plain, not flooded or flat, with a depth of at least 20 inches.

As mentioned above about the leftover after planting of sugarcane. Which has a lot of unused waste. Sugarcane production in Thailand is 5% of the world's production. And there are still other countries in the world that produce a large amount of sugarcane, such as China (7 %), India (19%), and Brazil (40%), which will create more waste from sugarcane. For this reason, we are interested in sugarcane leaves. In sugarcane leaves contain the composition of Lignin, hemicellulose and cellulose are the main components, which those components can be added to the value and can also be used for change to the chemical platform or producing chemicals.

The three main components of lignocellulosic in sugarcane leaves, from other research showing in **Table 3**.

Table 3 Three main components of lignocellulosic in sugarcane leaves.

Hemicellulose %	Cellulose %	Lignin %	Ref.
23	38.5	15.6	[31]
23	35.3	19.6	[32]
21	36	16	[33]
28.28	44	10.04	[34]

The research by A. Akaracharanya et al [31]. Study about ethanol production from sugarcane leaves, as a raw material. In this research, study about the susceptibility of sugarcane leaves to cellulose hydrolysis by GC220 cellulase at 72 hrs. After pretreatment by autoclaving at 121°C with dilute sulfuric acid and lime. Were found the acid pretreated sample give glucose more than the lime pretreated sample (5.7% and 3.9% weight by weight (w/w, (DS)), respectively). And this research study uses the Accellerase™ 1000 (160 FPU / g, DS) to hydrolysis of pretreatment with dilute sulfuric acid and in pretreatment hydrolysate of sugarcane leaves pretreatment at 6 hrs. Were found the yields 0.104 and 0.163 g glucose/ g (DS) respectively. The fermentation in both of the above sources received glucose from Saccharomyces cerevisiae at 12 and 24 hrs, respectively. Which produces ethanol yields at 4.8% and 8.0% (w / w, DS) respectively.

2.4 Pathways to furfural

The pathways of lignocellulosic to furfural have many ways, this topic discusses pathways to the formation of furfural from lignocellulose. Other research will mention to the mechanism of furfural production can be formed from both cellulose and hemicellulose (Xylose or arabinose).

In the research of M. Sert et al. [26], they study the direct conversion of cellulose into 5- hydroxymethylfurfural (5-HMF), levulinic acid, furfural, and formic acid by using deep eutectic solvents (DESs) in conventional and microwave reactors. And starting from sunflower stalk, based on cellulose. In this research, showing the effect of acidity on to yield of products, the acid using in DESs for hydrogen bond donor (HBD) behave both of solvent and catalyst. at 180 °C in a microwave reactor within only 1 min, this condition achieves 76.2% of levulinic acid,

4.07% of 5-HMF, 5.57% of furfural, and 15.24% of formic acid. And the conventional heating at 150°C in 1 h, the compositions of levulinic acid, 5-HMF, furfural, and formic acid remained at 48.24%, 2.08%, 1.10%, and 9.65%, respectively.

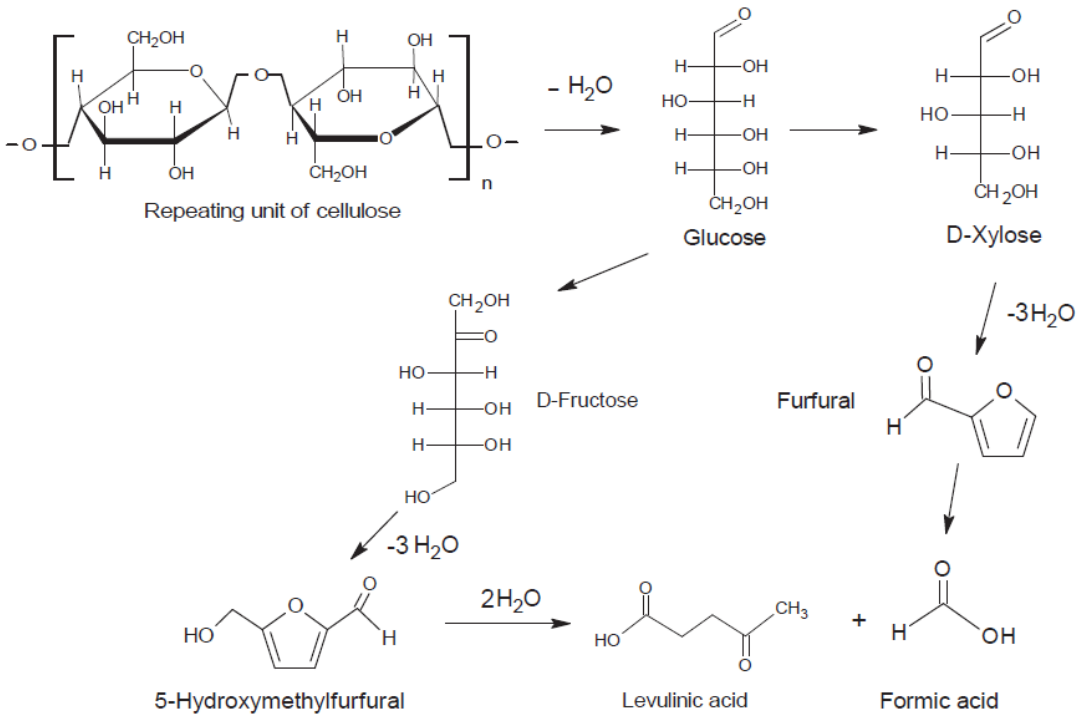

Figure 4 : The reaction mechanism of cellulose conversion., Renewable Energy, 2018, 118, 993-1000, [26]

From **Figure 4**, showing the conversion to other products of cellulose, it can be seen that cellulose also has the opportunity to change to other valuable hydrolysis products of hemicellulose, such as furfural and formic acid, etc.

And the next research, B. Girisuta et al [35], study a kinetic model of acid-catalyzed in hydrolysis process from sugar cane bagasse to levulinic acid (LA) to predict the yield of LA and the selectivity without side products. And investigate the optimum reaction conditions of this process, by varying the reaction temperature and acid concentration. The highest yield of LA was obtained at 63 mol%, at 150 °C, and 0.55 M H_2SO_4 (Acid catalyst), which equates to 194 kg of LA from 1 dry ton of sugarcane bagasse. This research shows the possible pathway of products from lignocellulosic biomass to confirm in previous research, according

to the topic. 2.3. And this research showing in **Figure 5** about furfural production formed from only xylose and arabinose, directly.

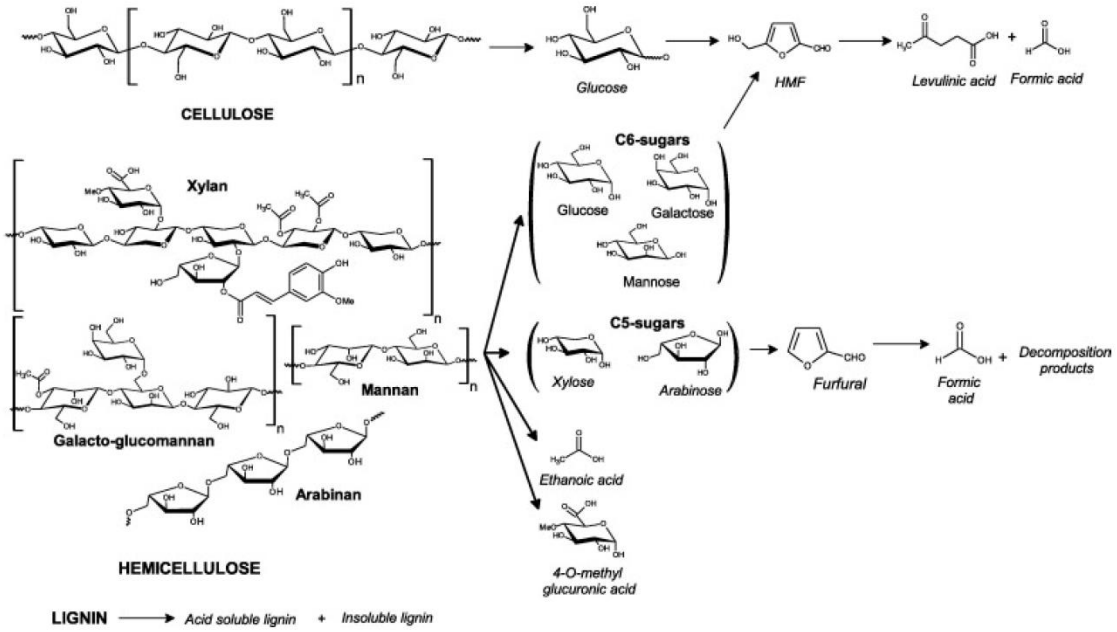

Figure 5 : Proposed pathway of acid-catalyzed hydrolysis of lignocellulosic biomass., Chemical Engineering Journal, 2013, 217, 61–70. [35]

N. W. Dulie, et al. [28]. This work is a review paper, using heterogeneous solid catalysts in furfural production. They mention using heterogeneous solid catalysts to modify the association problem of used homogeneous catalysts. Heterogeneous solid catalyst contains both of the Brønsted and Lewis acid sites for dehydration and isomerization reactions. A Lewis acid accepts electrons while Brønsted acid donates proton and Lewis acid sites can be promote furfural from xylose to xylulose, and finally xylulose to furfural path and the conversion of xylulose to furfural can be catalyzed with Brønsted acid sites. The rate of dehydration reaction and furfural product caused by the effect of Lewis/Brønsted acid site ratio. At low L/B ratio and high L/B ratio leads to form the side-reaction as the polymerization reaction, and carbonaceous by-products. An increase in acid content that affects the rate of reaction increased, but too strong acid accelerates side-reactions. The diffusional resistance by intercepting the diffusion rate caused from small pore size than xylose and furfural which the size of xylose approximates to be 0.68 nm and furfural approximates to be 0.57 nm. Larger sizes of the pore may be appropriate for furfural reorganization

into large molecules because the product inside the porous structure, has a longer residence time. And higher specific surface area advances the performance of a catalyst by increasing the accessibility of the active sites to xylose. And for other research in this review, the activities of sulfonic acid functionalized mesoporous SBA-15 material, at 160 °C, obtained 82% furfural yield and with 99% selectivity of furfural from d-xylose in water/toluene [36]. A sulfated tin ion-exchanged montmorillonite (SO_4^{2-} /Sn-MMT) in 2-Methyltetrahydrofuran (2-MTHF)/NaCl-water at 160 °C, gave a high furfural yield (79.64%) from xylose as a substrate. [37]. And other research, showing used SAPO-44 can achieve furfural 93% yield from lignocellulosic material such as wheat straw, bagasse, and rice husk [38]. They mention about used metal oxides with H_2SO_4, such as TiO_2, ZrO_2, SnO_2, and Al_2O_3 were also studied and demonstrated that it gives the highest of the conversion of xylose and furfural yield [86]. Using SO_4^{2-}/ ZrO_2– TiO_2 gave a higher yield than the zeolite catalysts [39].

2.5 One-pot conversion of biomass to furfural with solid acid catalysts

The furfural production from biomass has many ways such as using only solvents, using catalysts in medium water, or other solvents for high yield. This work is interesting in process of biomass converted to furfural with a solid acid catalyst, called “One-pot” process. Therefore, this topic mentions the researches of biomass converted to furfural with solid catalyst process and the effect in other parameters.

2.5.1 The effect of solvents

2.5.1.1 Water

The production of furfural from sugarcane bagasse using niobic acid (NbO) and niobium phosphate (NbP) in a one-step process in water, by variables temperature, the mass of catalyst, reaction time, and vibration time. This research show results, after 5 h at 150 °C, furfural, xylose, and arabinose yields were 52.1 g/kg, 69.7 g/kg, and 6.4 g/kg for NbO, respectively. And furfural, xylose, and arabinose yields were 59.3 g/kg, 147.4 g/kg, and 11.1 g/kg, respectively, when using NbP. And this research showing the yield of furfural and higher catalytic performance of NbP, because of the higher ratio of Brønsted to Lewis acid sites on its surface than NbO [11]. The routes of furfural production from sugarcane

bagasse in this research showing in **Figure 6**. Li H. et al., were studying the effects of corncob to water ratio, residence time, and reaction temperature on the performance of catalytic hydrothermal pretreatment of corncob to xylose and furfural by using a solid acid catalyst (SO_4^{2-} / TiO_2– ZrO_2 /La^{3+}). The highest furfural is 6.18 g/100 g and 6.80 g/100 g xylose when the corncob/water ratio was 10:10, 180 °C for 120 min. They reported, at a higher reaction temperature may be leading to the formation of humins and side reactions or the decomposition of product (furfural and HMF). The structure of substrate was destroyed under radical conditions and numbers of small particles. [40]. A novel core-shell sulfonated tin-loaded diatomite catalyst (SO_4^{2-}/CX-DMSn) with water as a solvent in xylose converted to furfural, the yield of furfural was 66.2% at 180°C for 5 h [41]. From research of I. Rakngam, et al., SBA-15 was stable mesoporous silica and aluminium (Al) added into the structure as catalyst (Al-SBA-15). By the Al prepared from different Al precursors were sodium aluminate (SA), aluminium sulfate (AS), and aluminium isopropoxide (AI). In the conversion of xylose to furfural, they were reported the highest yield of furfural was 63% at 170°C for 7 h and pressure 15 bar with water as solvent [42].

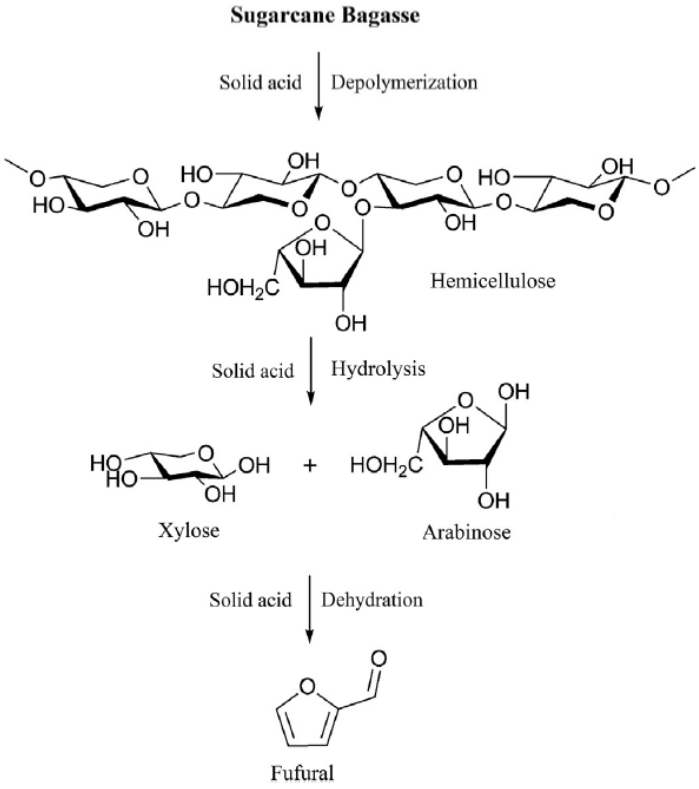

Figure 6 : General scheme of one-pot conversion of sugarcane bagasse to furfural using a solid acid catalyst., Fuel Processing Technology, 2020, 207, 106482, [11].

2.5.1.2 Other solvents

For the biphasic system, R. Sahu and P. L. Dhepe, they were study the conversion of crop waste to C_5 sugars and furfural by using solid acid catalysts in two solvent systems, as water and biphasic system. And show the yield of furfural 18% by using a solid catalyst (HUSY) in water as solvent from crop waste at 170 °C for 6 h, and using a solid catalyst in the biphasic system (water+p-xylene) gave increased yields of furfural 56% at the same condition. **Figure 7** showing the methods to produce the main product that is possible for the selective conversion of hemicellulose (without separation of other lignocellulosic material components, cellulose, and lignin) in this research. Using solid acid catalyst in aqueous, the main product is ß-D-xylose and L-arabinose. And using a solid acid catalyst in the biphasic system the main product is furfural [10]. In NaCl aqueous-toluene biphasic system with tin-loaded sulfonated diatomite (SO_4^{2-}/Sn-DM) as a solid acid catalyst in mild condition, showed a maximized furfural yield of 84.39% and 80.97% were obtained using water-soluble hemicelluloses and xylose. Q. Jia, et al., were

reported results, in the process, Cl^- from NaCl added, accelerated the isomerization of xylose and the reaction time was shorted [43]. Micro-mesoporous carbon-supported tin oxide catalyst (MC-SnOx) used in the conversion of xylose to furfural with low sodium chloride (NaCl) concentration and acid-free biphasic system. N. Zhou, et al., were achieve the highest furfural yield of 57.9% at 170 ◦C for 30 min with 2 mol/L NaCl and 0.1 g MC-SnOx were added [44].

In γ-valerolactone (GVL) solvent, Z. Xu, et al., were using a solid acid catalyst was prepared by the co-polymerization of p-toluenesulfonic acid and paraformaldehyde (PTSA-POM). Results for optimum conditions, 83.5% of furfural yield and 19.5% of HMF yield were obtained from corn stalk at 190 °C for 100 min in GVL. This work focuses on the effects of various reaction conditions including catalyst, solvent, residence time, reaction temperature, xylose loading, catalyst dosage, and water concentration on the dehydration of xylose to furfural. [45]. The sulfonation of carbonaceous material was used for preparation of carbon solid acid catalyst. Sulfonated carbon catalyst was prepared by carbonization of sucrose using 4-BDS as a sulfonating agent. Results from the experiment, 60.6% furfural yield from corn stalk was achieved in 100 min at 200 °C in GVL and furfural yield of 78.5% at 170 °C in 30 min from the dehydration of xylose [46]. To enhance the direct conversion of raw corn stover into furfural by using a novel heterogeneous strong acid catalyst (SC-CaCt-700) in different solvents. The effects of reaction temperature, residence time, catalyst loading, substrate concentration, and solvent were studied. They were report results, 93% furfural yield was obtained from 150 mg corn stover at 200 °C in 100 min using a 45 mg catalyst in GVL. Compared to, 51.5% furfural yield was achieved in aqueous media under the same conditions (200 °C, 5 h, and 45 mg catalyst) [47]. For the co-production of 5-hydroxymethylfurfural (5-HMF) and furfural from corncob via a new porous polytriphenylamine–SO_3H (SPTPA) solid acid catalyst in lactone solvents. The optimum reaction conditions, at 448 K yields of furfural (73.9%) and 5-HMF (32.3%) were achieved [48].

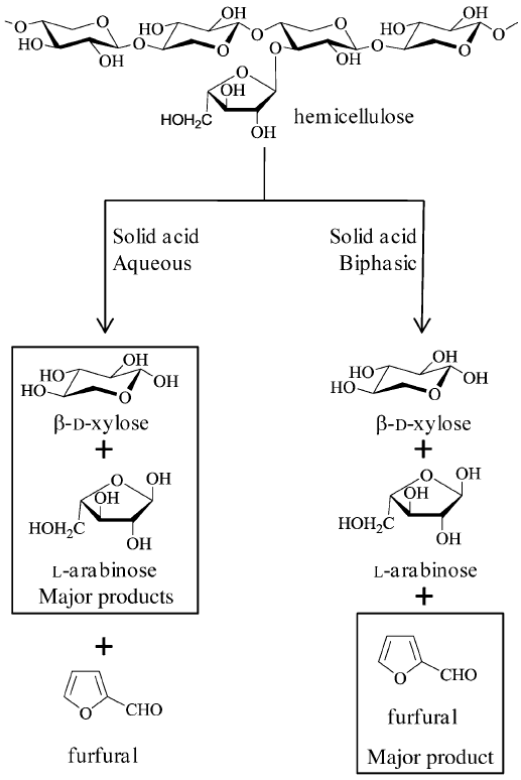

Figure 7 : Reaction for the conversion of hemicellulose by using solid acid catalysts., ChemSusChem 2012, 5, 751 – 761. [10]

In ionic liquid, $H_3PW_{12}O_{40}$, Amberlyst-15, and NKC-9 (macroporousstyrene-based sulfonic acid resin) were used as catalysts for the production of furfural from raw material as xylan, xylose, and lignocellulosic biomass in [BMIM]Cl at atmospheric pressure and under microwave irradiation. The results indicate that increasing the total acid sites of the catalysts affect to the furfural yields was increased. The total acid sites of catalysts decreased as follows: $H_3PW_{12}O_{40}$ > Amberlyst-15 > NKC-9. $H_3PW_{12}O_{40}$ at 160°C in 10 min give a high furfural yield of 93.7% from xylan, and this research, the furfural yields from substrates were lower than pure xylan and xylose at the same conditions, which could be attributed to three possible reasons. First, a network of lignin–cellulose–xylan in lignocellulosic biomass. Second, the components of biomass were more complex components. Third, the biomass components have strongly chelating groups, the formation of chelating compounds during the processing of biomass, that could make the reaction medium became aggressive to solid catalysts [49].

2.5.2 Solid acid catalysts

2.5.2.1 Active site, support, and general effect of catalysts

Metal elements could improve the formation of mesoporous structures catalyst, which increases the catalytic activity and performed the reaction medium transport. For the production of furfural, metal-doped catalysts with mesoporous structures should be an excellent carrier material. And the surface of the metal-doped on support catalyst increases the density of Brønsted acid sites and the strong acid acidity [50]. In the research from K. Sun, et al., they were used solid acidic resin (D008) and $FeCl_3$ as a catalyst (called ferric chloride modified D008) with GVL as a solvent in the conversion of xylose to furfural. When they used pure D008, the yield of furfural was 47.3%, and when $FeCl_3$ was added the yield of furfural was 65.5% [51]. SO_4^{2-}/CX-DM-Sn catalyst used in the furfural production from the report of D. Cai et al., they were used different DM derived materials, including DM, DMSn, CX-DMSn, SO_4^{2-}/CX-DM, SO_4^{2-}/DMSn, and SO_4^{2-}/CX-DMSn as catalysts. From the results, DMSn and DM were higher yields of furfural than other catalysts, but the furfural selectivity of DMSn and DM was lower than without catalyst. The effect of the inner Sn layer of SO_4^{2-}/CX-DMSn, when using SO_4^{2-}/CX-DM the furfural yield was lower than that using SO_4^{2-}/CX-DMSn. This result demonstrated that the Brønsted acid sites in SO_4^{2-}/CX-DM catalyzed the furfural production and avoid the catalyzed side reactions by Lewis acids [41]. The overloading of catalysts would lead to forming the side reactions such as fragmentation, resinification, and condensation, which limits the yield of products. By the fragmentation of furfural, as the formation of lactic and formic acids and the aldehydes such as formaldehyde, glyceraldehyde, glycolaldehyde, acetaldehyde, and pyruvaldehyde reported by N.W. Dulie, et al. [52].

2.5.2.2 Structural of catalysts

The mesoporous structures were productive for interaction between the reactive species and catalytic active phases, which could improve the catalytic activity in the conversions of biomass. There were confirmed by X.Li, et al., they were used sulfonated carbon microspheres (C-Co-S) as a catalyst, and they were reporting, the mesoporous structures of C-Co-S could improve the mass transfer of the furfural production [50]. For used the micro-mesoporous carbon-supported tin oxide catalyst (MC-SnO_x), the transformation of microstructure can explain the catalytic effect

distinction and from the XRD, prove the Sn added in MC-SnO_x was formed. The increase of annealing temperature in the preparation of catalysts affect to the crystallite of SnO_2 and Sn grow up. The growth of the crystallite means that the Sn concentration was distributed, which could reduce the effective contact area of the catalysts. From the results, C and CO were reacted with Sn^{4+} and lower valence species that is Sn^0, from the transformation of Sn^{4+}, and that is reductive substances, produced during the annealing process. The lower valence of Sn species was volatilized and cause of the decreasing of Sn surface content. However, found that the catalyst performance caused from a reduction reaction between tin oxide and carbon-based support in the annealing process. And noting that when the other carbon-supported metal oxide catalysts were synthesis, the reduction reactions was occured. [44]. From research of I. Rakngam, et al., SBA-15 was stable mesoporous silica, and aluminium (Al) added into the structure, acid sites were generated for catalysis. The generation of Al species define the meso-structure composites with different arrangements and geometry, the obtained catalyst samples could work as effective catalysts to encourage the furfural production from xylose [42].

2.5.2.3 Acidity of catalysts

The mechanism of Brønsted acid sites (BAS) and Lewis acid sites (LAS). In the general, the mechanism of xylose converted to furfural is well studied, xylose is isomerized by Lewis acid into xylulose and then dehydrated by Brønsted acid to formed furfural [11, 43, 44, 50, 51]. And I. Rakngam, et al., they were reported the furfural yield depends on the relative ratios of Lewis to Brønsted acid sites [42]. For example research from X.Li, et al. [50], showed in **Figure 8**, and in research from L. Zhang, et al., the Brønsted to Lewis acid ratios of the three catalysts followed the order: Amberlyst-15 > NKC-9 > $H_3PW_{12}O_{40}$. They were reported, a high number of Lewis acid sites catalyst was active in the production of furfural, and the Brønsted acid site that affect to the furfural selectivity, the selectivity of furfural was easied caused by a high ratio of the Brønsted to Lewis acid site. The Brønsted and Lewis sites were both catalyze the dehydration of xylose into furfural and the degradation of furfural to humins, and especially, the decreasing of furfural selectivity because the Lewis sites can explain the decomposition of xylose and the reaction between xylose and furfural. [49]. M. N. Catrinck, et al. [11],

study the production of furfural from sugarcane bagasse by using a solid acid catalyst as niobic acid (NbO) and niobium phosphate (NbP) in water, they report NbP have a high catalytic performance, because NbP have a higher ratio of Brønsted to Lewis acid sites on surface than NbO. And they report about the mechanism of furfural production, the xylose converted to xylulose and converted to furfural, this step is faster than the direct xylose converted to furfural. While the Brønsted acid sites (BAS) can help the dehydration of xylose to furfural, the Lewis acid sites (LAS) shift the reaction route to isomerized xylose to xylulose, and then BAS catalyze the dehydrate xylulose to furfural. However, the side reactions were performed when the acid site density and acidity were excess, including degradation of furfural, condensation between furfural and intermediates product, resinification, that caused the furfural was loss [50]. In used SO_4^{2-}/CX-DM-Sn as a catalyst from the research of D. Cai, et al., to develop the Brønsted acid of catalyst with -SO_3H groupsHence, the unification between Brønsted acid and hydrophobic carbon layer and the fixation of Lewis acid proves good potential in the production of furfural in water. And Lewis acid sites promote the side-reaction of humins, that explain the decreasing of the furfural selectivity [41]. For chitin/Ag co-modified $H_3PW_{12}O_{40}$ composites (Chx-AgPW) as a catalyst in the H_2O/MIBK for production of furans from carbohydrates and biomass. In the report of F. Lai, et al., the dehydration to furans and the depolymerization of biomass were promoted by the Brønsted acid sites from $H_2[PW_{12}O_{40}]^-$ anion [53].

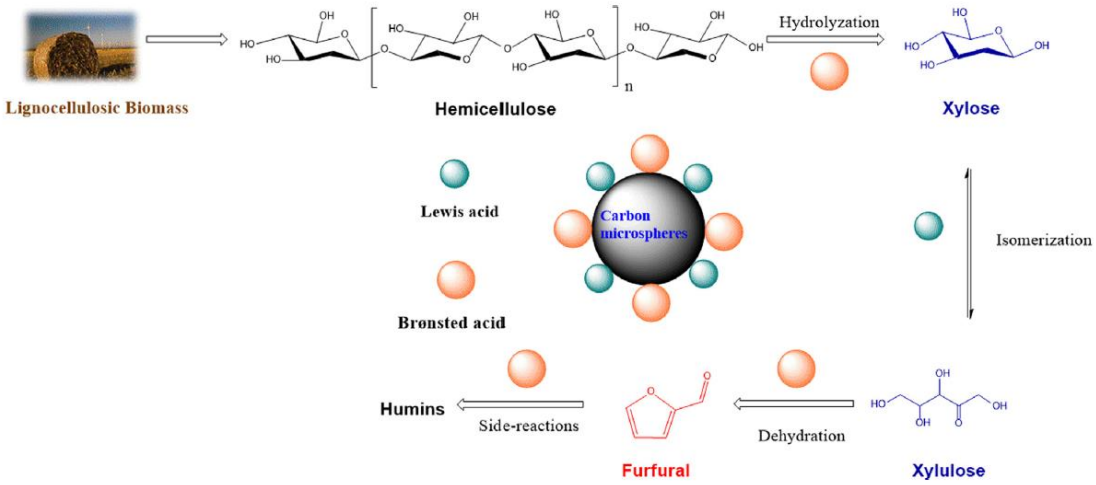

Figure 8 : The proposed reaction pathways for the transformation of lignocellulosic biomass to furfural over C-Co-S catalyst., Waste Management, 2020, 108, 119–126 [50].

2.6 Alumina (Al_2O_3)

Supported metal oxides were studied widely to control the catalytic properties and the structure of the surface of metal oxides, with different precursors, calcination temperatures, and supports [54]. For this research was cite the mechanism of biomass converted to furfural from Catrinck, M.N., et al (2020) [11] (**Figure 6**). The whole process starts from the conversion of biomass to hemicellulose, converted to xylose and arabinose, and finally converted to furfural, each process required the efficient conversion, one of the properties crucial to the conversion of biomass to furfural was the acidity. Several previous studies have indicated that Brønsted and Lewis's acid-base theory affects the processes described above [11, 28]. Therefore, for this research, the solid acid heterogeneous catalyst was selected, with Al_2O_3 as the support. In addition to the acidity properties, Al_2O_3 support has other properties, which is beneficial to the furfural production, for example, having a high surface area [12, 13], helps the metal to be added to dispersed well (Compared to silica (SiO_2)) [14], etc. However, the other properties will be discussed next.

The specific surface area of 220 m^2/g of Al_2O_3 for calcination temperature at 600°C was achieved γ-Al_2O_3 and aluminum oxide is a solid Lewis acid [12]. The acidity of Al_2O_3 is 110 μmol/m^2 of Lewis acid site and Brønsted acid site ≈ 47 μmol/m^2. And specific surface area of

146 m^2/g was achieved by M. Saito, et al. [54]. For Solution combustion synthesis (SCS), at $\Phi < 1$, mesoporous alumina (pore size ≈ 3.5 nm) is formed with a specific surface area as high and at low pH, the amorphous alumina formed and Al_2O_3 is inert ceramic support allows for produce highly dispersed metal nanoparticles by SCS. [15]. The fructose dehydration to 5-HMF in a biphasic system by using solid acid catalysts, they report about the Brønsted and Lewis acidity of Al_2O_3 by Py adsorption, 135 μmol/g of Lewis acid site of Al_2O_3 achieved. And in the report, Al_2O_3 was very weak of Brønsted acid (it was not detected). Therefore, it's confirmed to Al_2O_3 is the strong Lewis acid site [16, 17]. L. Gong, et al., used SO_4^{2-}/SnO_2- Al_2O_3-CFA (coal fly ash) as catalyst was achieved furfural yield of 84.7% was achieved in the NH_4Cl-toluene biphasic system, from the report, doping a small amount of Al_2O_3, could inhibit SnO_2 crystallized and the growth of SnO_2 grains, and thus enhanced the catalytic activity [55].

2.7 Metal-promoted alumina catalyst

2.7.1 Tungsten-promoted alumina catalyst (W-Al_2O_3) and the effect of tungsten

M. Saito, et al., they were study the effects of alumina-based supports on the structure (Al_2O_3, Al_2O_3–TiO_2, Al_2O_3–ZrO_2, SiO_2–Al_2O_3, and SiO_2) and acid properties of supported tungsten oxide catalysts (WO_3/Al_2O_3). They were prepared catalysts by the sol-gel method and show the maximum Brønsted acid at 20 wt% of WO_3/Al_2O_3 was achieved. At 20 wt% of WO_3/Al_2O_3 was achieve 115 m^2/g for specific surface area. And they were reporting about Brønsted acid sites, might be generated at tungsten oxide monolayer domain boundaries. [54]. The various WO_3 contents indicating different acidic sites confirmed that the ratio of acidic to basic sites of the catalyst was the key parameter affecting selectivity by László T. Mika, et al. [25]. WO_3/Al_2O_3 are synthesized using a facile hydrothermal method followed by calcination and various WO_3/Al_2O_3 ratio 1/10, 5/10, and 10/10. When increasing WO_3, the specific surface area and pore volume were decreased but the yield of products was increased [13]. The Brønsted and Lewis acidity of WO_3, that tungstite exhibits weak Brønsted acidity. It has 6.8 μmol/g of Brønsted acid site and 10.2 μmol/g of Lewis acid site. [56].

2.7.2 Cerium-promoted alumina catalyst (Ce-Al_2O_3) and the effect of cerium

The acidity of Ceria, was both Brønsted and Lewis acid on ceria surface. And specific surface area of ceria was 81 m^2/g (Calcined at 600°C). [57]. The ceria−alumina catalyst was prepared by the SCS process. It was in crystalline form and a low specific surface area was found for ceria−alumina [15]. The study of Cerium loading supported on Al_2O_3 was prepared by a basic precipitation route. Cerium was good dispersion over the surface of the Al_2O_3 support. And for the 5 %Ce-Al and 10 %Ce-Al, as a strong interaction with the Al_2O_3 [18]. For hydrothermal stability and doping, Ce could improve the ability of the catalyst to hydrothermal aging and against the water vapor effect. [19-21]

2.7.3 Iron-promoted alumina catalyst (Fe-Al_2O_3) and the effect iron

The study of Fe_2O_3 supported on Al_2O_3 and SiO_2 catalysts were prepared by an incipient wetness impregnation technique. They mention the dispersion of Fe_2O_3 on both support catalysts, the dispersion of iron on the surface of silica is less than on the surface of alumina. From the SEM image, particles of iron oxide supported on the silica are on average larger in diameter when compared to those on the alumina support. Results from TEM, confirmed agglomerated and larger particle sizes of iron oxide on the surface of silica support. Acidity, on the surface of alumina was measured higher density of acid sites and acid site concentration, than on the surface of silica. And data from BET of iron oxide on alumina, specific surface area, BJH adsorption pore volume, BJH average pore diameter is 168 m^2/g, 0.42 cm^2/g, and 9.4 nm, respectively. [14]. The Fe_2O_3/HY catalyst used for Friedel–Crafts acylation of m-xylene with benzoyl chloride. They report about the Brønsted and Lewis acid of Fe_2O_3, the Brønsted acid site of the HY catalyst decreased but the Lewis acid site increased with Fe_2O_3 added to the HY catalyst. That confirms, the Fe_2O_3 has a Lewis acid site than the Brønsted acid site. And this research showing the effect of Fe_2O_3 load in $Fe_2O_3$3/HY, the conversion of benzoyl chloride increased rapidly when the Fe_2O_3 loading increased from 10 to 15 wt.%. With the Fe_2O_3 loading increased, Lewis acidic sites increase, led to enhance the activity of Fe_2O_3/HY. But when the load increased to 20 wt.%, the conversion of benzoyl chloride displayed a slight drop as compared to 15 wt.% loadings at the same reaction conditions. [22]

2.8 Sulfated metals catalyst

As mentioned in previous topics, for the process of biomass converted to furfural, the acidity was needed to help the formation of products at each step, both of Brønsted and Lewis acid. It can be seen that in the catalyst to be used in the research, both types of acidity were present. For the development of more catalyst activities in this research, it was interesting to develop a catalyst by adding sulfated to the metal catalyst for catalytic properties, such as acid sites on the surface area of metals catalyst. The addition of sulfated was expected to enhance the yield of furfural in the process of biomass converted to furfural.

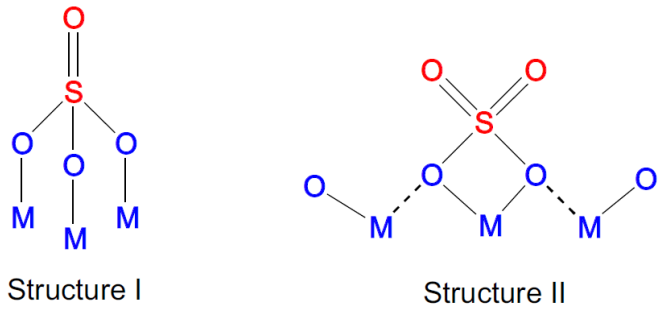

Figure 9 : Triply bridging sulfate (I) and bridged bidentate sulfate(II)., Arabian Journal of Chemistry, 2016, 9, 550–573 [58].

The reviews of R. Varala, et al., and H. A. Khalaf, et al., confirmed the presence of the sulfate group from FT-IR results. In general, the sulfated structure included the triply bridging sulfate and bridged bidentate sulfate (in **Figure 9**) [58, 59]. G. A. H. Mekhemer, et al., were studying the sulfated added to alumina by various the SO_4^{2-} content to 3, 6, and 10 wt.%. The results confirm that the presence of sulfated species of more than 3 wt.% generates Brønsted acid sites and at least of Lewis acid sites [60]. And Lewis acid sites on sulfated catalyst were stronger than those exposed on pure alumina. The structure between sulfate and metal oxide showed in **Figure 10** (SO_4^{2-} and SnO_2). And it was considered that the Brønsted acid sites and the Lewis acid sites present on the SO_4^{2-}/SnO2 catalyst surface could function as active sites independently [58].

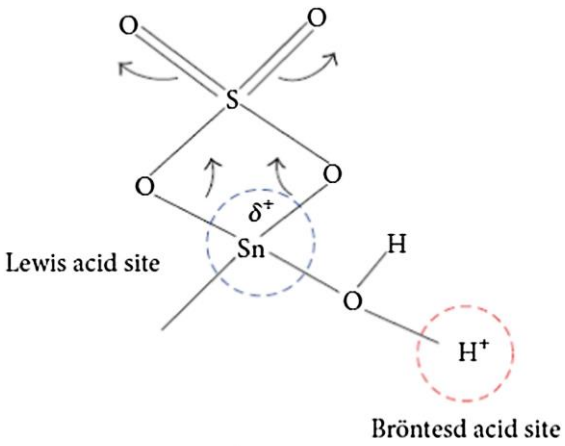

Figure 10 : Lewis and Bronsted acid sites, Arabian Journal of Chemistry, 2016, 9, 550–573 [58].

2.9 Preparation catalyst

2.9.1 Solution combustion synthesis (SCS)

The preparation catalyst using solution combustion synthesis (SCS). Most of this method for nanoscale materials synthesis was invented in the 1980s. For SCS method, the reaction component consists of metal precursor (solution), fuel (C, H), and oxidizer (e.g., O). When the components are complete, they will cause thermal decomposition and combustion. In the occurrence of the decompose reaction in the air at a relatively low temperature and combustion. Due to their exothermic and autocatalytic features, can proceed in a self-sustained thermal. And without any additional external energy input. While synthesis causes a large of gaseous products. In which a large amount of gas causes the expansion to solid (metal) oxides and. While after the reaction, the temperature drops quickly, making the solid product is porous and finely dispersed [15]. Generally, the solution combustion synthesis consists of three main steps which are (1) formation of the combustion mixture (2) formation of the gel (3) combustion of the gel, as shown in **Figure 11**. The formation of large quantities of these gaseous byproducts from Flaming reactions such as NO, NO_2, NH_3, CO, CO_2, etc., will affect the distinctive properties of the catalyst. The properties depend on synthesis parameters such as the fuel type, (the reducers or fuel)-to-oxidizers ratio (Φ), the fuel-to-metal cations ratio (F/M), and many other parameters [61]. So many of these factors have been studied in many of researches.

For combustion synthesis reactions are highly exothermic self-sustaining without additional energy. Duo to combustion reaction was fast and completed in a few seconds, it was being assumed as an adiabatic process. The features are controlled through the enthalpy of combustion and flame temperature resulting from fuel and oxidizer. In testing fuel types, the amount of fuel was determined by the fuel-to-oxidant ratio (Φ=1 or stoichiometric balance). In conclusion, when using urea as fuel at the higher surface area, higher dispersion, and lower nickel particle size in comparison with using the other fuels. The combustion with urea as fuel is instead by a moderate increment of temperature, before the light-off of the combustion reaction, with a more controlled release of gases and subsequent dissipation of heat. And less voluminous powders compared to other fuels that violent combustion with high temperature causes the spread of heat throughout, resulting in voluminous powders. Therefore, the choice of the fuel is important, because it determines the exothermicity of the redox reaction and, consequently, the properties of the resulting powder [62]. The fuel-to-oxidizer ratio (Φ) is divided into 3 main stages: fuel-lean (Φ<1), fuel-rich (Φ>1), and stoichiometrically balanced (Φ=1). The fuel-to-oxidizer ratio is used in the stoichiometric equations by defining Φ in the equation [63]. The results of the types parameter have different effects on the temperature, type, or amount of gas released, which affects the structure depending on the selection, but the result of the fuel-to-oxidizer ratio is different [57]. W. Kang, et al. [23]. They studied have varied the fuel-to-oxidizer ratio (Φ, 0.5−3). When increasing the ratio of fuel-to-oxidizer, the adiabatic temperature and maximum temperature increase to maximum value after that will be decreased significantly. In which temperature increases came from increasing fuel. And decrease in temperature due to the dilution of the oxidizer in precursor solution resulting in incomplete combustion. The effect of temperature will affect the generating gas and the properties of the catalyst such as darker colors from black carbon, pore-volume, crystallite size, and surface area, etc. When using different fuels in SCS, the maximum value of the fuel-to-oxidizer will be different. Because different energy values or changes to other forms before combustion is sufficient for the combustible mixture, fuel-rich or lean needs to affect the property of catalyst. And the most of fuels for SCS in other research, urea and glycine are known to be among the most popular fuels for synthesizing highly uniform oxide ceramic powders [64].

The reaction for catalyst preparation in SCS is as follows [15].

(1) Combustion reaction (Urea)

$$nNH_2CONH_2 + 2nO_2 \rightarrow nN_2 + nCO_2 + 2nH_2O$$

(2) Redox reaction

$$Me^v(NO_3)_v \rightarrow Me^vO_{2/v} + vN_2 + 3v/2O_2$$

(3) Solution combustion synthesis

$$Me^v(NO_3)_v + 3\varphi/4vNH_2CONH_2 + 3v/2(\varphi-1)O_2 \rightarrow Me^vO_{2/v} + (v+3\varphi/4v)N_2 + 3\varphi/4vCO_2 + 3\varphi/2vH_2O$$

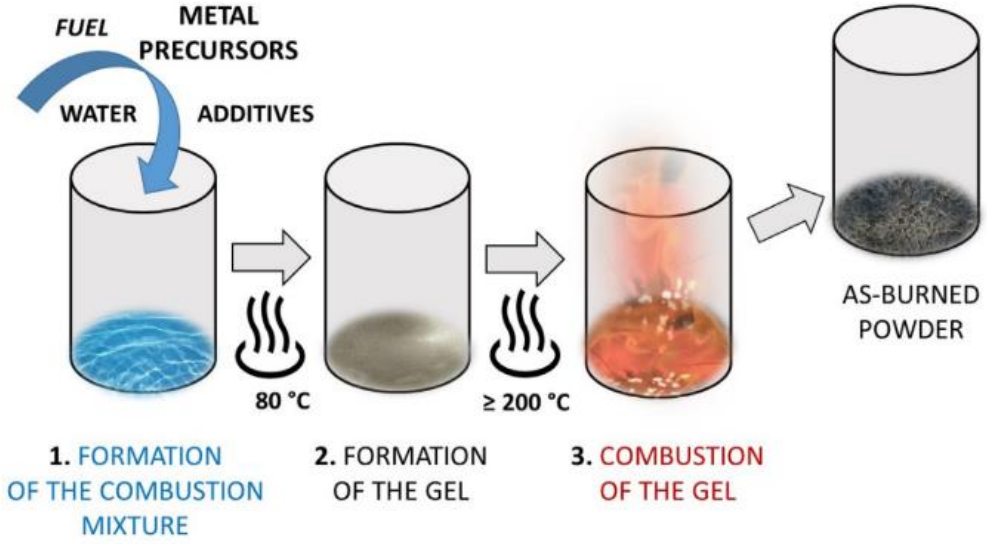

Figure 11 : Schematic description of the three main steps in SCS., Progress in Crystal Growth and Characterization of Materials, 2018, 64, 23–61, [61].

Chapter III
Methodology

In the experiment, which will be used chemicals in different experiments like in preparation characterization and reaction, which can be viewed from **Table 4**, **Table 5**, and **Table 6**, respectively.

3.1 Chemicals

Table 4 Chemicals of preparation.

Name	**Chemicals**	**Formula**	**Grade %**
Aluminium	Aluminium nitrate 9-hydrate	$Al(NO_3)_3$•9H2O	98
Tungsten	Ammonium metatungstate hydrate	$H_{26}N_6O_{40}W_{12}$ •xH_2O	85
Iron	Iron (III) nitrate	$Fe(NO_3)_3$•9H2O	98
Cerium	Cerium (III) nitrate hexahydrate	$Ce(NO_3)_3$•6H_2O	99
Urea	Urea crystalline	NH_2CONH_2	99
Water	Deionized water	H_2O	-
Sulfated	Ammonium sulfate	$(NH_4)_2SO_4$	99

Table 5 Chemicals of characterization.

Name	**Chemicals**	**Formula**	**Grade %**
Liquid nitrogen	Liquid nitrogen	LN_2	100
Nitrogen gas	Nitrogen	N_2	99.99
Helium gas	Helium	He	99.99
Ammonia gas	Ammonia	NH_3	99.99
Sodium hydroxide	Sodium hydroxide	NaOH	99
Hydrochloric acid	Hydrochloric	HCl	37

Table 6 Chemicals of reaction.

Name	**Chemicals**	**Formula**	**Grade %**
Water	Deionized water	H_2O	-

3.2 Catalyst preparation

3.2.1 Preparation of unpromoted Al_2O_3, WO_3-Al_2O_3, CeO_2-Al_2O_3, and Fe_2O_3-Al_2O_3

In the catalyst preparation of tungsten, cerium and iron-promoted alumina were prepared by solution combustion synthesis (SCS). Ammonium metatungstate hydrate/Aluminium nitrate 9-hydrate, Cerium (III) nitrate hexahydrate/Aluminium nitrate 9-hydrate, and Iron (III) nitrate /Aluminium nitrate 9-hydrate mixed. And add urea as fuel, then solute by DI water. The solution was prepared by various wt.% of metal oxide (1, 5, 10, 20 wt.%) with a 0.8 fuel/oxidizer ratio. After that, the solution was stirred at room temperature for 1 h. Then, the solution was placed in a pre-heated furnace at 400 °C until the combustion was completed, cooled down to room temperature, and calcined at 600 °C for 6 h with a heating rate of 10 °C/min.

3.2.2 Preparation of SO_4^{2-}/MOx^a-Al_2O_3

In the catalyst preparation of sulfated metal-promoted alumina was prepared by impregnation method. The metal-promoted alumina and an aqueous solution of $(NH_4)_2SO_4$ were mixed by various wt.% of SO_4^{2-} (5, 10, and 15 wt.%). After that, the catalyst was dried in an oven overnight at 110 °C, and calcined at 600 °C for 3 h, with a heating rate of 10 °C/min.

3.3 Catalyst reaction

For the sugarcane leaves (SCL) converted to furfural, the reaction used 1 g of SCL, 0.1 g of catalysts, and 20 ml of DI water. The reaction was run in batch-type stainless-steel autoclave with a magnetic stirrer at 170 °C and 10 bars of N_2 for 0.5, 1, 2 and 5 h. Then, the reaction was stopped by cold water and 50 ml of deionized water was added to wash the solid from the reactor. Finally, the solid was separated from the liquid with filter paper and the liquid was taken to HPLC for analysis products.

3.4 Catalyst characterization and analysis products

3.4.1 X-ray diffraction (XRD)

The XRD measurement was used to determine the bulk crystalline phases of the catalysts sample. The XRD patterns were recorded by SIEMENS D-5000 in the range 2θ from 20° to 80° with Cu Kα using the conditions of 30 kV and 20 mA. The crystallite sizes were determined from XRD data using the Scherer equation.

3.4.2 Temperature-programmed desorption of ammonia (NH_3 -TPD)

Temperature-programmed desorption of ammonia (NH_3 -TPD) was used to detect the acidity of the catalyst. The catalysts were installed to the adsorption part for pretreatment in 25 ml/min of Helium gas for hours at 485.15 K to remove moisture on the surface area of catalysts and cool down at ambient temperature. Then ammonia gas flowed in 25 ml/min for 1 hour to catalysts to adsorb gas. After the absorption, the ammonia gas was desorbed by heating at 823.15 K for 1 hour.

3.4.3 The titration

The titration was used to detect the acidity (Brønsted acid sites) of the catalyst, 0.1 g of catalyst was stirred with 20 ml of 0.01 M NaOH at room temperature for 6 h. Finally, the solution was separated, and the liquid was titrated with 0.01 M HCl to find the Brønsted acid sites which were absorbed by the catalyst.

3.4.4 Scanning electron microscopy (SEM)

Scanning electron microscopy (SEM) was used to focus the beam of high-energy electrons to generate a variety of signals at the surface of catalysts specimens.
The morphology of the catalysts powder were observed by field emission scanning electron microscopy (Mira 3, TESCAN) just after coating with Ag.

3.4.5 Nitrogen physisorption

N_2 physisorption was used to determine the BET surface area of the catalyst, the average pore size diameter, and the pore size distribution using BELSORP MINI II. The BET surface areas were calculated in the range of 0.05–0.3 P/P_0 [13]. The catalysts were firstly pretreated in helium gas flow of 50 ml/min at 180 °C for 3 h. Sample pretreatment for remove water bound to the particle surface. After cooled down to the ambient temperature, the weight of the dried sample was collected. The sample cell was installed on the adsorption part, which contained liquid nitrogen in the Dewar. The volume of N_2 was measured at a different partial pressure of N_2 at -196 °C.

3.4.6 High-performance liquid chromatography (HPLC)

HPLC was used to analyze the components such as organic component, bio component, polymer, etc. molecule that used for sampling to analyze must be 100 % soluble solid or liquid state. The component separation will be succeeded if the compound has a different rate of diffusion in the column. The separated component will move along the length of the column by the mobile phase. The concentration of the product and all of the byproducts were quantified using HPLC with reflective index and UV in wavelength 195 nm for detect sugar, 254 nm for detect acid, and the product using column Aminex-87H (BioRad), 8 µm, and using 0.005 M H_2SO_4 as a mobile phase.

Chapter IV
Results and Discussion

This chapter shows the results of catalyst characterization, the products analysis and discusses the effect of tungsten loading and the effect of reaction time.

4.1 Tungsten-promoted alumina (WO_3-Al_2O_3)

4.1.1 XRD

The structural analysis of tungsten-promoted alumina from XRD indicated that amorphous tungsten was formed with alumina **Figure 12**, showed that the catalysts derived by SCS were γ-phase alumina at 2θ of 36.9˚, 45.4˚ and 66.7˚ [13, 54]. The reduction of the peak intensity of the γ-alumina when loading tungsten was increased, which suggested the highly dispersed on the alumina surface of tungsten. The report by Guntida was consistent with the results, the peak intensity of the crystalline phase of tungsten was increased with the increment of tungsten loading. This indicated that higher tungsten loading showed a higher aggregation of tungsten [65].

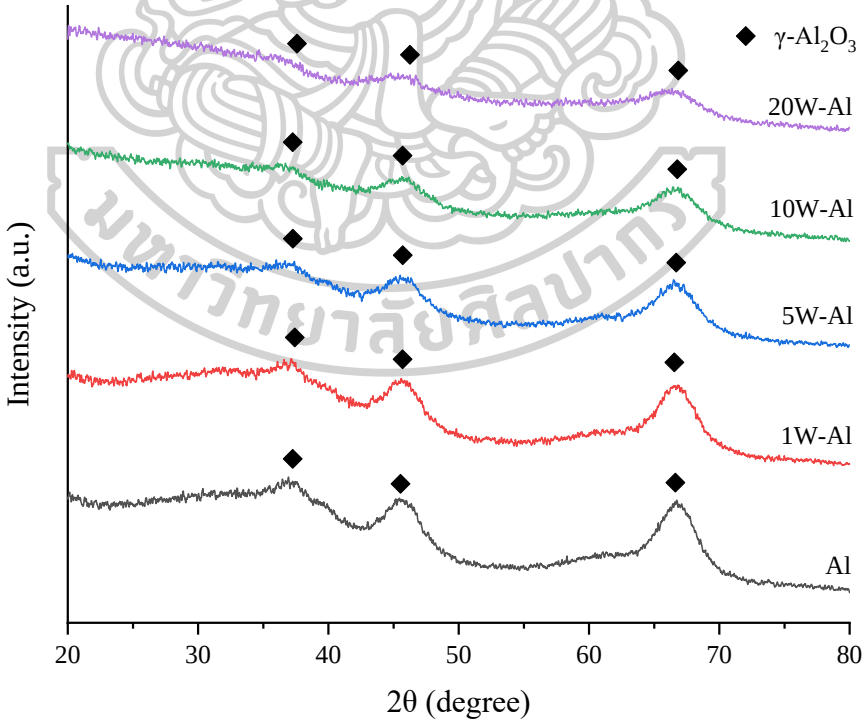

Figure 12 : The XRD patterns of tungsten-promoted alumina series.

4.1.2 Nitrogen physisorption

Table 7 showed the results of nitrogen physisorption including the Brunauer−Emmett−Teller (BET) surface area (m^2/g), pore volume (cm^3/g), and average pore size (nm). The specific surface area of catalysts increased with increasing tungsten loadings. The highest at 272 m^2/g of 20 wt.% tungsten was obtained. The high specific surface area of all catalysts was obtained even after the calcination at 600 °C for 6 h, which may mean that the synthesized tungsten-promoted alumina had very high thermal stability which can occur from thick pore walls. The pore volume increased from 0.24 cm^3/g of unpromoted alumina to 0.31 cm^3/g when increasing loading of tungsten 1, 5, and 10 but decreased to 0.28 cm^3/g when loading at 20 wt.% tungsten. The decrease of alumina in 20W-Al may be the main reason for the hollow structure, leading to the pore of catalyst collapses during the calcination at high temperatures. The average pore size decreased with increasing tungsten loadings, which may be due to the difference in the dimensionality of molecules of alumina and tungsten [13].

Table 7 Properties of tungsten-promoted alumina catalysts.

Catalyst	**S_{BET} (m^2/g)**	**Pore volume (cm^3/g)**	**Average pore size (nm)**
Al	189	0.24	5.0
1W-Al	249	0.31	5.0
5W-Al	253	0.31	4.9
10W-Al	270	0.31	4.6
20W-Al	272	0.28	4.1

4.1.3 NH_3 -TPD

The acidity of catalysts showed the comparison of unpromoted alumina (Al) and tungsten-promoted alumina by NH_3-TPD **Figure 13**. **Figure 14** showed the deconvolution of NH_3-TPD results. **Table 8** showed acidity calculated from deconvolution peaks to compare unpromoted alumina and tungsten-promoted alumina. The NH_3-TPD profile of γ-Al_2O_3 consists of three peaks approximately 150, 250, and 490 °C synonymous with the weak, medium, and strong acid sites, respectively [66]. These results show that the adsorbed NH_3 molecules on the surface of 1W-Al catalysts can be removed more easily than on Al at low, medium, and high temperatures. Otherwise, the addition of 1 wt.% tungsten into γ-Al_2O_3, decreases the acid sites. For the 5W-Al catalyst, the adsorbed NH_3 molecules can be removed easied than on Al at high temperature but opposite at low temperature, which means the addition of 5 wt.% tungsten into γ-Al_2O_3, increases weak acid sites but decreases strong acid sites, and at medium acid sites nearby with Al. For other catalysts, for 10W-Al, when tungsten was added into γ-Al_2O_3, weak, medium, and strong acid sites were increased. But in 20W-Al, the weak and medium acid sites were increased and highest but it has the lowest strong acid sites.

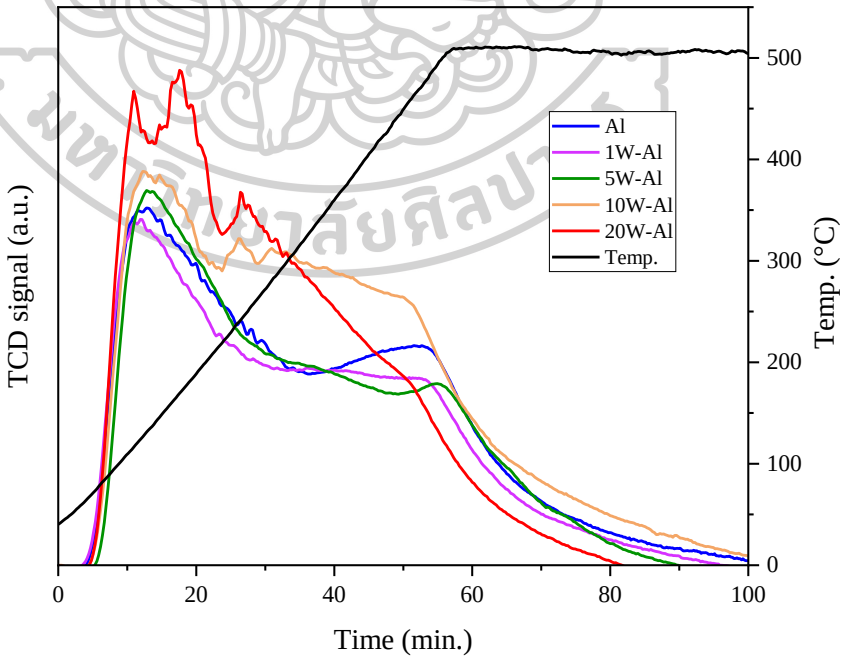

Figure 13 : NH_3-TPD profiles of unpromoted alumina (Al), and tungsten-promoted alumina series.

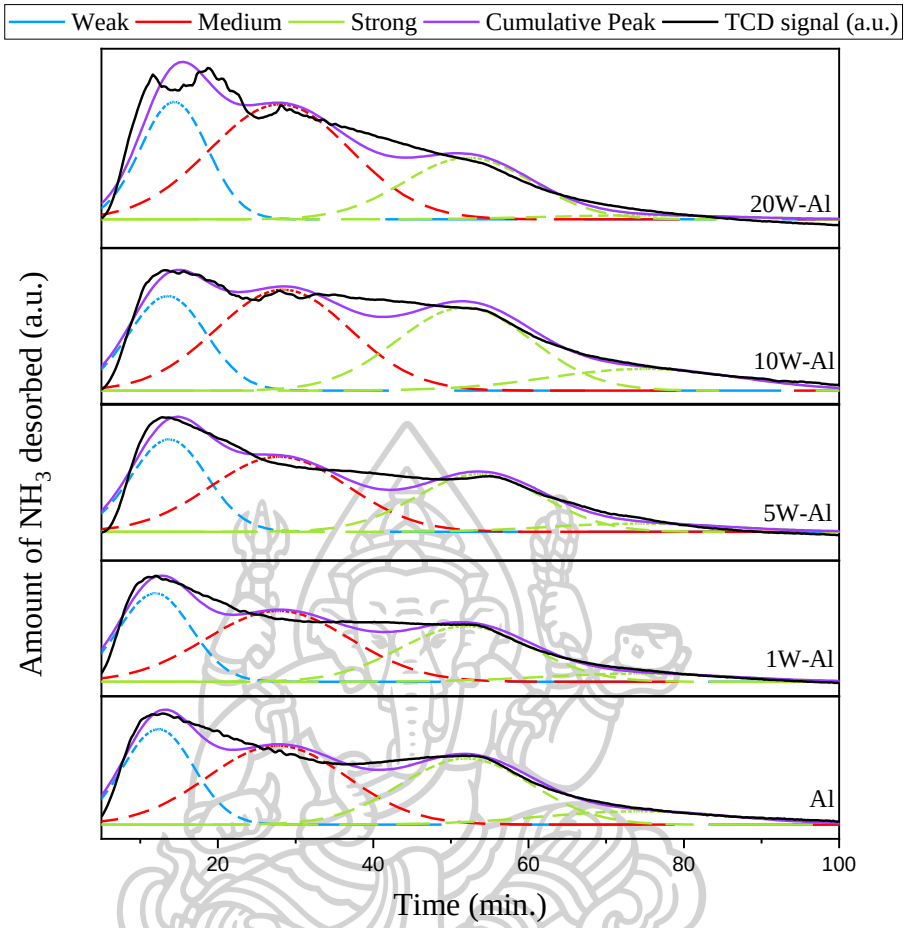

Figure 14 : Deconvolution of NH_3-TPD profiles of unpromoted alumina (Al), and tungsten-promoted alumina series.

Table 8 The acidity of tungsten-promoted alumina catalysts.

Catalyst	Weak (mmol/g)	Medium (mmol/g)	Strong (mmol/g)	Total (mmol/g)	Brønsted (mmol/g)
Al	0.18	0.3	0.31	0.79	0.25
1W-Al	0.17	0.28	0.24	0.69	0.27
5W-Al	0.19	0.28	0.24	0.71	0.47
10W-Al	0.2	0.37	0.42	0.99	0.57
20W-Al	0.22	0.44	0.24	0.9	1.69

The effect of tungsten loading on the Brønsted-Lewis acid sites had shown in **Table 8**. M. Saito reported that, Brønsted acid sites were generated by tungsten oxide monolayer at the boundaries between the WO_3 domains and Al_2O_3. The Brønsted acid site on the amorphous WO_3 is related to the support properties and surface area of support. Thus, the amorphous tungsten oxide is the source of the Brønsted acid sites. They were shown the relationship between surface hydroxyl groups density and the Lewis acid density on the Brønsted acid density. Al_2O_3 supported WO_3 catalysts showed a high Lewis acid density and a high Brønsted acidity. These results show that the high density of Lewis acids has an keys role in the generation of Brønsted acid site when the support is loading by WO3, and Al2O3 with a high surface hydroxyl groups density and Lewis acid density that affect to high Brønsted acid density. These results propose that a high density of the surface hydroxyl groups and the Lewis acid are significant for the amorphous tungsten oxide monolayer domains formed, which the generation of Brønsted acid sites. [54].

However, the report by Guntida discusses the Lewis acid transformation to new Brønsted acid sites occurred when a process engages with metal, and hydrogen accessibility on tungsten oxide directly affected the transformation of Lewis acid sites to new Brønsted acid sites on its surface. That means the increase of Brønsted acid sites of catalysts in this work may be led by the Lewis acid transformation to new Brønsted acid sites [65].

4.1.4 SEM

The morphology and surface structures of the tungsten-promoted alumina series were analyzed with SEM. The comparison of SEM images (**Figure 15)** indicated a negligible change in the morphology of the catalysts. The particle of catalysts was mostly spherical but these small particles aggregated uniform for all catalysts. This was found that the catalysts were synthesized by using urea as a fuel, successfully in nanoscale [67].

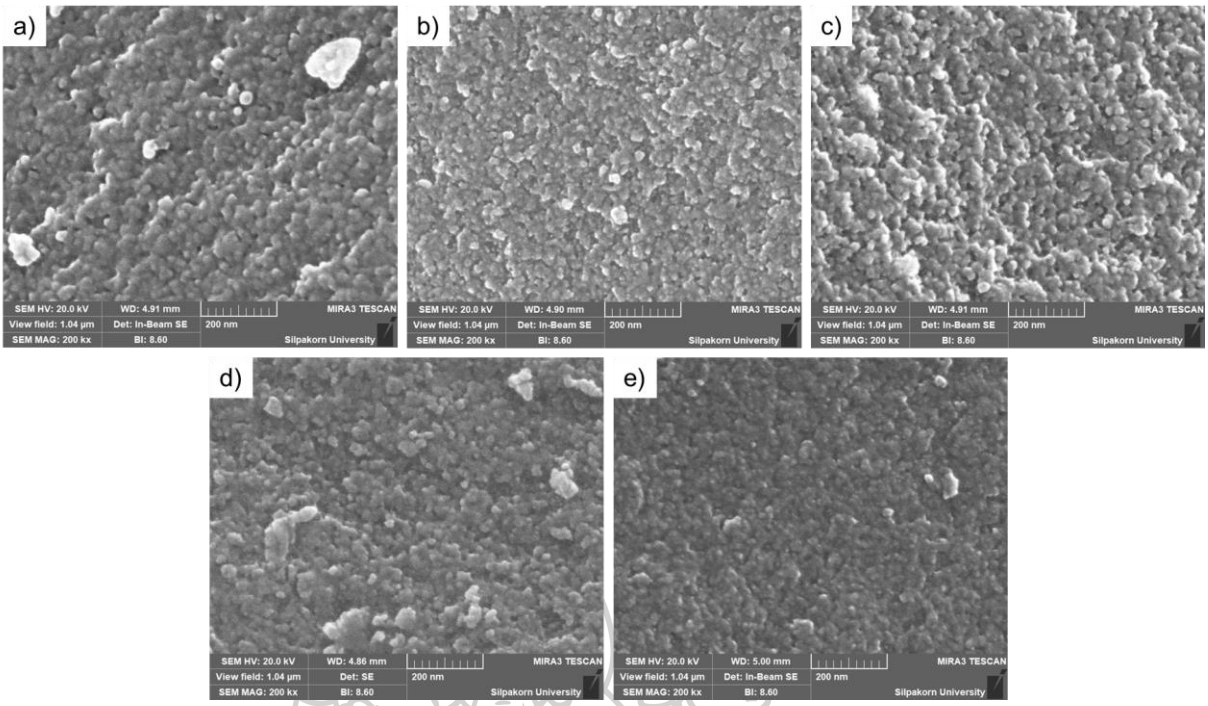

Figure 15 : SEM images of unpromoted alumina and tungsten-promoted alumina series; a) Al, b) 1W-Al, c) 5W-Al, d) 10W-Al, and e) 20W-Al.

4.2 Cerium-promoted alumina (CeO_2-Al_2O_3)

4.2.1 XRD

The structural analysis of cerium-promoted alumina from XRD indicated that amorphous cerium was formed with alumina (**Figure 16**). The reflections typical of the γ-alumina phase had the same the pattern of tungsten-promoted alumina series. The XRD pattern showed the reflections typical of cerium oxide of 2θ at 28.5, 33.2, 47.5, and 56.5° [18],[68]. The reduction of peak intensity of the γ-alumina when loading cerium was increased, which may suggest the highly dispersed on the alumina surface of cerium, same as the results of the tungsten-promoted alumina series, and the reflections typical of cerium oxide increased with increasing cerium loading [69].

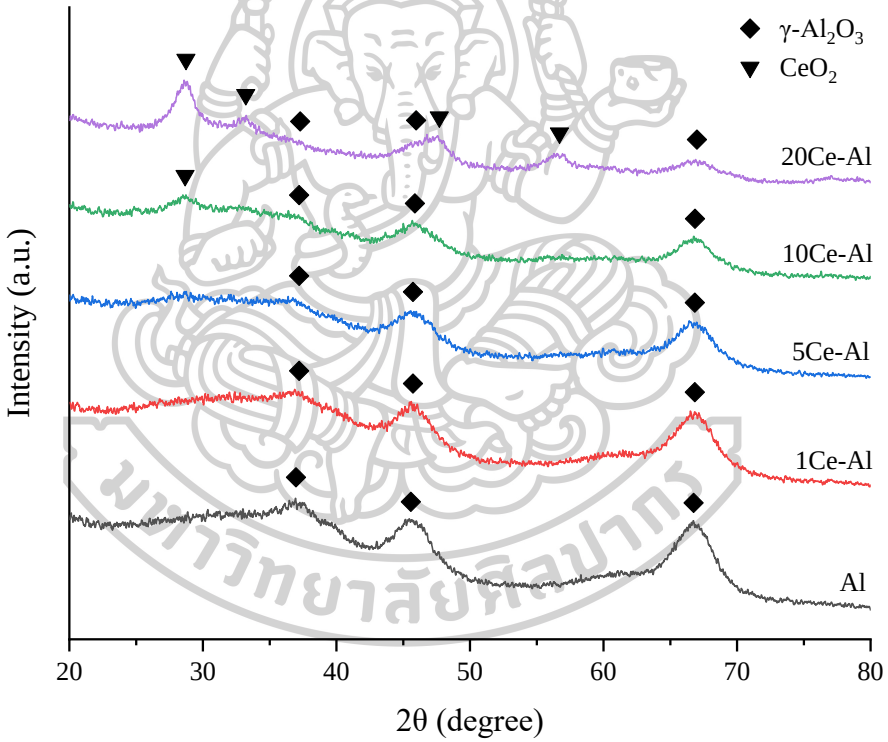

Figure 16 : The XRD patterns of cerium-promoted alumina series.

4.2.2 Nitrogen physisorption

The results of nitrogen physisorption including the Brunauer−Emmett−Teller (BET) surface area (m^2/g), pore volume (cm^3/g), and average pore size (nm) showed in **Table 9**. The specific surface area of cerium-promoted alumina catalysts decreased with decreasing cerium loadings for Al to 5Ce-Al and was highest at 212 m^2/g of 10 wt.% cerium. The high specific surface area of all catalysts derived from SC method more than other methods was obtained even after the calcination at 600 °C for 6 h, which may mean that the synthesized cerium-promoted alumina had very high thermal stability which can occur from thick pore walls [13]. The pore volume decreased from 0.24 cm^3/g of unpromoted alumina to 0.19 cm^3/g when increasing loading of cerium 1, and 5 but decreased to 0.23 cm^3/g when loading at 10 wt.% tungsten, and decreased to 0.18 when increasing loading of cerium at 20wt%. The average pore size decreased with increasing cerium loadings. Thus, this loss was around 14-25 % (with compare to the unpromoted alumina for the specific surface area of 5Ce-Al, 189 vs 162 m^2/g., and pore volume of 20Ce-Al, 0.24 vs 0.18 cm^3/g), maybe judging from these results the effect of cerium-promoted was considered moderate [18].

Table 9 Properties of cerium-promoted alumina catalysts.

Catalyst	**S_{BET} (m^2/g)**	**Pore volume (cm^3/g)**	**Average pore size (nm)**
Al	189	0.24	5.0
1Ce-Al	179	0.21	4.7
5Ce-Al	162	0.19	4.7
10Ce-Al	212	0.23	4.3
20Ce-Al	169	0.18	4.2

4.2.3 NH_3 -TPD

The acidity of catalysts, showed the comparison of unpromoted alumina and cerium-promoted alumina by NH_3-TPD **Figure 17**. **Figure 18** showed the deconvolution of NH_3-TPD results. **Table 10** showed acidity calculated from deconvolution peaks to compare unpromoted alumina and cerium-promoted alumina. The NH_3-TPD profile of γ-Al_2O_3 consists of three peaks approximately 150, 250, and 490 °C synonymous with the weak, medium, and strong acid sites same as the results of tungsten-promoted alumina. These results show that the adsorbed NH_3 molecules on the surface of 5 and 20Ce-Al catalysts can be removed more easily than on Al at low, medium, and high temperatures. Otherwise, the addition of cerium into γ-Al_2O_3, decreases the acid sites.

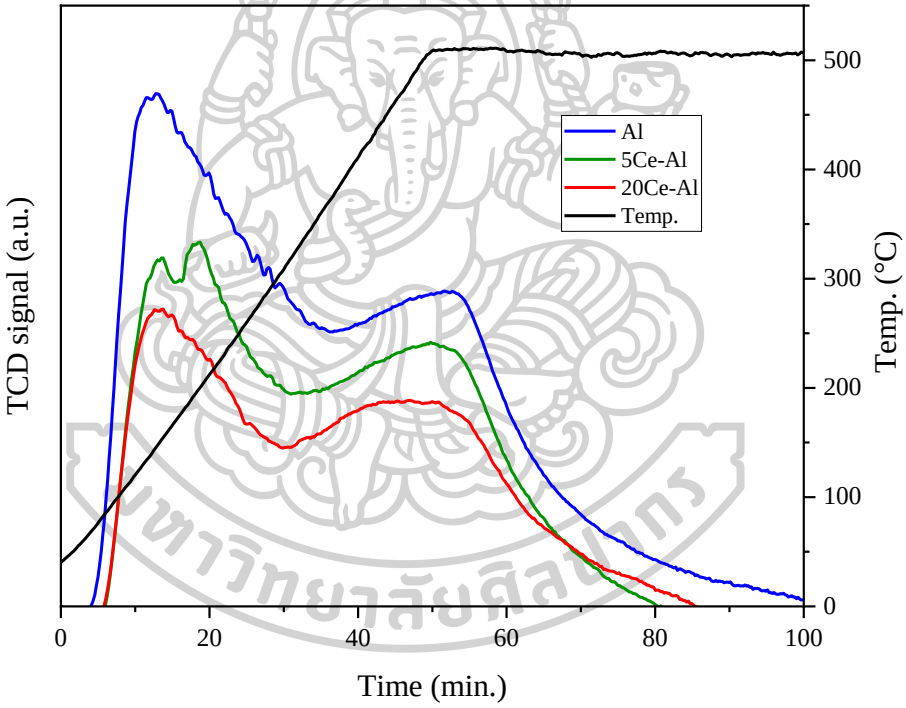

Figure 17 : NH_3-TPD profiles of unpromoted alumina (Al), and cerium-promoted alumina series.

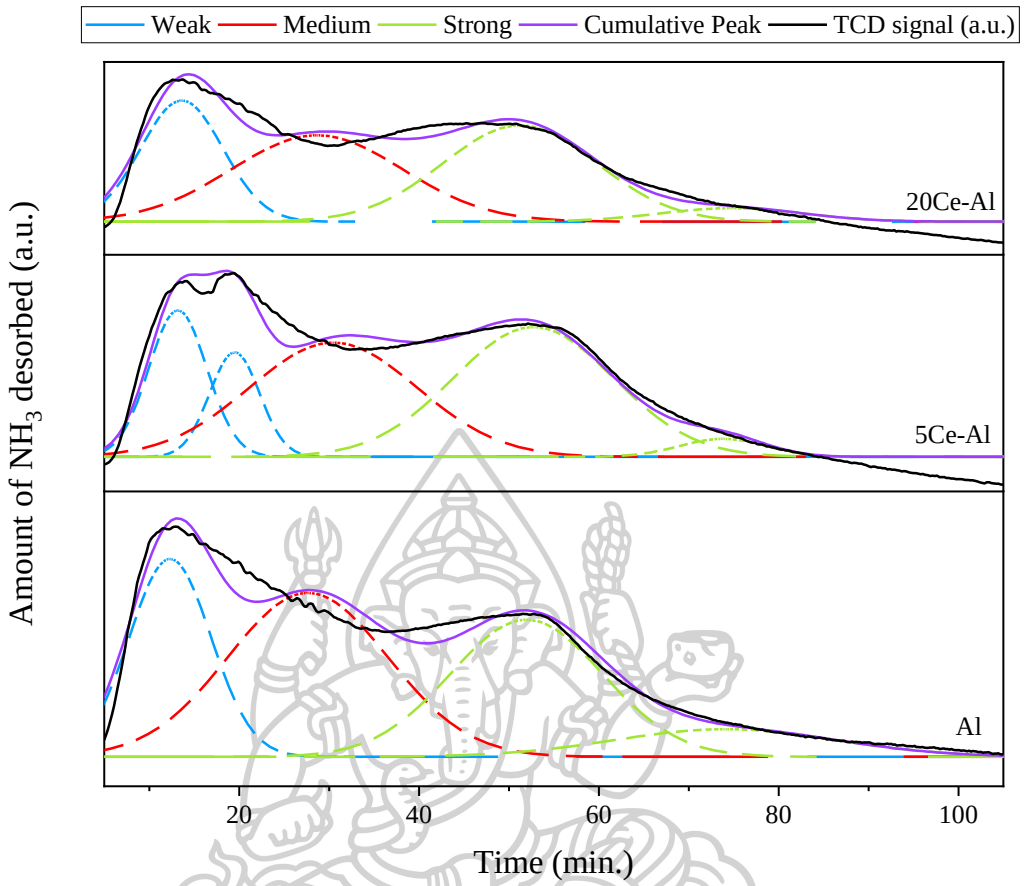

Figure 18 : Deconvolution of NH_3-TPD profiles of unpromoted alumina (Al), and cerium-promoted alumina series.

Table 10 The acidity of cerium-promoted alumina catalysts.

Catalyst	**Weak (mmol/g)**	**Medium (mmol/g)**	**Strong (mmol/g)**	**Total (mmol/g)**
Al	0.18	0.3	0.31	0.79
5Ce-Al	0.13	0.18	0.21	0.52
20Ce-Al	0.1	0.16	0.18	0.44

4.2.4 SEM

The morphology and surface structures of the cerium-promoted alumina series were analyzed with SEM. The comparison of SEM images **(Figure 19)** same as the SEM of tungsten-promoted series, indicated a negligible change in the morphology of the catalysts. The particle of catalysts was mostly spherical but these small particles aggregated uniform for all catalysts. This was found that the catalysts were synthesized by using urea as a fuel, successfully in nanoscale [67].

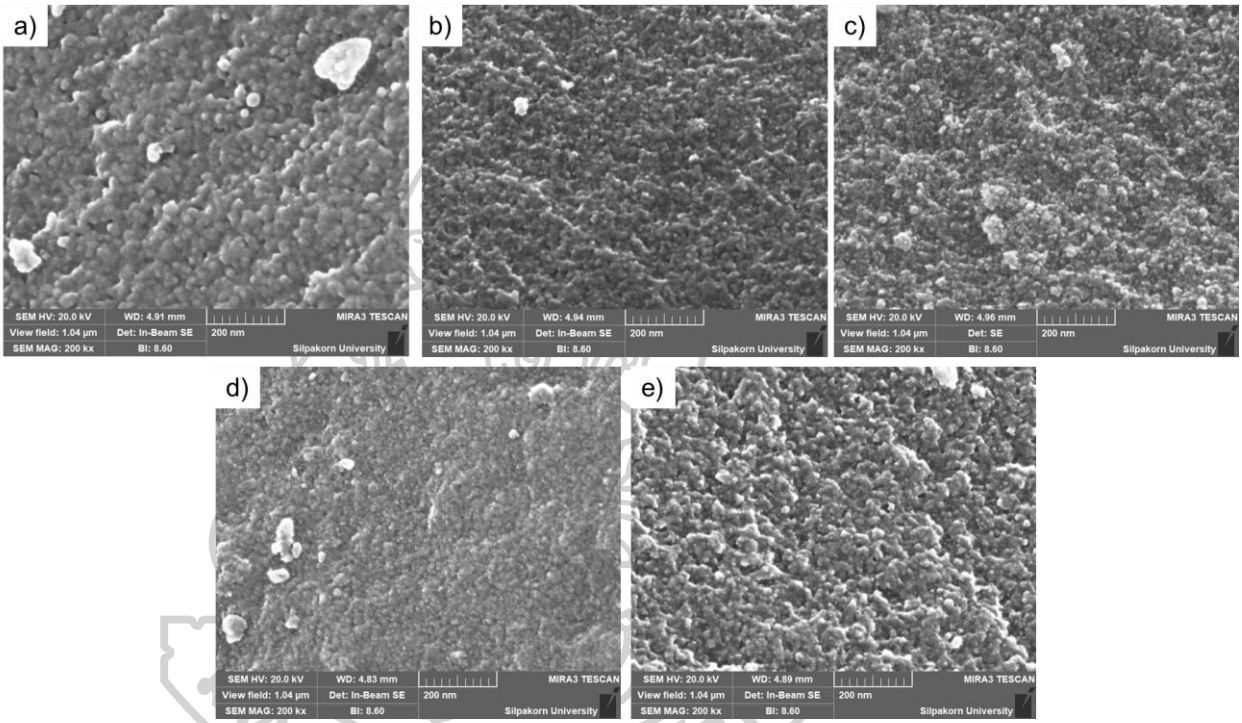

Figure 19 : SEM images of unpromoted alumina and cerium-promoted alumina series; a) Al, b) 1Ce-Al, c) 5Ce-Al, d) 10Ce-Al, and e) 20Ce-Al.

4.3 Iron-promoted alumina (Fe_2O_3-Al_2O_3)

4.3.1 XRD

The structural analysis of iron-promoted alumina from XRD indicated that amorphous iron was formed with alumina (**Figure 20**), showing the reflections typical of the γ-alumina phase at same the pattern of tungsten-promoted alumina series. The XRD pattern showed the reflections typical of iron oxide were obtained at 24.2, 33.3, 35.7, 41.1, 49.7, 54.2, 62.7, and 64.8° [70, 71]. The reduction of peak intensity of the γ-alumina when loading iron was increased, which may suggest the highly dispersed on the alumina surface of iron, same as the results of the tungsten- and cerium-promoted alumina series, and the reflections typical of iron oxide increased with increasing iron loading [72].

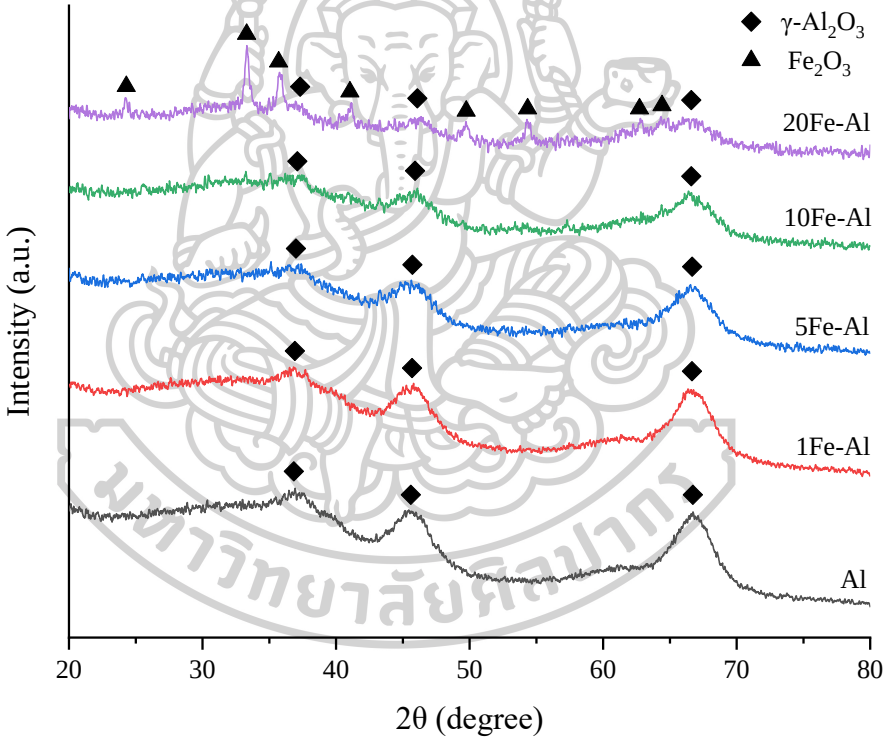

Figure 20 : The XRD patterns of iron-promoted alumina series.

4.3.2 Nitrogen physisorption

The results of nitrogen physisorption including the Brunauer−Emmett−Teller (BET) surface area (m^2/g), pore volume (cm^3/g), and average pore size (nm) showed in **Table 11**. From the results, the high specific surface area of all catalysts was obtained even after the calcination at 600 °C for 6 h, which may mean that the synthesized iron-promoted alumina had very high thermal stability which can occur from thick pore walls. The specific surface area of the iron-promoted alumina catalyst series increased at 1 wt.% loading of iron and was highest at 245 m^2/g, and significantly decrease to 214 m^2/g of 20Fe-Al. The pore volume increased from 0.24 cm^3/g of unpromoted alumina to 0.29 cm^3/g when increasing the loading of iron 1 wt.% but decreased to 0.28, 0.27, and 0.24 cm^3/g when loading at 5, 10, and 20 wt.% tungsten. The decrease of alumina in iron-promoted alumina catalysts may be the main reason for the hollow structure, leading to the pore of catalyst collapses during the calcination at high temperatures [13]. The average pore size decreased with increasing iron loadings. The increase in specific surface area and pore volume of iron-promoted alumina more than unpromoted alumina relate to the nitrogen sorption isotherms **(Appendix. B)** demonstrate that iron-promoted alumina composites with the mesoporous structure were successfully synthesized. The high specific surface area and mesoporous structure of iron-promoted alumina allow the iron to disperse well. However, the specific surface area, pore volume, and average pore size decrease with increasing iron loading, It can be accounted to the pore blockage by the loading of iron [72].

Table 11 Properties of iron-promoted alumina catalysts.

Catalyst	**S_{BET} (m^2/g)**	**Pore volume (cm^3/g)**	**Average pore size (nm)**
Al	189	0.24	5.0
1Fe-Al	245	0.29	4.8
5Fe-Al	241	0.28	4.7
10Fe-Al	245	0.27	4.5
20Fe-Al	214	0.24	4.5

4.3.3 NH_3 -TPD

The acidity of catalysts, showed the comparison of unpromoted alumina and iron-promoted alumina by NH_3-TPD **Figure 21**. **Figure 22** showed the deconvolution of NH_3-TPD results. **Table 12** showed acidity calculated from deconvolution peaks to compare unpromoted alumina and iron-promoted alumina. The NH_3-TPD profile of γ-Al_2O_3 consists of three peaks approximately 150, 250, and 490 °C synonymous with the weak, medium, and strong acid sites same as the results of tungsten-promoted alumina. These results show that the adsorbed NH_3 molecules on the surface of 5Fe-Al catalysts can be removed easied than on Al at low, medium, and high temperatures and for 20Fe-Al the adsorbed NH_3 molecules on the surface catalyst can be removed easied than on Al at low, and high temperatures. Otherwise, for 5Fe-Al the addition of iron into γ-Al_2O_3 decreases all acid sites but for 20Fe-Al the addition of iron into γ-Al_2O_3 decreases the weak and strong acid sites, increases the medium acid sites.

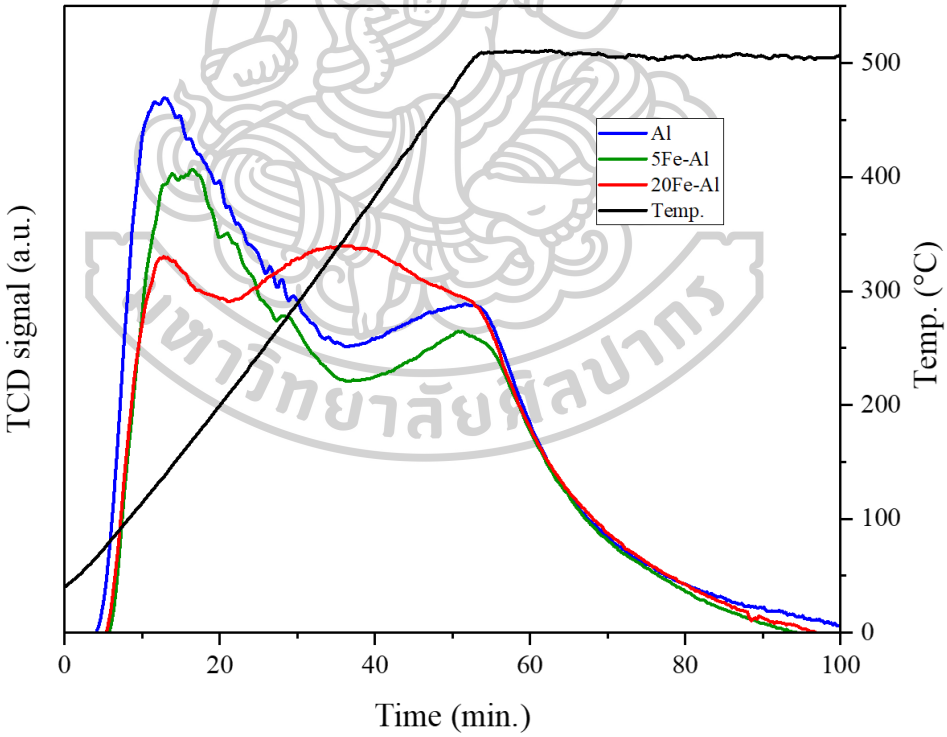

Figure 21 : NH_3-TPD profiles of unpromoted alumina (Al), and iron-promoted alumina series.

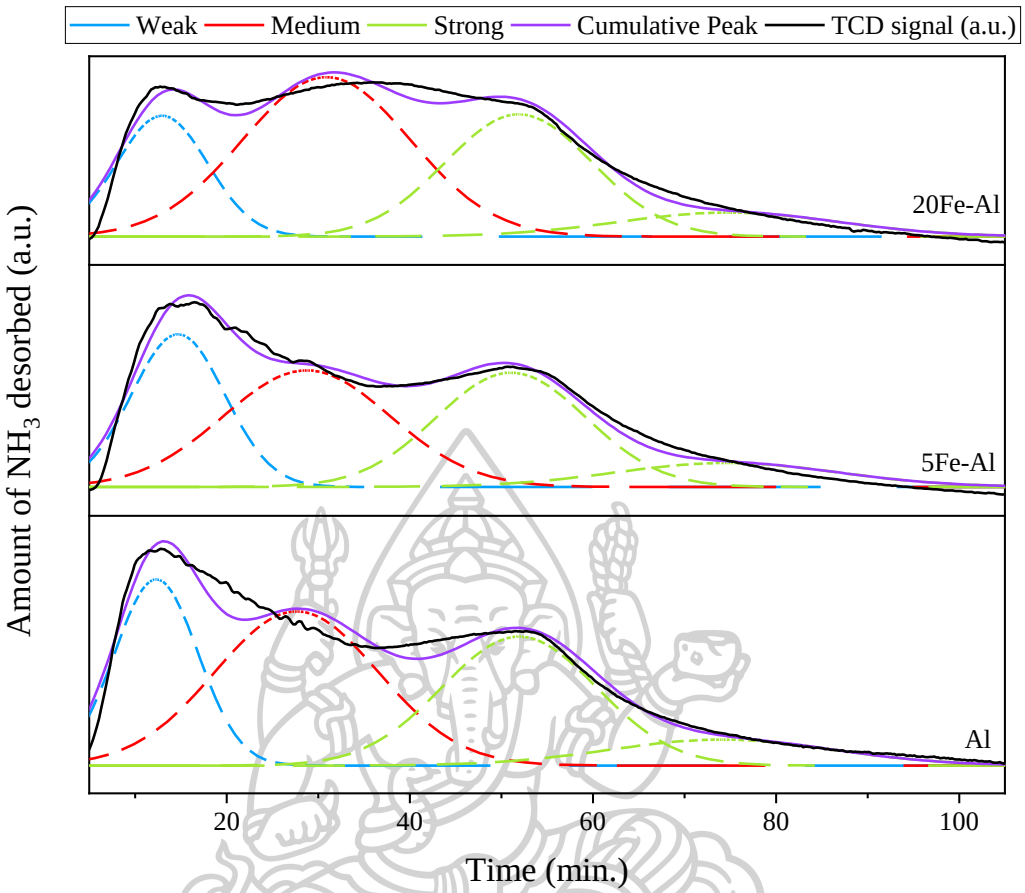

Figure 22 : Deconvolution of NH_3-TPD profiles of unpromoted alumina (Al), and iron-promoted alumina series.

Table 12 The acidity of iron-promoted alumina catalysts.

Catalyst	**Weak (mmol/g)**	**Medium (mmol/g)**	**Strong (mmol/g)**	**Total (mmol/g)**
Al	0.18	0.3	0.31	0.79
5Fe-Al	0.17	0.23	0.27	0.67
20Fe-Al	0.13	0.32	0.28	0.73

4.3.4 SEM

The morphology and surface structures of the iron-promoted alumina series were analyzed with SEM. The comparison of SEM images **(Figure 23)** same as the SEM of tungsten-promoted series, indicated a negligible change in the morphology of the catalysts. The particle of catalysts was mostly spherical but these small particles aggregated uniform for all catalysts. This was found that the catalysts were synthesized by using urea as a fuel, successfully in nanoscale [67]. For the 20Fe-Al sample, SEM image showed the formation of particles on the surface, the particles were featured mostly regular cubical and spherical shapes (the diameter of the particles on the surface is approximately 40 nm) [71].

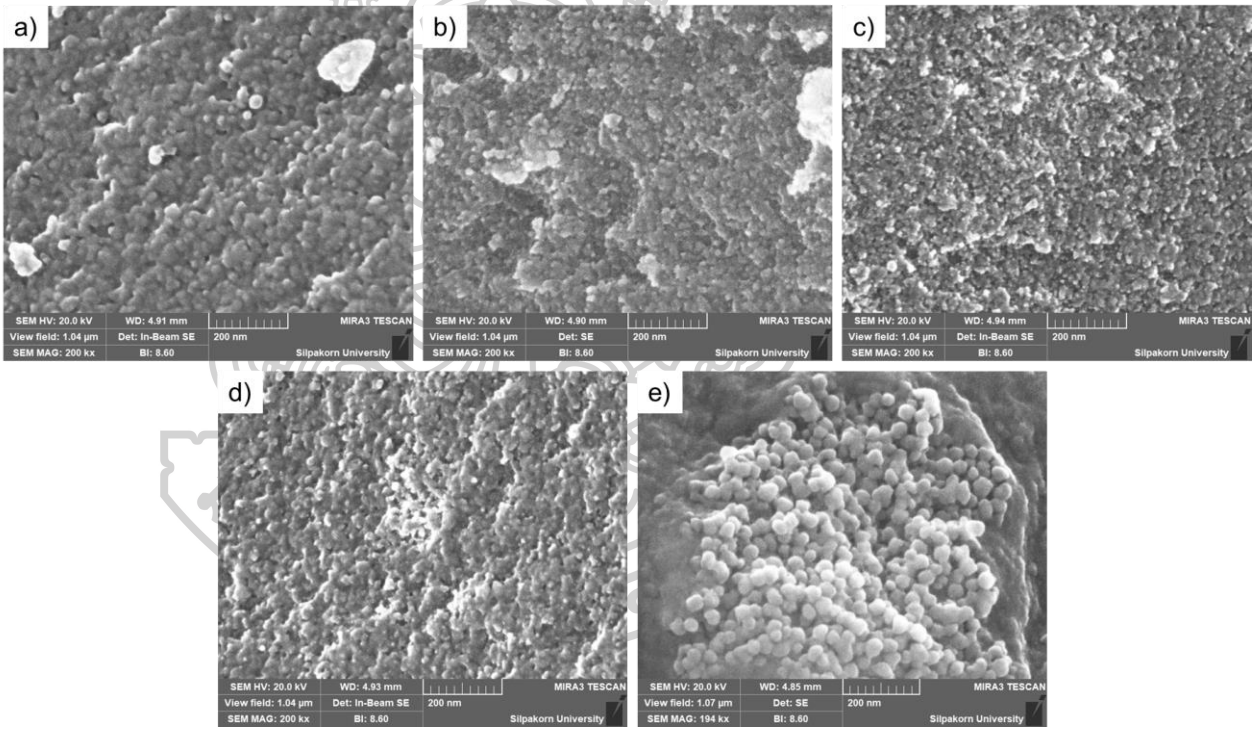

Figure 23 : SEM images of unpromoted alumina and iron-promoted alumina series; a) Al, b) 1Fe-Al, c) 5Fe-Al, d) 10Fe-Al, and e) 20Fe-Al.

4.4 Furfural production

The catalysts were tested for furfural production from sugarcane leaves at 170°C and under N_2 pressure of 10 bar. All of the catalysts tested, first at 5 h (**Figure 24**) according to the literature review, about the condition of the reaction such as the report by Catrinck [11], etc. According to the results, the best of each catalysts series is 5W-Al, 5Ce-Al, and 5Fe-Al, and these results in this condition are not following the literature review and the effect of acidity observed from the NH_3-TPD (**Figure 13, Figure 14, and Table 8**).

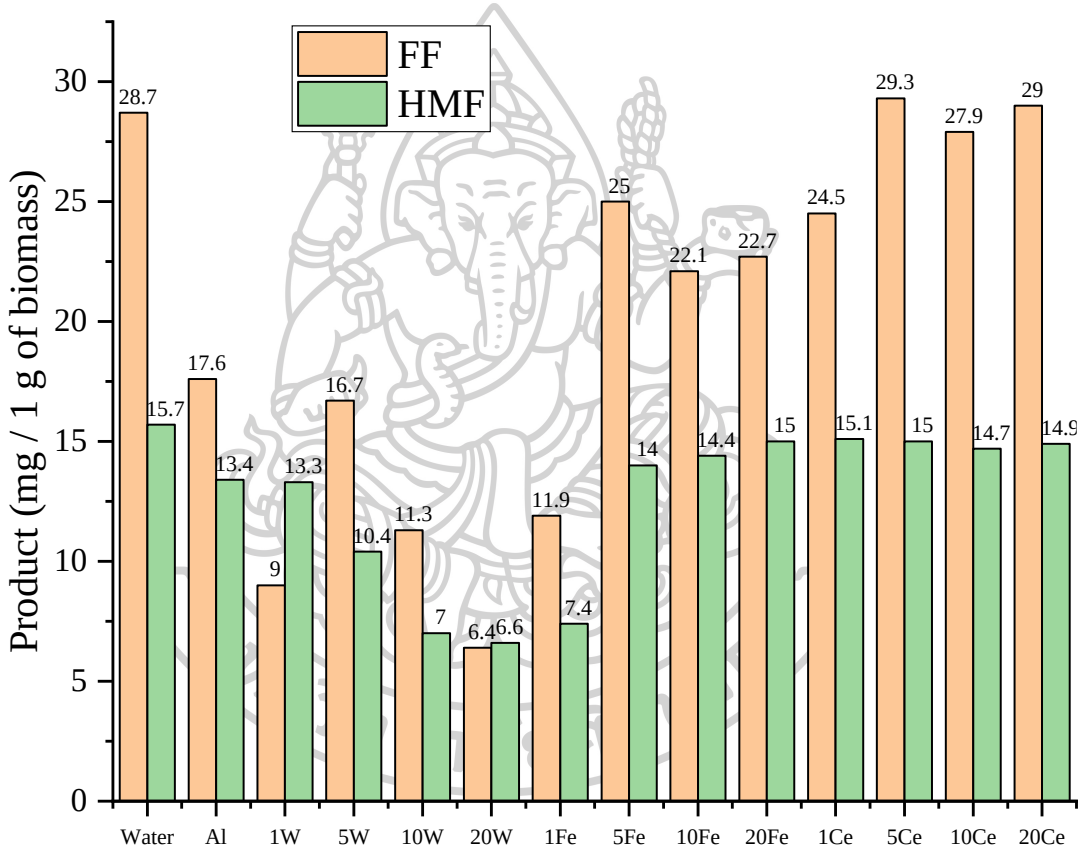

Figure 24 : The results from all reactions at 170°C, 10 bar for 5 h.

The tungsten-promoted alumina series, there was the highest acidity compared to the cerium- and iron-promoted alumina series. It is believed that this is the reason for less product yield than both cerium- and iron-promoted alumina series [40, 50]. That is why try to reduce the reaction time. The reduction of reaction time, **Figure 25** shows the furfural and HMF product trend of water, 5Fe, and 5Ce were decreased by reducing the reaction time to 2 h. In contrast, the furfural product for Al and 5W was increased by decreasing the reaction time but HMF was

decreased by decreasing the reaction time. Therefore, the highest acidity and trend of products of tungsten-promoted alumina series were further studied for reaction time as shown in **Figure 26**.

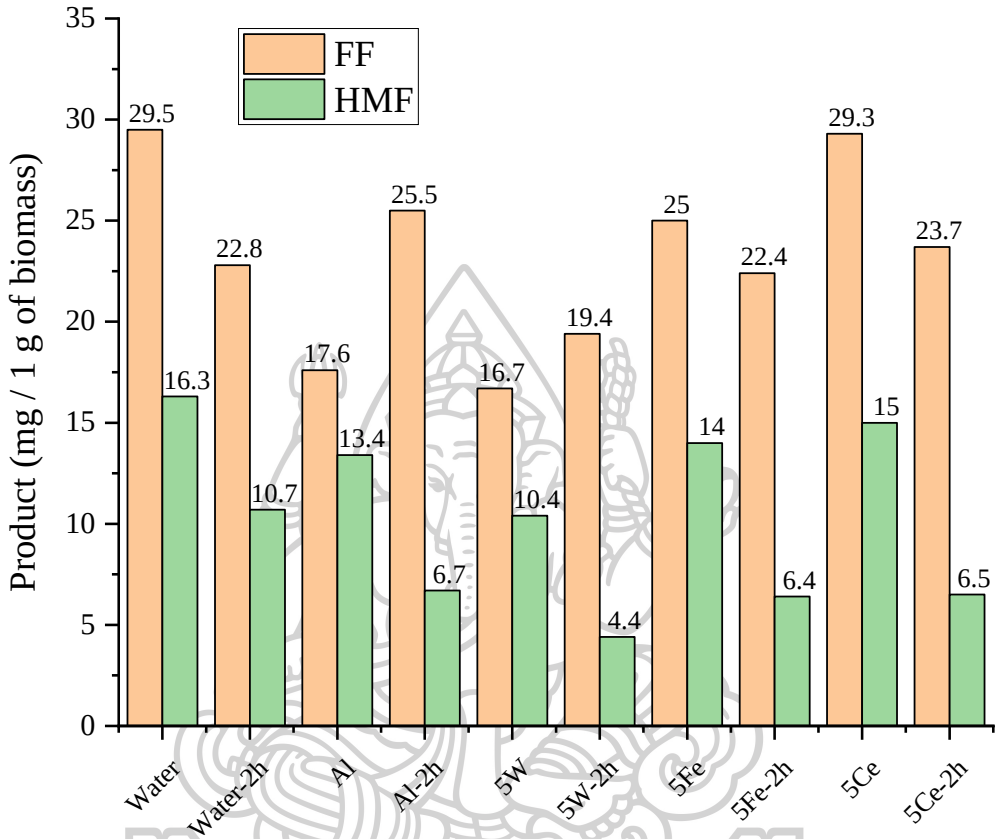

Figure 25 : The comparison of results from the reaction at 170°C, 10 bar for 2 and 5 h.

For tungsten-promoted alumina series was tested for various reaction times. **Figure 26** shows the results of furfural from the reaction of all catalysts in the tungsten-promoted alumina series compared at 0.5, 1, 2, and 5 h. At 2 and 1 h, for these reaction times, the furfural product decreased when increasing tungsten loading as shown in **Figure 26**. That may be mentioned the Brønsted acid sites affect to main product, from acidity of catalyst in **Table 8** show the Brønsted acid sites increased when increasing tungsten loading, in contrast to the furfural results, which has an optimum at 1 wt.% of tungsten. From this result may be concluded to the same result with the report of Li H. and Li X. about the excess acidity enhanced the side reactions, humins formation, and decreased product was facilitated by Brønsted acid [40, 50]. Therefore, the catalyst having too high Brønsted acid sites maybe lead to furfural degradation and lead

to biomass being converted to other byproducts such as humins [7, 50, 73-77], etc. Thus, this reason may be attributed to the report of Jiménez-Morales and Shirai, they explained about the Brønsted catalyst promoted HMF and another byproduct [78, 79].

Moreover, this process may be similar to the liquid hot water (LHW) process, is also known as hydrothermal pretreatment. Which in batch-type reactors, it was a process that reacts at temperatures and pressures of 100-300◦C and 1-220 bar. The process that occurs, is divided into 3 main steps as follows: 1) The creation of products from biomass surface reactions, 2) the products dissolute in water, and 3) the product decomposition. Under that conditions, the auto-ionization of water occurs, in which the water dissociated into H+ and OH- ions. Which H+ or hydronium ions dissociate will increase the acidity of the solvent water and act as the primary catalysts for the hydrolysis of biomass (**Figure 27-28**). It is believed that, altogether with the acidity obtained from the catalyst, the hydronium ion was another reason that the acidity of the process is too high, causing other products such as humins to form and the main product to decompose [80-82].

However, if considering the results, at 0.5 and 5 h of reaction time, these have furfural results an optimum at 10 and 5 wt.% of tungsten, respectively. It can be seen that for each reaction time from 0.5 to 5 h., the optimum was only a range of 1-10 wt.% of tungsten but not more than 20%. This may be proof that increasing the amount of tungsten to a certain point will too high Bronsted acidity, leading to lower results, which in each condition may be different.

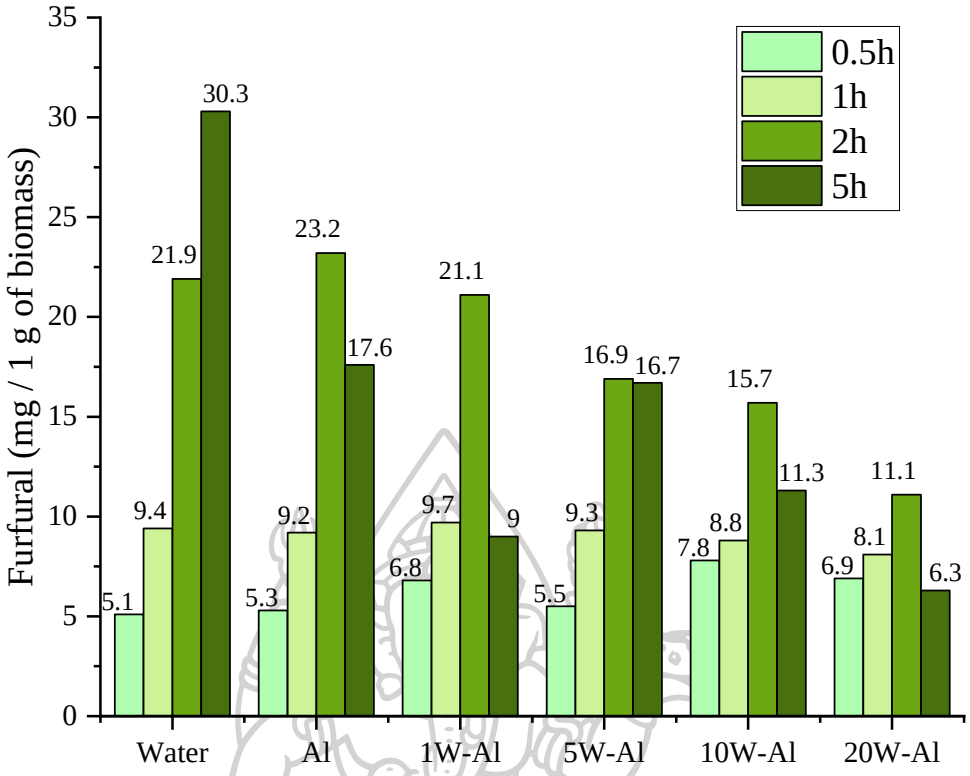

Figure 26 : The comparison of furfural product from the reaction (Tungsten-promoted alumina series) at 170°C, 10 bar for 0.5, 1, 2, and 5 h.

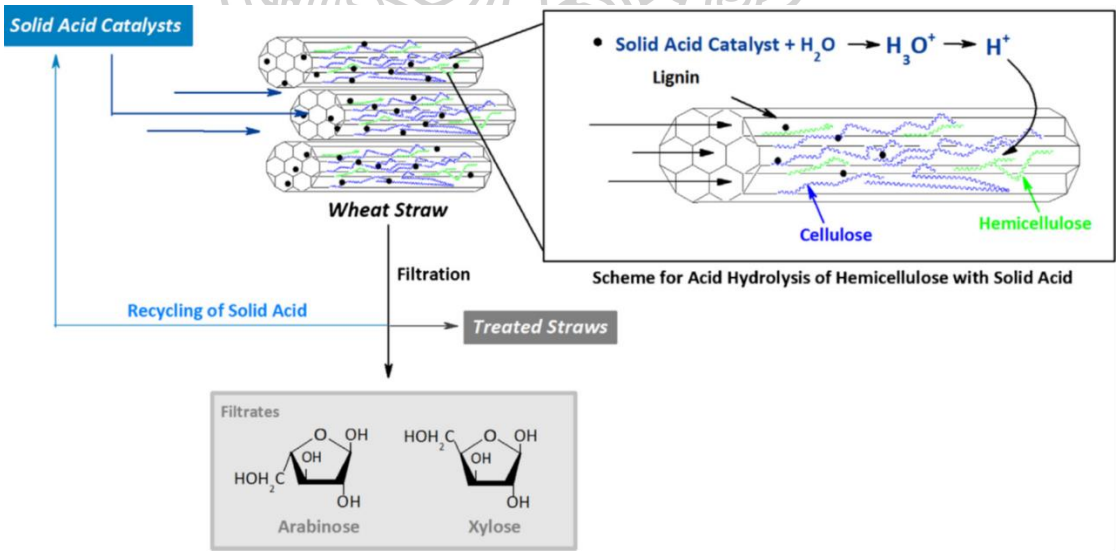

Figure 27 : Scheme for selective hemicellulose hydrolysis from wheat straw with solid acid [82].

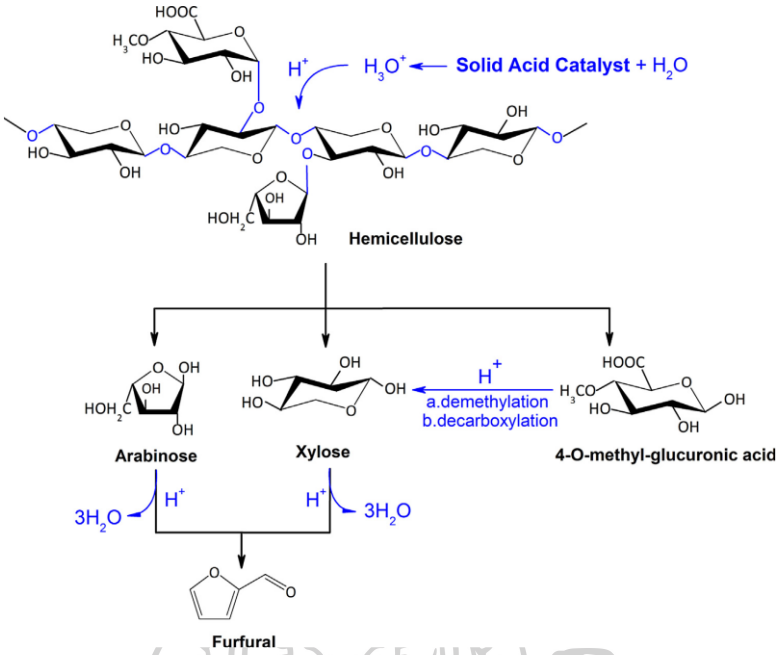

Figure 28 : Scheme for mechanism of hemicellulose hydrolysis with solid acid SO_4^{2-}/Fe_2O_3 [82].

For the condition at 170°C believed that this is radical condition, thus that is the reason for low product yield. Therefore, from that reason the temperature was reduced to 130°C. **Figure 29** show the results when temperature reduced, furfural decreased with a decreasing of temperature. It could be said that this condition it was not harsh enough for furfural production and gave a low furfural yield, and this condition cannot show the performance of the catalysts.

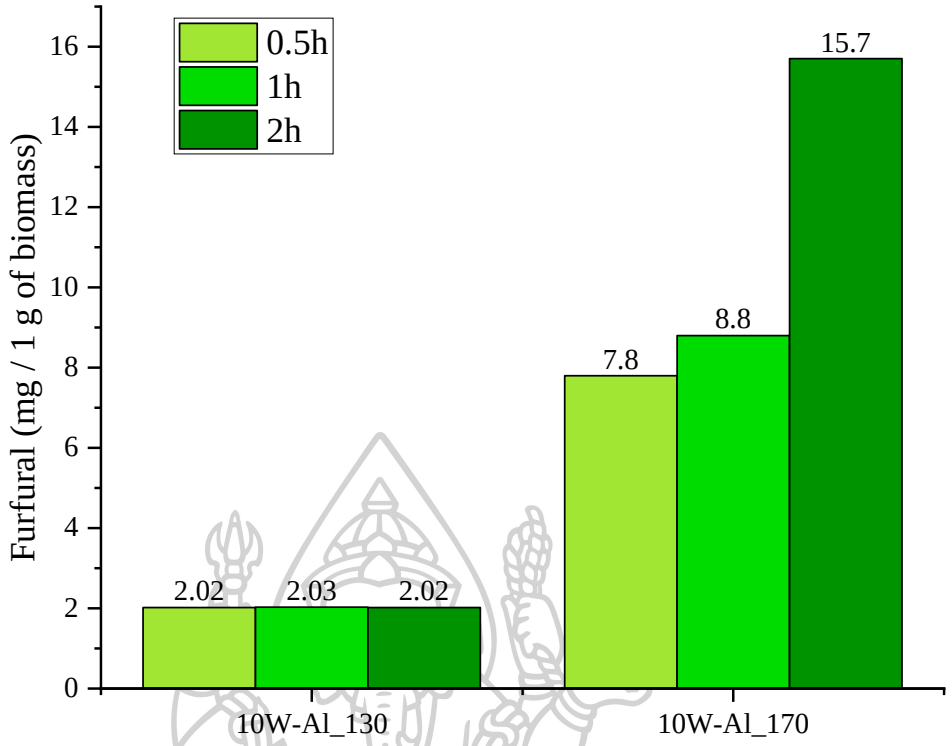

Figure 29 : The comparison of furfural product from the reaction at 130 and 170°C, 10 bar for 0.5, 1, and 2 h.

For the cerium-promoted alumina series, the comparison of furfural product from the reaction at 0.5, 2, and 5 h showed in **Figure 30**. These results show some activities of catalysts between 5Ce-Al and 20Ce-Al. At 5 h, for Al may be too high the acidity and too high reaction time that reason to lowest furfural content, and for 5Ce-Al and 20Ce-Al may have acidity lower than Al that why to give a high content of furfural (**Table 10**) [7, 40, 50, 74, 75]. At 2 h, It cannot compare because for 20Ce-Al does not have data but the trend was nearby the tungsten-promoted alumina at 1 h (**Figure 26**), the furfural content of all reactions was approximately the same. At 0.5 h, gave the furfural content 20Ce-Al, 5Ce-Al, and Al, respectively. These results may be related to the acidity of catalysts. Thus, the results that may be predicted about the cerium-promoted alumina catalyst were not too high acidity that why it can perform the reaction in both long and short time.

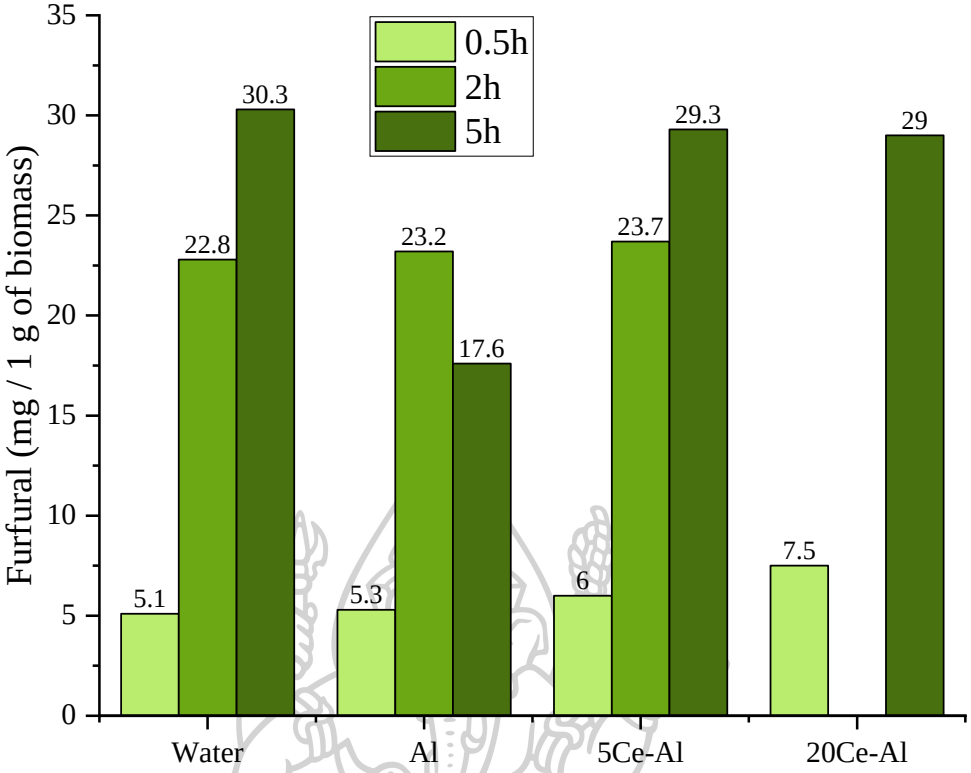

Figure 30 : The comparison of furfural product from the reaction (Cerium-promoted alumina series) at 170°C, 10 bar for 0.5, 2, and 5 h.

For the iron-promoted alumina series, the results of furfural product from the reaction at 0.5, 2, and 5 h showed in **Figure 31.** At 5 h, the results were the same the cerium-promoted alumina series for Al may be too high the acidity and too high reaction time that reason for the lowest furfural content, and for 5Fe-Al and 20Fe-Al may have acidity lower than Al that why to give a high content of furfural (**Table 12**) [7, 40, 50, 74, 75]. At 2 h, It cannot compare because for 20Fe-Al does not have data but the trend was nearby the tungsten-promoted alumina at 1 h (**Figure 26**) and cerium-promoted alumina at 2 h (**Figure 30**), the furfural content of all reactions was approximately the same. Finally, at 0.5 h the furfural content of all reactions was approximately the same but highest at 5Fe-Al. Thus, the results that may be predicted about the iron-promoted alumina catalyst were not too high acidity same as the cerium-promoted alumina catalyst why it can perform the reaction in both long and short time.

Figure 31 : The comparison of furfural product from the reaction (Iron-promoted alumina series) at 170°C, 10 bar for 0.5, 2, and 5 h.

Finally, **Table 13** try to show the comparison of conversion of biomass to furfural, called “One-pot” method. The results from other research compared to result from this work starting from biomass converted to furfural product with solid catalyst in water as a solvent.

Table 13 "One-pot" method for conversion of biomass to furfural in water as a solvent.

Raw material	Catalyst	Solvent	Conditions	Yield	Ref.
Corncob	SO_4^{2-}/TiO_2–ZrO_2/La^{3+}	Water	180°C,2 h.	6%	[40]
Softwood	HUSY	Water	160°C, 1 h.	< 1%	[83]
Unpurified hemicellulose	Al-SBA-15	Water	170°C, 3 h, 5 MPa of N_2.	< 2%	[10]
Bagasse	HUSY	Water	160°C, 1 h.	< 1%	[2]
Sugarcane leaves	1W-Al	Water	170°C, 2 h, 10 bars of N_2	2.1%	This work
Sugarcane leaves	5Ce-Al	Water	170°C, 5 h, 10 bars of N_2	2.9%	This work
Sugarcane leaves	5Fe-Al	Water	170°C, 5 h, 10 bars of N_2	2.5%	This work

4.5 Sulfated metal-promoted alumina (SO_4^{2-}/MOx^a-Al_2O_3)

4.5.1 XRD

The structural analysis of sulfated tungsten-promoted alumina from XRD indicated that amorphous sulfated was formed with tungsten-promoted alumina (**Figure. 32**). The reflections typical of the γ-alumina phase had the same the pattern of tungsten-promoted alumina series. The XRD patterns of sulfated tungsten-promoted alumina series, this result could be concluded as the only formation of the γ-Al_2O_3 phase which means the presence of sulfate, in low loading is not able of changing the structure of γ-Al_2O_3 [60, 84, 85].

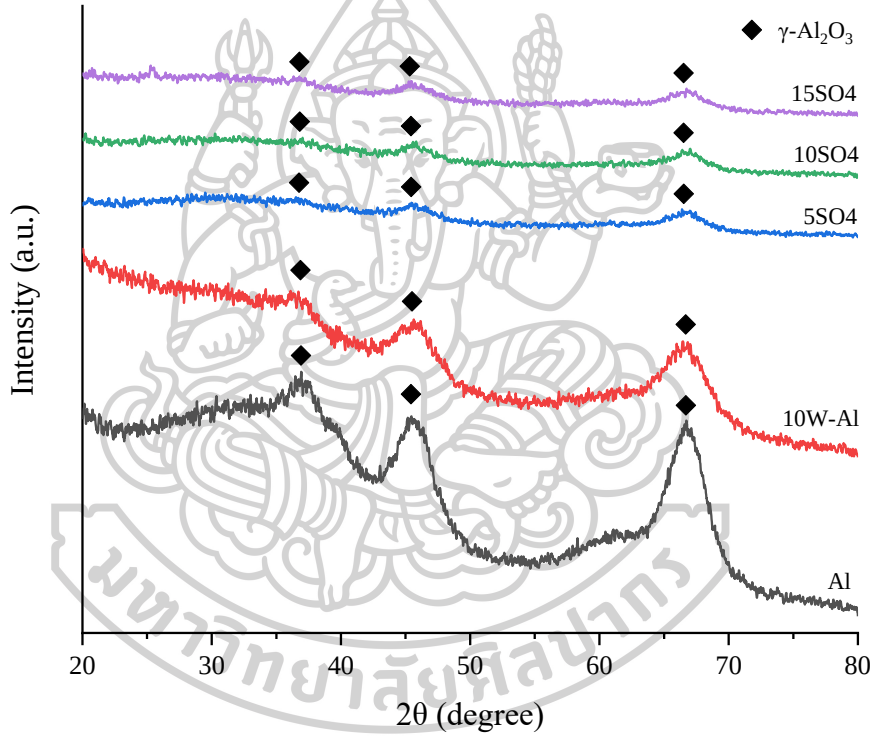

Figure 32 : The XRD patterns of sulfated tungsten-promoted alumina series.

4.5.2 Nitrogen physisorption

Table 14 showed the results of nitrogen physisorption including the Brunauer−Emmett−Teller (BET) surface area (m^2/g), pore volume (cm^3/g), and average pore size (nm). The specific surface area and pore volume of catalysts decreased with increasing sulfate loadings [60]. The lowest was obtained at 222 m^2/g and 0.20 cm^3/g of 15 wt.% of sulfate, but the average pore size is constant at 3.9 nm. These results can be accounted means by a report by M. Naghavi, the specific surface area and pore volume slowly decreased after sulfate impregnation [85]. These can be attributed to the covering of pores by the sulfate and demonstrated well impregnation of sulfate over the alumina catalyst, no destructive effects on the porosity of the alumina, and this reason may be leading to the average pore size being constant.

Table 14 Properties of sulfated tungsten-promoted alumina catalysts.

Catalyst	**S_{BET} (m^2/g)**	**Pore volume (cm^3/g)**	**Average pore size (nm)**
Al	189	0.24	5.0
10W-Al	248	0.24	3.9
5%SO_4^{2-}	241	0.23	3.9
10%SO_4^{2-}	235	0.21	3.9
15%SO_4^{2-}	222	0.20	3.9

4.5.3 NH_3 -TPD

The acidity of catalysts, showed the comparison of unpromoted alumina, 10 wt.% tungsten-promoted alumina catalyst, and sulfated tungsten-promoted alumina by NH_3-TPD **Figure 33**. **Figure 34** showed the deconvolution of NH_3-TPD results. **Table 15** showed acidity calculated from deconvolution peaks to compare unpromoted alumina, 10 wt.% tungsten-promoted alumina, and sulfated tungsten-promoted alumina. The NH_3-TPD profile of γ-Al_2O_3 consists of three peaks approximately 150, 250, and 490 °C synonymous with the weak, medium, and strong acid sites same as the results of tungsten-promoted

alumina. These results show that the adsorbed NH_3 molecules on the surface of 5, 10, and 15%SO_4^{2-} catalysts can be removed with more difficulty than on 10W-Al at low and medium temperatures and the adsorbed NH_3 molecules can be removed easied than on 10W-Al at high temperature. Otherwise, the addition of sulfate into 10 wt.% tungsten-promoted alumina decreases only the strong acid sites but increases weak and medium acid sites.

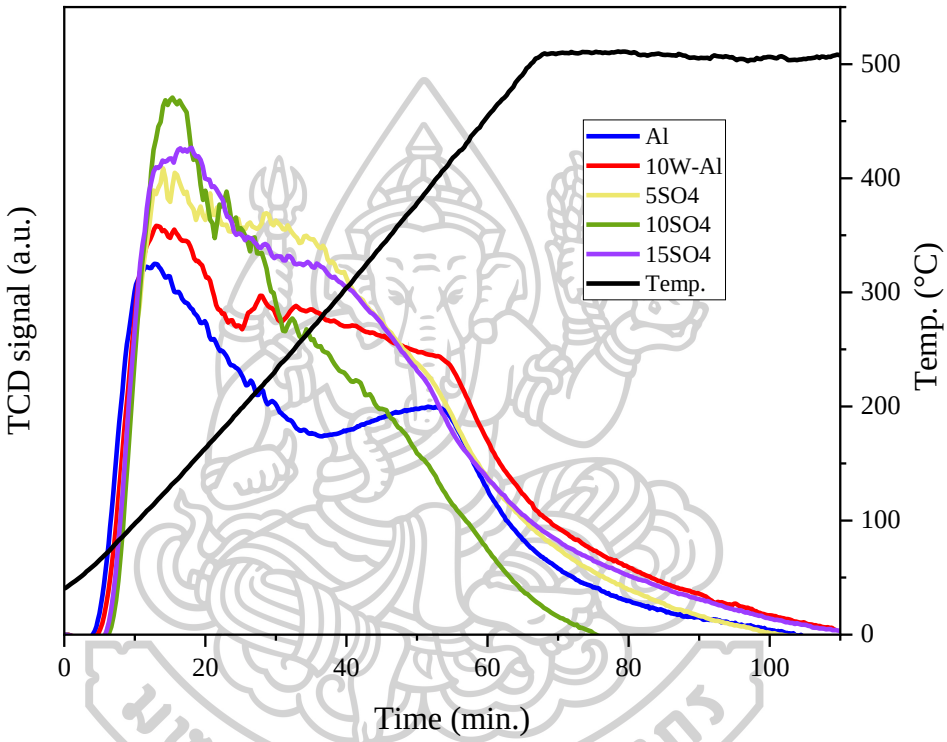

Figure 33 : NH_3-TPD profiles of sulfated tungsten-promoted alumina series.

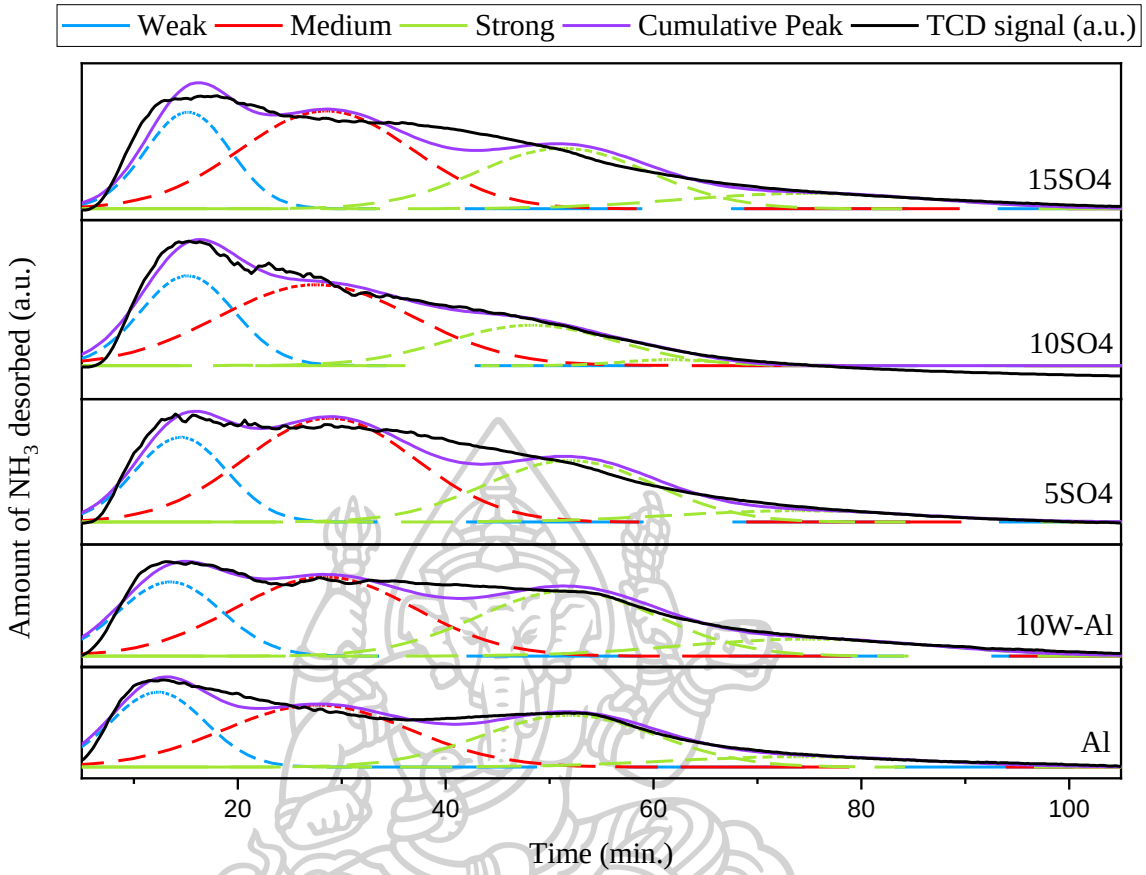

Figure 34 : Deconvolution of NH_3-TPD profiles of sulfated tungsten-promoted alumina series.

Table 15 The acidity of sulfated tungsten-promoted alumina catalysts.

Catalyst	Weak (mmol/g)	Medium (mmol/g)	Strong (mmol/g)	Total (mmol/g)	Brønsted (mmol/g)
Al	0.18	0.3	0.31	0.79	0.25
10W-Al	0.2	0.37	0.42	0.99	0.57
5%SO_4^{2-}	0.2	0.46	0.35	1.01	1.87
10%SO_4^{2-}	0.22	0.41	0.19	0.82	1.88
15%SO_4^{2-}	0.21	0.44	0.37	1.02	1.86

4.5.4 The effect of sulfate concentrations on furfural production

The furfural product content from the reaction of sulfated catalyst series showed in **Figure 35** and the results of sulfated catalyst series compared with water, Al, and 10W-Al. The furfural trend from sulfated tungsten-promoted alumina is lower than 10W-Al which is undoped by sulfate. This trend was consistent with the acidity of catalysts and the physical properties as specific surface area and pore volume. For the acidity, the sulfate impregnation effects in higher acidity than 10W-Al, especially for Brønsted acid. The catalyst having too high Brønsted maybe lead to furfural degradation and lead to biomass being converted to HMF or other byproducts such as humins [7, 73-77], etc. Thus, this reason may be attributed to the report of Jiménez-Morales and Shirai, they discuss about the Brønsted catalyst promoted HMF and another byproduct, and the effect of physical properties as specific surface area and pore volume were affected byproduct as well (The reduction of specific surface area and pore volume, **Table 14**) [78, 79]. However, for confirm about Brønsted acid effect in this work. The report of Li H. and Li X. explain about the excess acidity enhanced the side reactions and humins formation was facilitated by Brønsted acid [40, 50].

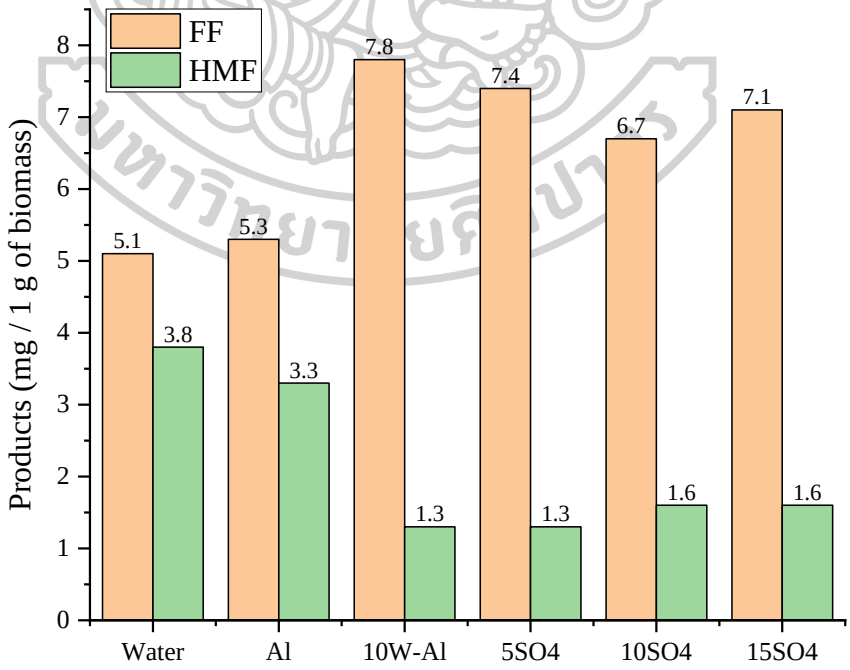

Figure 35 : The results from the reaction of sulfated series for 170°C, 10 bar, and 0.5 h.

However, humins in this work, the other researches that confirm the occurrence of humins can be summarized as the reaction in water at high temperature, high acidity and long reaction time causes the conversion of products to humins and decomposition of HMF and furfural, and the formation of humins on the catalyst, it was the reason for the impaired surface and pore activity of the catalyst resulted in a decreased product yield [7, 40, 50, 73-77, 86, 87]. The formation of humins can take many forms, as illustrated in **Figure 36-37**. The various formations of humins make the analysis used more the instrumental and difficult because must be analyzed according to the state of the humins that occur, eg. humins solid and soluble humins oligomers etc.

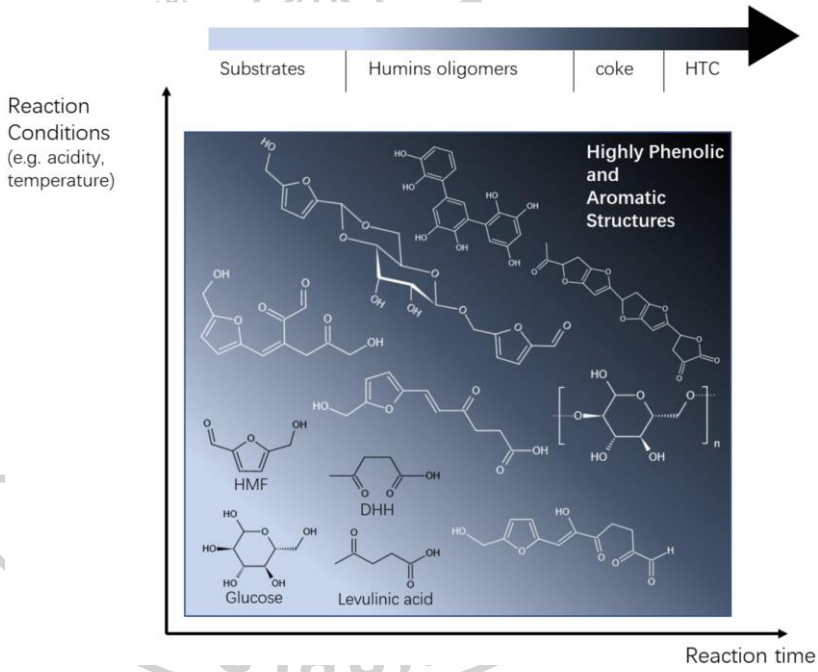

Figure 36 : Formation process of humins and other cellulosic solid byproducts. The depth of black color means the degree of polymerization and dehydration [88].

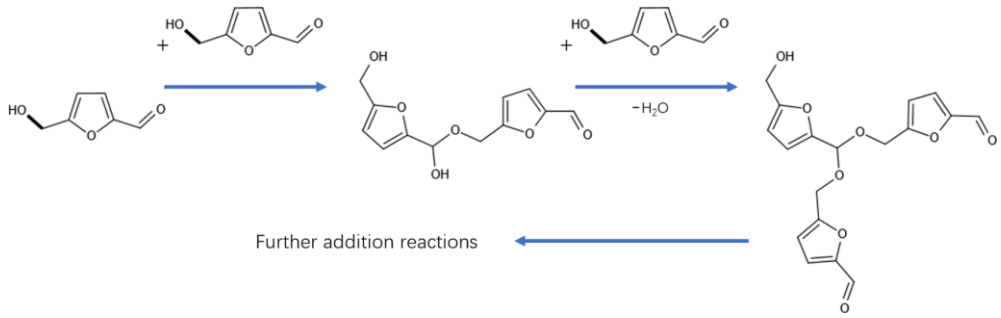

Figure 37 : Structure of cellulose-based humins proposed by Sumerskii et al. [89]

To prove the generation of humins in the reaction, xylose was used as the reactant and 10W-Al was used as catalyst at 170 °C for 2 and 5 h. **Figure 38** shows that the xylose converted to furfural but there are also other by-products such as HMF and HPLC can also detect lactic acid and levulinic acid, 5.5 mg of lactic acid at 2 h, and at 5 h. 2.9 mg of lactic acid and 7 mg of levulinic acid. The results were shown at this condition xylose converted to other substances besides furfural, and humins that cover on the catalyst were shown in **Appendix B** it is believed that is humins and calculated 0.1 mg at 2 h and 0.8 mg at 5 h.

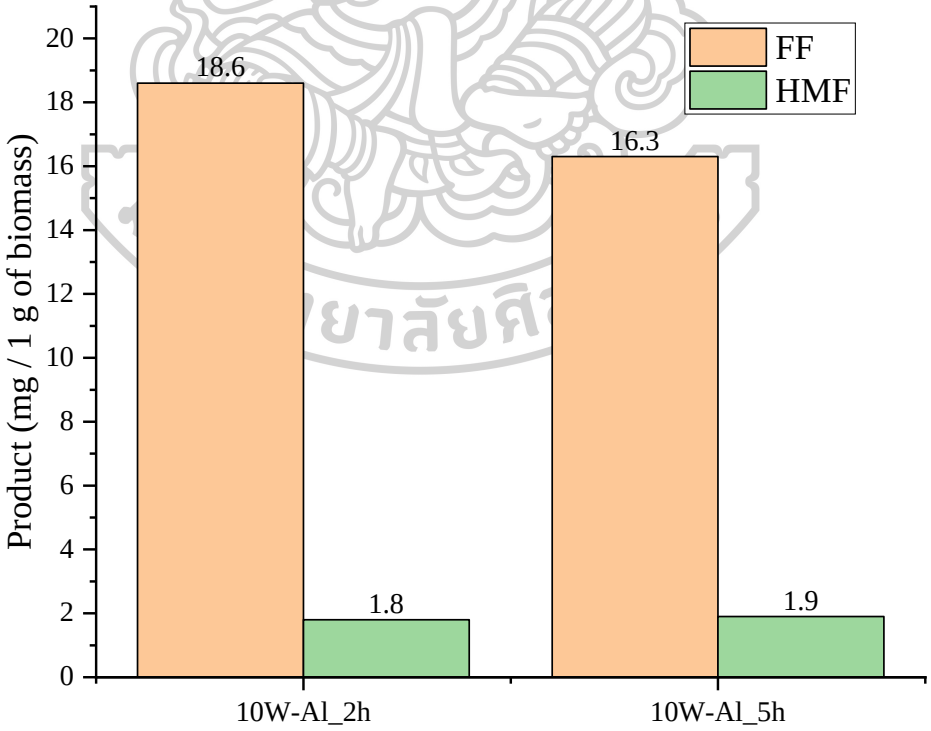

Figure 38 : The results from the reaction of xylose as substrate for 170°C, 10 bar, 2 and 5 h.

Chapter V
Conclusion

5.1 Conclusion

This work demonstrates the furfural production from sugarcane leaves in one-pot using metal-oxides catalyst synthesized by solution combustion method. The catalysts used in this work were cerium-, iron-, and tungsten-promoted alumina. The results revealed that high content of furfural can be achieved (29.3 mg / 1 g of sugarcane leaves), at 170 °C under N2 pressure 10 bar for 5 h conditions using the 5Ce-Al catalysts. A series of tungsten-promoted alumina showed higher acidity compared to the cerium and iron-promoted alumina. Therefore, effect of time were studied for tungsten-promoted alumina. The highest furfural yield can be obtained (21.1 mg / 1 g of sugarcane leaves) at 2 h using the 1W-Al catalyst. The sulfate impregnation on 10W-Al significantly boosted the Brønsted acid, leading to furfural degradation by converting to byproducts such as humins. This work demonstrated the facile and fast method for synthesizing mixed-oxide catalysts with high surface area and acidity, which plays a crucial role for upgrading biomass to value-added products.

5.2 Recommendations

The catalysts should be characterized by pyridine-adsorbed IR-spectroscopy to understand the relationship between acidity and furfural yield in order to designing more effective catalysts for conversion of biomass to furfural.

REFERENCES

Reference

1. Department of Alternative Energy Development and Efficiency, M.o.e. ฐานข้อมูลศักยภาพชีวมวลในประเทศไทยประจ าปีเพาะปลูก พ.ศ. *2556*. 2013; Available from: http://webkc.dede.go.th/testmax/node/2450.
2. Matsagar, B.M., et al., *Direct production of furfural in one-pot fashion from raw biomass using Brønsted acidic ionic liquids.* Scientific reports, 2017. **7**(1): p. 1-7.
3. Lee, C., et al., *Md. Jahim, J., & Mohammad, AW (2019). One-pot furfural production using choline chloride-dicarboxylic acid based deep eutectic solvents under mild conditions.* Bioresource Technology, 2019. **278**: p. 486-489.
4. Tian, D., et al., *Acidic deep eutectic solvents pretreatment for selective lignocellulosic biomass fractionation with enhanced cellulose reactivity.* International journal of biological macromolecules, 2020. **142**: p. 288-297.
5. Zhou, P. and Z. Zhang, *One-pot catalytic conversion of carbohydrates into furfural and 5-hydroxymethylfurfural.* Catalysis Science & Technology, 2016. **6**(11): p. 3694-3712.
6. Du, J., et al. *Furfural Formation from Corn Cobs in a One-Pot Method Catalyzed by ZSM-5*. in *2015 3rd International Conference on Advances in Energy and Environmental Science*. 2015. Atlantis Press.
7. Hoang, P.H. and T.D. Cuong, *Simultaneous Direct Production of 5-Hydroxymethylfurfural (HMF) and Furfural from Corncob Biomass Using Porous HSO3-ZSM-5 Zeolite Catalyst.* Energy & Fuels, 2020.
8. Choudhary, V., et al., *Xylose isomerization to xylulose and its dehydration to furfural in aqueous media.* Acs Catalysis, 2011. **1**(12): p. 1724-1728.
9. Choudhary, V., S.I. Sandler, and D.G. Vlachos, *Conversion of xylose to furfural using Lewis and Brønsted acid catalysts in aqueous media.* Acs Catalysis, 2012. **2**(9): p. 2022-2028.
10. R.Sahu and P.L. Dhepe, *A One-Pot Method for the Selective Conversion of Hemicellulose from Crop Waste into C5 Sugars and Furfural by Using Solid Acid Catalysts.* ChemSusChem, 2012. **5**: p. 751-761.
11. Catrinck, M.N., et al., *One-step process to produce furfural from sugarcane bagasse over niobium-based solid acid catalysts in a water medium.* Fuel Processing Technology, 2020. **207**: p. 106482.

12. Ivanova, A., *Aluminum oxide and systems based on it: Properties and applications.* Kinetics and catalysis, 2012. **53**(4): p. 425-439.
13. Kerenkan, A.E., et al., *Synthesis of mesoporous tungsten oxide/γ-alumina and surfactant-capped tungsten oxide nanoparticles and their catalytic activities in oxidative cleavage of oleic acid.* International Journal of Chemical Reactor Engineering, 2016. **14**(4): p. 899-907.
14. Mosallanejad, S., et al., *On the chemistry of iron oxide supported on γ-alumina and silica catalysts.* ACS omega, 2018. **3**(5): p. 5362-5374.
15. Varma, A., et al., *Solution combustion synthesis of nanoscale materials.* Chemical reviews, 2016. **116**(23): p. 14493-14586.
16. Ordomsky, V.V., et al., *Fructose dehydration to 5-hydroxymethylfurfural over solid acid catalysts in a biphasic system.* ChemSusChem, 2012. **5**(9): p. 1812-1819.
17. Li, R., et al., *Brønsted acid-driven conversion of glucose to xylose, arabinose and formic acid via selective C–C cleavage.* Applied Catalysis B: Environmental, 2021. **286**: p. 119862.
18. Choya, A., et al., *Oxidation of lean methane over cobalt catalysts supported on ceria/alumina.* Applied Catalysis A: General, 2020. **591**: p. 117381.
19. Yang, X., et al., *Effect of hydrothermal aging treatment on decomposition of NO by Cu-ZSM-5 and modified mechanism of doping Ce against this influence.* Materials, 2020. **13**(4): p. 888.
20. Wang, Q., et al., *Nature of cerium on improving low-temperature hydrothermal stability of SAPO-34.* Journal of Rare Earths, 2021. **39**(5): p. 548-557.
21. Dey, S. and G.C. Dhal, *Cerium catalysts applications in carbon monoxide oxidations.* Materials Science for Energy Technologies, 2020. **3**: p. 6-24.
22. Mu, M., et al., *An efficient Fe 2 O 3/HY catalyst for Friedel–Crafts acylation of m-xylene with benzoyl chloride.* RSC advances, 2014. **4**(70): p. 36951-36958.
23. Kang, W., D.O. Ozgur, and A. Varma, *Solution combustion synthesis of high surface area CeO2 nanopowders for catalytic applications: reaction mechanism and properties.* ACS Applied Nano Materials, 2018. **1**(2): p. 675-685.
24. Pawongrat, R., *Pretreatment processes for enhancing the efficiency of ethanol production from lignocellulosic agricultural wastes.* Veridian E-Journal, Science and Technology Silpakorn University, 2015. **1**: p. 143-157.

25. Mika, L.s.T., E. Cséfalvay\, and A.r. Németh, *Catalytic Conversion of Carbohydrates to Initial Platform Chemicals: Chemistry and Sustainability.* Chem. Rev., 2018. **118**: p. 505−613.
26. Sert, M., A. Arslanoglu, and L. Ballice, *Conversion of sunflower stalk based cellulose to the valuable products using choline chloride based deep eutectic solvents.* Renewable Energy, 2018. **118**: p. 993-1000.
27. online, T. *Virtual School Online*. 2017; Available from: http://www.digitalschool.club/digitalschool/science1_2_2/science2_1/more/lignin_1.php.
28. Dulie, N.W., et al., *An insight into the valorization of hemicellulose fraction of biomass into furfural: Catalytic conversion and product separation.* Waste and Biomass Valorization, 2020: p. 1-22.
29. Luo, Y., et al., *The production of furfural directly from hemicellulose in lignocellulosic biomass: A review.* Catalysis Today 2019. **319** p. 14–24.
30. ศูนย์สารสนเทศข้อมูลพลังงานทดแทนและการอนุรักษ์พลังงาน, บทที่ *4* การศึกษาข้อมูลด้านศักยภาพเชิงพื้นที่ในการส่งเสริมการใช้ใบและยอดอ้อยเป็นพลังงานทดแทน *4.* ศักยภาพและพื้นที่ในการส่งเสริมการผลิตพลังงานจากใบอ้อย *4.1* ภาพรวมของอ้อยและอุตสาหกรรมอ้อย *4.1.1* ข้อมูลทั่วไปของอ้อย. 2016, Department of Alternative Energy Development and Efficiency, Ministry of energy. 4-1,4-2.
31. Jutakanoke, R., et al., *Sugarcane leaves: Pretreatment and ethanol fermentation by Saccharomyces cerevisiae.* biomass and bioenergy, 2012. **39**: p. 283-289.
32. Krishnan, C., et al., *Alkali-Based AFEX Pretreatment for the Conversion of Sugarcane Bagasse and Cane Leaf residues to Ethanol.* Biotechnol. Bioeng., 2010. **107**: p. 441–450.
33. Eggleston, G., et al., *Brown and green sugarcane leaves as potential biomass: How they deteriorate under dry and wet storage conditions.* Industrial Crops and Products, 2014. **57**: p. 69–81.
34. Moodley, P. and E.B.G. Kana, *Optimization of xylose and glucose production from sugarcane leaves (Saccharum officinarum) using hybrid pretreatment techniques and assessment for hydrogen generation at semi-pilot scale.* International journal of hydrogen energy, 2015. **40**: p. 3859-3867.
35. Girisuta, B., et al., *A kinetic study of acid catalysed hydrolysis of sugar cane bagasse to levulinic acid.* Chemical Engineering Journal, 2013. **217**: p. 61–70.

36. Agirrezabal-Telleria, I., et al., *Dehydration of d-xylose to furfural using selective and hydrothermally stable arenesulfonic SBA-15 catalysts.* Applied catalysis B: environmental, 2014. **145**: p. 34-42.
37. Lin, Q., et al., *SO4 2−/Sn-MMT Solid Acid Catalyst for Xylose and Xylan Conversion into Furfural in the Biphasic System.* Catalysts, 2017. **7**.
38. Bhaumik, P. and P.L. Dhepe, *A Novel One-Pot Method for Furfural Synthesis from Crop Wastes using Stable SAPO-44 Catalysts.* 2015.
39. Zhang, J., L. Lin, and S. Liu, *Efficient production of furan derivatives from a sugar mixture by catalytic process.* Energy & fuels, 2012. **26**(7): p. 4560-4567.
40. Li, H., et al., *Catalytic hydrothermal pretreatment of corncob into xylose and furfural via solid acid catalyst.* Bioresource technology, 2014. **158**: p. 313-320.
41. Cai, D., et al., *Carbonized core-shell diatomite for efficient catalytic furfural production from corn cob.* Journal of Cleaner Production, 2021. **283**: p. 125410.
42. Rakngam, I., et al., *Properties of mesoporous Al-SBA-15 from one-pot hydrothermal synthesis with different aluminium precursors and catalytic performances in xylose conversion to furfural.* Microporous and Mesoporous Materials, 2021. **317**: p. 110999.
43. Jia, Q., et al., *Production of furfural from xylose and hemicelluloses using tin-loaded sulfonated diatomite as solid acid catalyst in biphasic system.* Bioresource Technology Reports, 2019. **6**: p. 145-151.
44. Zhou, N., et al., *Conversion of xylose into furfural over MC-SnOx and NaCl catalysts in a biphasic system.* Journal of Cleaner Production, 2021: p. 127780.
45. Xu, Z., et al., *Conversion of corn stalk into furfural using a novel heterogeneous strong acid catalyst in γ-valerolactone.* Bioresource technology, 2015. **198**: p. 764-771.
46. Zhang, T., et al., *Catalytic conversion of xylose and corn stalk into furfural over carbon solid acid catalyst in γ-valerolactone.* Bioresource technology, 2016. **209**: p. 108-114.
47. Li, W., et al., *Enhanced furfural production from raw corn stover employing a novel heterogeneous acid catalyst.* Bioresource technology, 2017. **245**: p. 258-265.
48. Zhang, L., et al., *Efficient catalytic system for the direct transformation of lignocellulosic biomass to furfural and 5-*

hydroxymethylfurfural. Bioresource technology, 2017. **224**: p. 656-661.
49. Zhang, L., H. Yu, and P. Wang, *Solid acids as catalysts for the conversion of d-xylose, xylan and lignocellulosics into furfural in ionic liquid.* Bioresource technology, 2013. **136**: p. 515-521.
50. Li, X., et al., *Conversion of waste lignocellulose to furfural using sulfonated carbon microspheres as catalyst.* Waste Management, 2020. **108**: p. 119-126.
51. Sun, K., et al., *A solid iron salt catalyst for selective conversion of biomass-derived C5 sugars to furfural.* Fuel, 2021. **300**: p. 120990.
52. Dulie, N.W., B. Woldeyes, and H.D. Demsash, *Synthesis of lignin-carbohydrate complex-based catalyst from Eragrostis tef straw and its catalytic performance in xylose dehydration to furfural.* International Journal of Biological Macromolecules, 2021. **171**: p. 10-16.
53. Lai, F., et al., *Efficient conversion of carbohydrates and biomass into furan compounds by chitin/Ag co-modified H3PW12O40 catalysts.* Journal of Cleaner Production, 2021: p. 128243.
54. Saito, M., et al., *Brønsted acid property of alumina-based mixed-oxides-supported tungsten oxide.* Catalysis Today, 2020.
55. Gong, L., et al., *Composite coal fly ash solid acid catalyst in synergy with chloride for biphasic preparation of furfural from corn stover hydrolysate.* Bioresource technology, 2019. **293**: p. 122065.
56. Yue, C., et al., *Dehydration of glucose to 5-hydroxymethylfurfural using Nb-doped tungstite.* ChemSusChem, 2016. **9**(17): p. 2421.
57. Kamachi, T., et al., *Combined theoretical and experimental study on alcoholysis of amides on CeO2 surface: A catalytic interplay between Lewis acid and base sites.* Catalysis Today, 2018. **303**: p. 256-262.
58. Varala, R., et al., *Sulfated tin oxide (STO)–Structural properties and application in catalysis: A review.* Arabian Journal of Chemistry, 2016. **9**(4): p. 550-573.
59. Khalaf, H.A., S.E. Mansour, and E.A. El-Madani, *The influence of sulfate contents on the surface properties of sulfate-modified tin (IV) oxide catalysts.* Journal of the Association of Arab Universities for Basic and Applied Sciences, 2011. **10**(1): p. 15-20.
60. Mekhemer, G.A., et al., *Sulfated alumina catalysts: consequences of sulfate content and source.* Monatshefte für Chemie/Chemical Monthly, 2005. **136**(12): p. 2007-2016.

61. Deganello, F. and A.K. Tyagi, *Solution combustion synthesis, energy and environment: Best parameters for better materials.* Progress in Crystal Growth and Characterization of Materials, 2018. **64**(2): p. 23-61.
62. Vita, A., et al., *Influence of Ce-precursor and fuel on structure and catalytic activity of combustion synthesized Ni/CeO2 catalysts for biogas oxidative steam reforming.* Materials Chemistry and Physics, 2015. **163**: p. 337-347.
63. Jain, S., K. Adiga, and V.P. Verneker, *A new approach to thermochemical calculations of condensed fuel-oxidizer mixtures.* Combustion and flame, 1981. **40**: p. 71-79.
64. Thoda, O., et al., *Review of recent studies on solution combustion synthesis of nanostructured catalysts.* Advanced Engineering Materials, 2018. **20**(8): p. 1800047.
65. Guntida, A., et al., *Lewis acid transformation to Bronsted acid sites over supported tungsten oxide catalysts containing different surface WOx structures.* Catalysis Today, 2020. **358**: p. 354-369.
66. Kosri, C., et al., *Selective conversion of xylose to lactic acid over metal-based Lewis acid supported on γ-Al2O3 catalysts.* Catalysis Today, 2021. **367**: p. 205-212.
67. Pehlivan, M., et al., *An extensive study on the synthesis of iron based magnetic aluminium oxide nanocomposites by solution combustion method.* Journal of Materials Research and Technology, 2019. **8**(2): p. 1746-1760.
68. Cam, T.S., et al., *Urea–nitrate combustion synthesis of CuO/CeO2 nanocatalysts toward low-temperature oxidation of CO: the effect of Red/Ox ratio.* Journal of Materials Science, 2020. **55**(26): p. 11891-11906.
69. Nhiem, D.N., et al., *Catalytic oxidation of carbon monoxide over nanostructured CeO2–Al2O3 prepared by combustion method using polyvinyl alcohol.* Ceramics International, 2013. **39**(3): p. 3381-3385.
70. Liu, X., et al., *IRON OXIDE AND Fe2O3/Al2O3 USED TO CATALYZE REMOVING HYDROGEN FROM TAIL CHLORINE AT LOW TEMPERATURE.* Química Nova, 2019. **42**(3): p. 319-328.
71. Zhang, J., et al., *Preparation and characterization of Fe2O3/Al2O3 using the solution combustion approach for chemical looping combustion.* Industrial & engineering chemistry research, 2012. **51**(39): p. 12773-12781.

72. Zhang, X., et al., *Selective catalytic oxidation of H2S over iron oxide supported on alumina-intercalated Laponite clay catalysts.* Journal of hazardous materials, 2013. **260**: p. 104-111.
73. Lee, C.B.T.L. and T.Y. Wu, *A review on solvent systems for furfural production from lignocellulosic biomass.* Renewable and Sustainable Energy Reviews, 2021. **137**: p. 110172.
74. Ji, L., et al., *Improved one-pot synthesis of furfural from corn stalk with heterogeneous catalysis using corn stalk as biobased carrier in deep eutectic solvent–water system.* Bioresource Technology, 2021. **340**: p. 125691.
75. Möller, M. and U. Schröder, *Hydrothermal production of furfural from xylose and xylan as model compounds for hemicelluloses.* Rsc Advances, 2013. **3**(44): p. 22253-22260.
76. Kanchanalai, P., et al., *Reaction kinetics of concentrated-acid hydrolysis for cellulose and hemicellulose and effect of crystallinity.* BioResources, 2016. **11**(1): p. 1672-1689.
77. Dussan, K., et al., *Kinetics of levulinic acid and furfural production from Miscanthus× giganteus.* Bioresource technology, 2013. **149**: p. 216-224.
78. Shirai, H., S. Ikeda, and E.W. Qian, *One-pot production of 5-hydroxymethylfurfural from cellulose using solid acid catalysts.* Fuel Processing Technology, 2017. **159**: p. 280-286.
79. Jimenez-Morales, I., et al., *Production of 5-hydroxymethylfurfural from glucose using aluminium doped MCM-41 silica as acid catalyst.* Applied Catalysis B: Environmental, 2015. **164**: p. 70-76.
80. Chen, W.-H., et al., *Liquid hot water as sustainable biomass pretreatment technique for bioenergy production: A review.* Bioresource technology, 2022. **344**: p. 126207.
81. Zhuang, X., et al., *Liquid hot water pretreatment of lignocellulosic biomass for bioethanol production accompanying with high valuable products.* Bioresource technology, 2016. **199**: p. 68-75.
82. Zhong, C., et al., *Selective hydrolysis of hemicellulose from wheat straw by a nanoscale solid acid catalyst.* Carbohydrate polymers, 2015. **131**: p. 384-391.
83. Matsagar, B.M. and P.L. Dhepe, *Brönsted acidic ionic liquid-catalyzed conversion of hemicellulose into sugars.* Catalysis Science & Technology, 2015. **5**(1): p. 531-539.
84. Ramesh, A., et al., *Catalytic conversion of glucose to 5-hydroxymethylfurfural productions over sulphated Ti-Al2O3 catalysts.* Biomass and Bioenergy, 2021. **154**: p. 106261.

85. Naghavi, M., et al., *Deep oxidative desulfurization by sulfated alumina catalyst using ferrate (Fe (VI)) oxidant derived from scrap iron.* Chemical Engineering Research and Design, 2021. **174**: p. 454-462.
86. Delbecq, F., et al., *Hydrolysis of hemicellulose and derivatives—A review of recent advances in the production of furfural.* Frontiers in chemistry, 2018. **6**: p. 146.
87. Joshi, S.S., et al., *Efficient conversion of cellulose to levulinic acid by hydrothermal treatment using zirconium dioxide as a recyclable solid acid catalyst.* Industrial & Engineering Chemistry Research, 2014. **53**(49): p. 18796-18805.
88. Liu, S., et al., *Advances in understanding the humins: Formation, prevention and application.* Applications in Energy and Combustion Science, 2022. **10**: p. 100062.
89. Sumerskii, I.V., S. Krutov, and M.Y. Zarubin, *Humin-like substances formed under the conditions of industrial hydrolysis of wood.* Russian Journal of Applied Chemistry, 2010. **83**(2): p. 320-327.

APPENDIX A

Calculations for preparing a catalyst.

Solution combustion method (SCS).

<u>For example</u>, preparation of tungsten-promoted alumina by SCS method was calculated as follow:

For alumina:

Redox reaction: $2Al(NO_3)_3 \rightarrow Al_2O_3 + 3N_2 + 15/2O_2$ …….(1)

Combustion reaction (Urea): $nCO(NH_2)_2 + 3n/2O_2 \rightarrow nN_2 + nCO_2 + 2nH_2O$ ……(2)

(1) + (2): $2Al(NO_3)_3 + nCO(NH_2)_2 + (3n/2\text{-}15)O_2 \rightarrow Al_2O_3 + (n+3)N_2 + nCO_2 + 2nH_2O$

$2Al(NO_3)_3 + nCO(NH_2)_2 + 3/2(n\text{-}5)O_2 \rightarrow Al_2O_3 + (n+3)N_2 + nCO_2 + 2nH_2O$

∴ $n = 5\Phi$

$2Al(NO_3)_3 + 5\Phi CO(NH_2)_2 + 3/2(5\Phi\text{-}5)O_2 \rightarrow Al_2O_3 + (5\Phi+3)N_2 + 5\Phi CO_2 + 2(5\Phi)H_2O$

$\Phi = 0.8$ (stoichiometric mixture)

$2Al(NO_3)_3 + 4CO(NH_2)_2 + 0.5O_2 \rightarrow Al_2O_3 + 7N_2 + 4CO_2 + 8H_2O$ …(SCS reaction)

Ratio of alumina : urea (precursor) = 1 : 2

For tungsten:

Redox reaction: $H_{26}N_6O_{40}W_{12} + 4HNO_3 \rightarrow 12WO_3 + 5N_2 + 1/2O_2 + 15H_2O$ …….(3)

Combustion reaction (Urea): $nCO(NH_2)_2 + 3n/2O_2 \rightarrow nN_2 + nCO_2 + 2nH_2O$ …….(4)

(3) + (4): $H_{26}N_6O_{40}W_{12} + 4HNO_3 + nCO(NH_2)_2 + (3n/2 - 1/2)O_2 \rightarrow 12WO_3 + (5+n)N_2 + 1/2O_2 + (15+2n)H_2O$

$H_{26}N_6O_{40}W_{12} + 4HNO_3 + nCO(NH_2)_2 + 1/2(3n - 1)O_2 \rightarrow 12WO_3 + (5+n)N_2 + 1/2O_2 + (15+2n)H_2O$

$\therefore$ n = $\Phi/3$

$H_{26}N_6O_{40}W_{12}$ + 4HNO_3 + $\Phi/3CO(NH_2)_2$ + 1/2(3($\Phi/3$) - 1)O_2 -> 12WO_3 + (5+ $\Phi/3$)N_2 +1/2O_2 + (15+2($\Phi/3$))H_2O

Φ = 0.8 (stoichiometric mixture)

$H_{26}N_6O_{40}W_{12}$ + 4HNO_3 + 0.27$CO(NH_2)_2$ + -0.095O_2 -> 12WO_3 + (5.27)N_2 +1/2O_2 + (15.54)H_2O

$H_{26}N_6O_{40}W_{12}$ + 4HNO_3 + 0.27$CO(NH_2)_2$ -> 12WO_3 + (5.27)N_2 +1/2O_2 + (15.54)H_2O + 0.095O_2 ……(SCS reaction)

Ratio of tungsten : urea (precursor) = 1 : 0.27

For basis 2 g catalyst of 1W-Al.

For example, preparation of 1% tungsten-promoted alumina by solution combustion method was calculated as follow: Basis 2 g of 1W-Al and $H_{26}N_6O_{40}W_{12}$ •xH_2O and $Al(NO_3)_3$•9H2O were used as tungsten and alumina precursor.

1.98 g of Al_2O_3	1 mol of Al_2O_3	2 mol of $Al(NO_3)_3$	375.13 g of $Al(NO_3)_3$	1
	101.96 g of Al_2O_3	1 mol of Al_2O_3	1 mol of $Al(NO_3)_3$	0.99

= 26.017 g of $Al(NO_3)_3$ for 1W-Al or 0.069 mol of $Al(NO_3)_3$

0.02 g of WO_3	1 mol of WO_3	1 mol of $H_{26}N_6O_{40}W_{12}$	2956.3 g of $H_{26}N_6O_{40}W_{12}$	1
	231.84 g of WO_3	12 mol of WO_3	1 mol of $H_{26}N_6O_{40}W_{12}$	0.85

= 0.044 g of $H_{26}N_6O_{40}W_{12}$ for 1W-Al or 0.0000148 mol of $H_{26}N_6O_{40}W_{12}$

Total gram of urea for 1W-Al = (mol of Al precursor * ratio of urea in alumina : urea) + (mol of W precursor ratio of urea in tungsten : urea)

= (0.069*2) + (0.0000148*0.27)

∴ Urea for 1W-Al = 0.139 mol or 8.35g.

Impregnation method

For example, preparation of 5 wt.%SO_4^{2-} on 10W-Al by impregnation method was calculated as follow: Basis 2 g of 10W-Al support and $(NH_4)_2SO_4$ solution used as SO_4^{2-}precursor.

2 g of support	5 g of SO_4^{2-}	1 mol of SO_4^{2-}	1 mol of $(NH_4)_2SO_4$	132.14 g of $(NH_4)_2SO_4$	1
	95 g of support	96.06 g of SO_4^{2-}	1 mol of SO_4^{2-}	1 mol of $(NH_4)_2SO_4$	0.99

= 0.146 g or 0.083 ml of $(NH_4)_2SO_4$ for 5 wt.%SO_4^{2-} on 10W-Al.

APPENDIX B

Calibration of furfural and 5-HMF by HPLC.

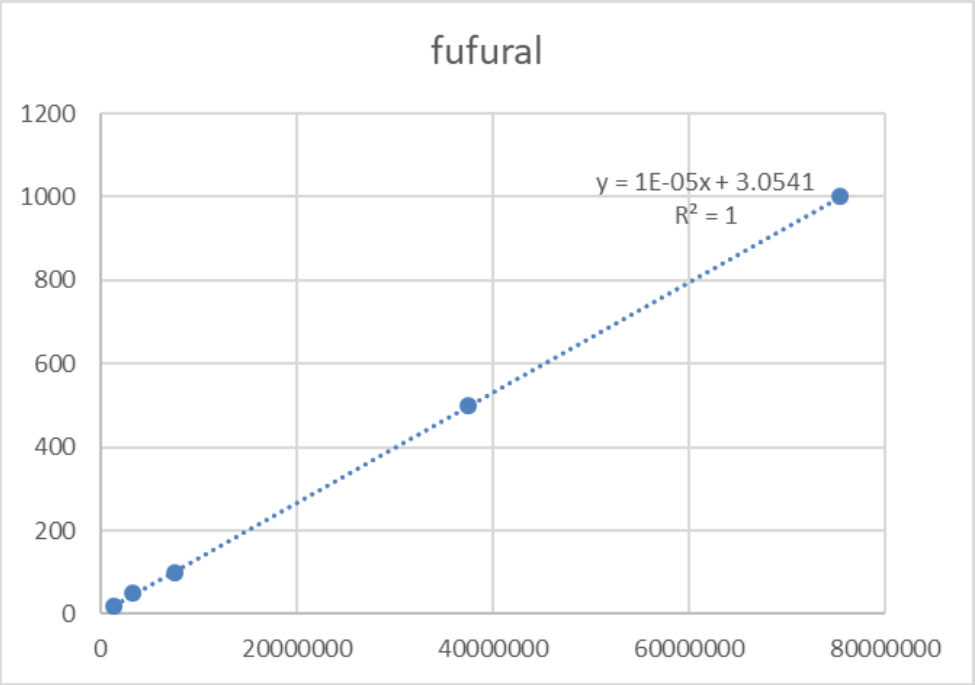

Table B1. Furfural calibration data.

Furfural calibration data	
Area	conc.(ppm)
75430261	1000
37540236	500
7529158	100
3295305	50
1378246	20

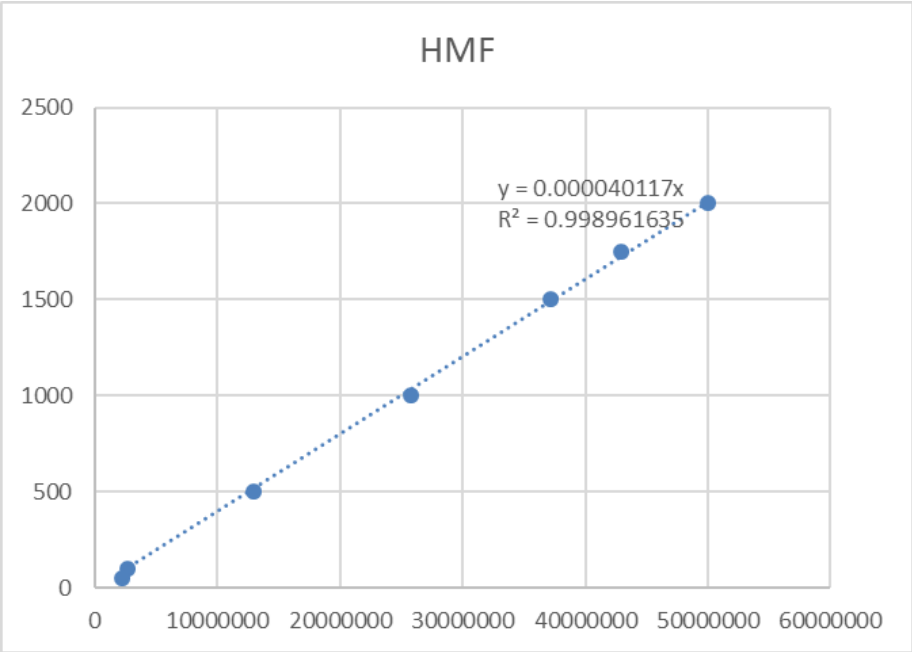

Table B2. 5-HMF calibration data.

5-HMF calibration data	
Area	con. (ppm)
49987107	2000
42974534	1750
37155104	1500
25741628	1000
12957775	500
2615546	100
2255806	50

Chromatogram from HPLC

For example I : 5W-Al at 170°C, 5 h.

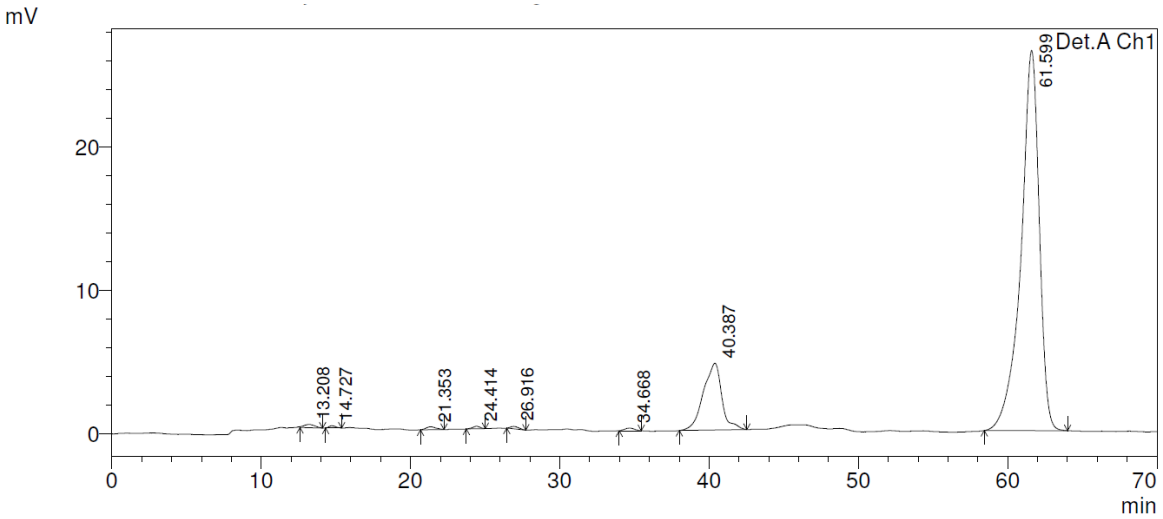

For example II : 5W-Al at 170°C, 0.5 h.

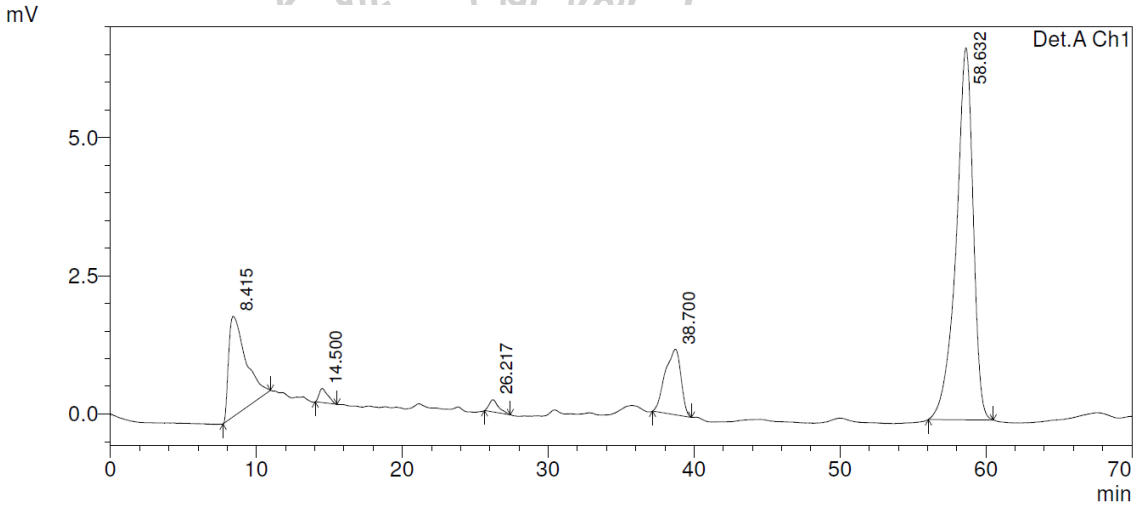

Adsorption-Desorption isotherm.

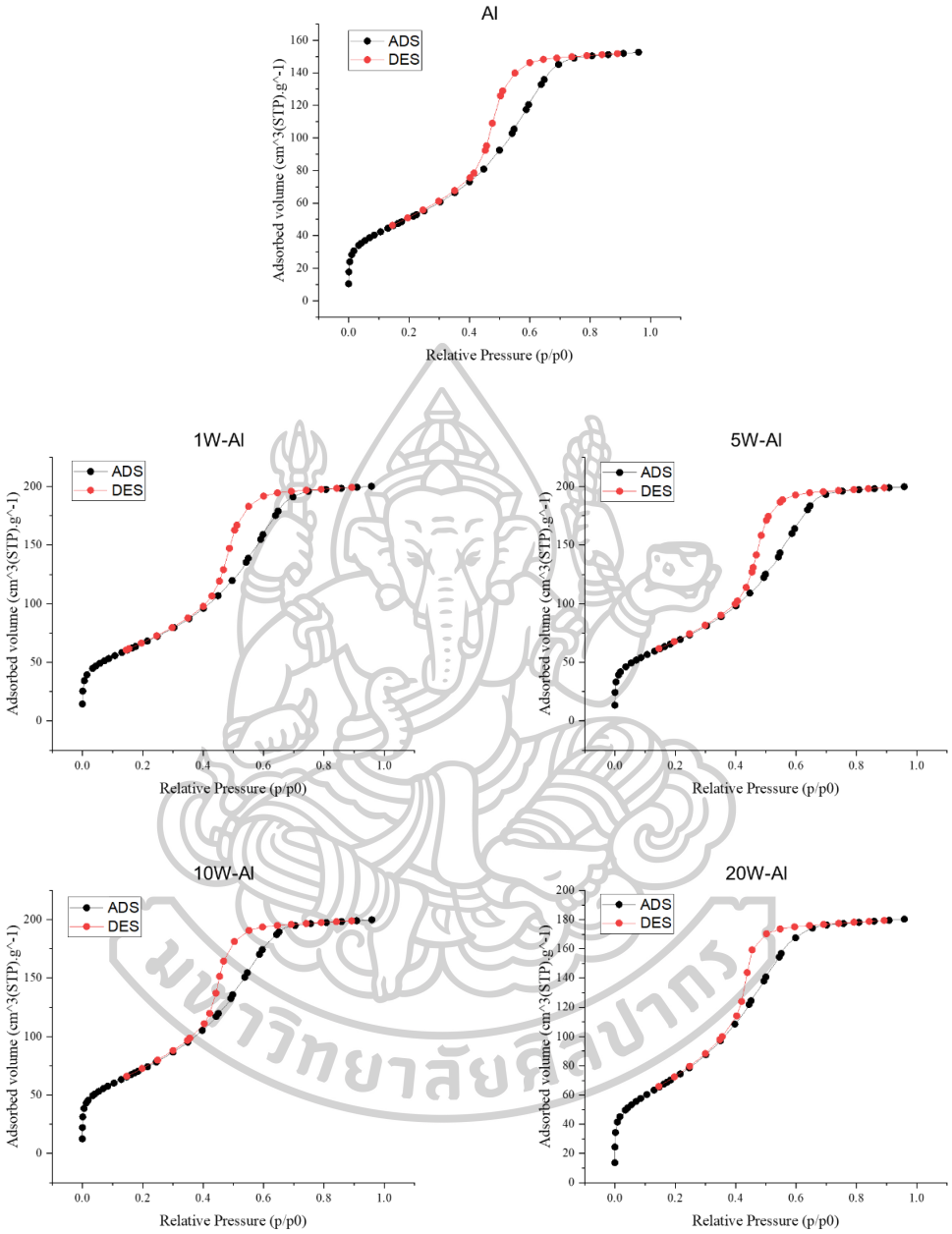

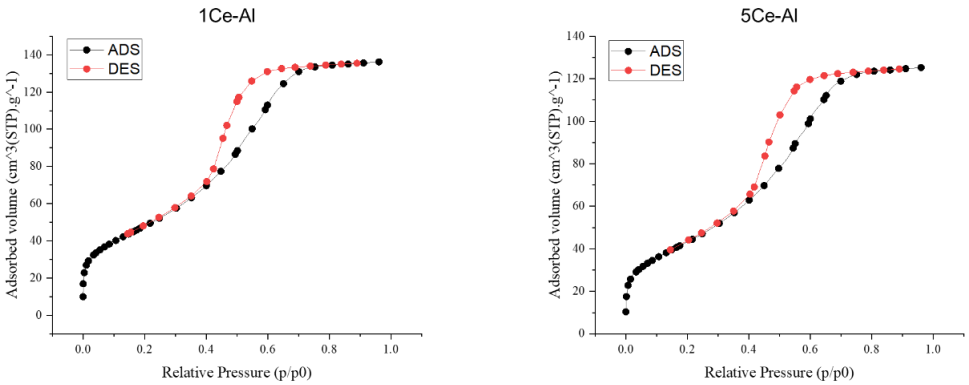
1Ce-Al
ADS
DES
Adsorbed volume (cm^3(STP).g^-1)
Relative Pressure (p/p0)

5Ce-Al
ADS
DES
Adsorbed volume (cm^3(STP).g^-1)
Relative Pressure (p/p0)

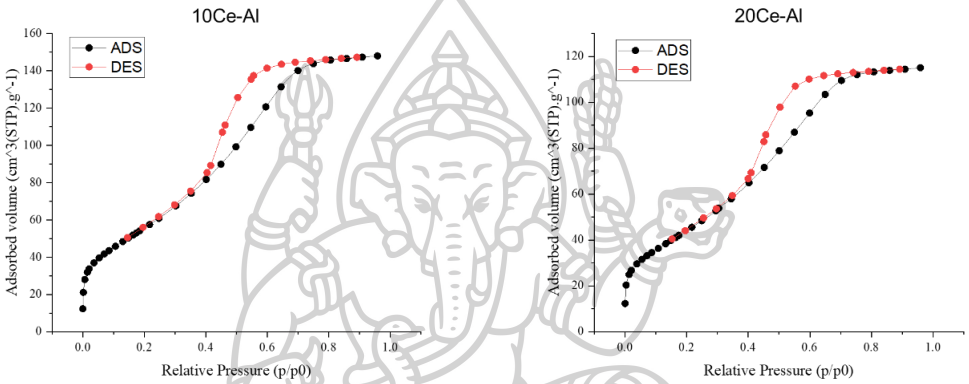
10Ce-Al
ADS
DES
Adsorbed volume (cm^3(STP).g^-1)
Relative Pressure (p/p0)

20Ce-Al
ADS
DES
Adsorbed volume (cm^3(STP).g^-1)
Relative Pressure (p/p0)

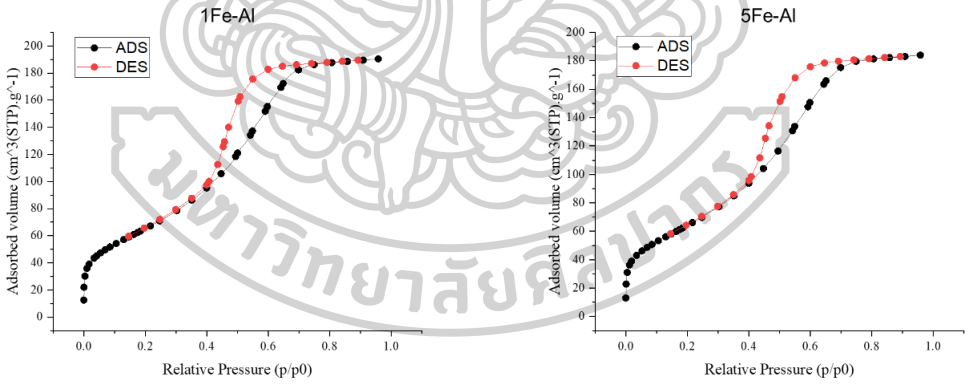
1Fe-Al
ADS
DES
Adsorbed volume (cm^3(STP).g^-1)
Relative Pressure (p/p0)

5Fe-Al
ADS
DES
Adsorbed volume (cm^3(STP).g^-1)
Relative Pressure (p/p0)

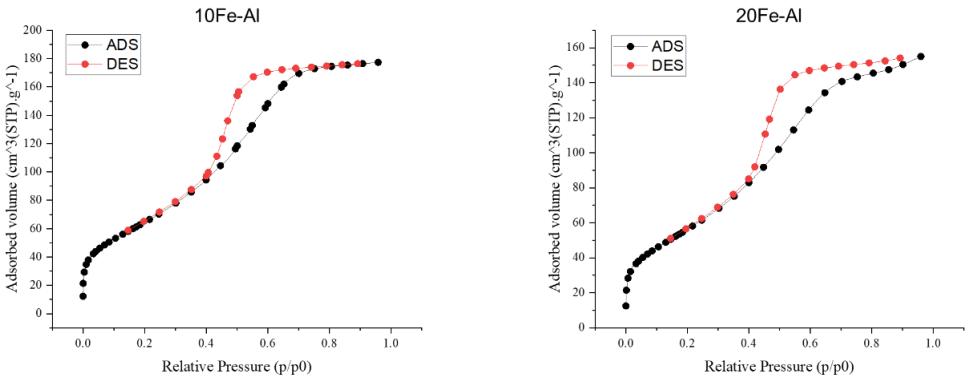
10Fe-Al
ADS
DES
Adsorbed volume (cm^3(STP).g^-1)
Relative Pressure (p/p0)

20Fe-Al
ADS
DES
Adsorbed volume (cm^3(STP).g^-1)
Relative Pressure (p/p0)

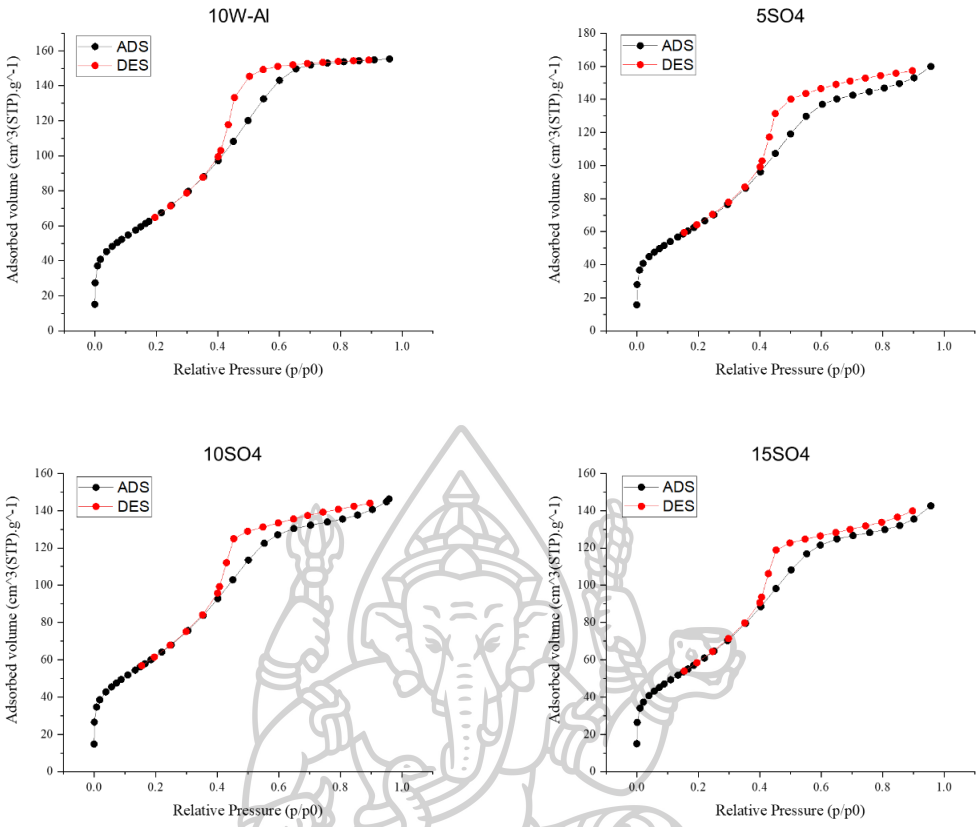
10W-Al
ADS
DES
Adsorbed volume (cm^3(STP).g^-1)
Relative Pressure (p/p0)
5SO4
ADS
DES
Adsorbed volume (cm^3(STP).g^-1)
Relative Pressure (p/p0)
10SO4
ADS
DES
Adsorbed volume (cm^3(STP).g^-1)
Relative Pressure (p/p0)
15SO4
ADS
DES
Adsorbed volume (cm^3(STP).g^-1)
Relative Pressure (p/p0)

Acidity calculation from deconvolution of NH_3-TPD results.

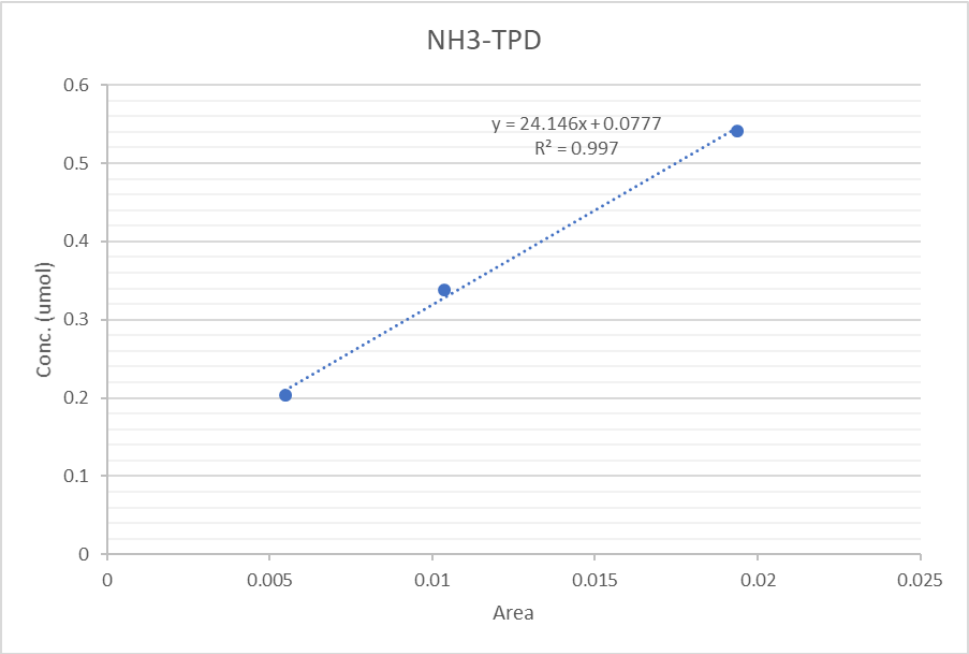

Table B3. NH_3-TPD calibration data.

NH_3-TPD calibration data	
Area	con. (umol)
0.005482	0.203188304
0.0103675	0.338647173
0.019376667	0.541835476

Humins on surface catalyst

For xylose as substrate and 10W-Al at 170°C, 2 h

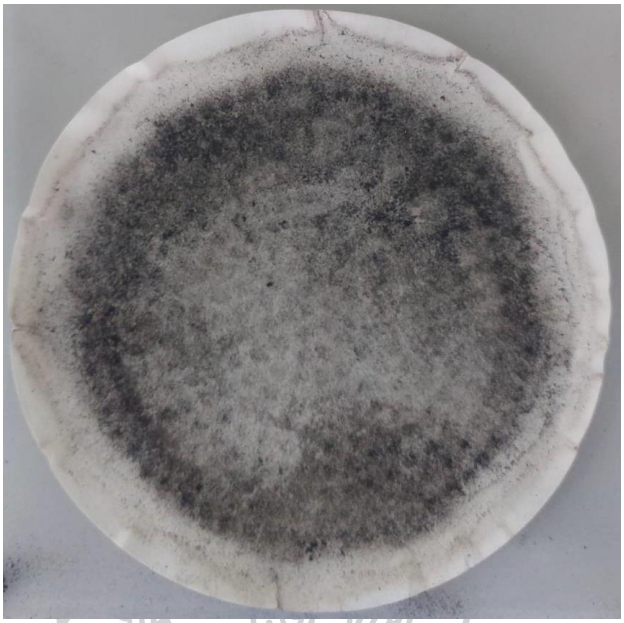

For xylose as substrate and 10W-Al at 170°C, 5 h

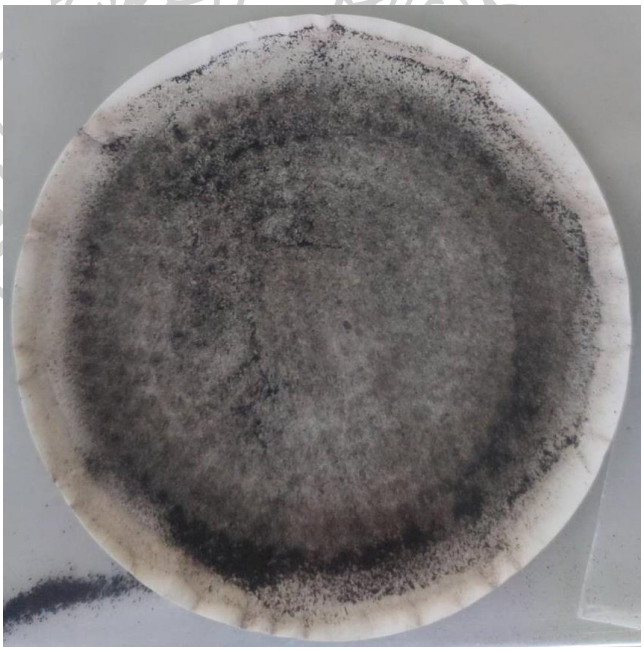

VITA

NAME	Mr.Navee Ampolsing
DATE OF BIRTH	29 April 1997
PLACE OF BIRTH	Bangkok, Thailand
INSTITUTIONS ATTENDED	Bachelor's degree : Department of chemical engineering, Faculty of Engineering and Industrial Technology, Silpakorn University
HOME ADDRESS	93/232, Moo 3, Tambon Nadi , Amphur Muang, Samut Sakhon 74000